Ph.D. DISSERTATION

Process Optimization and Parameter Estimation in Pilot Plant Experiments via Bayesian Theorem for the CO_2 Capture Process with a New Water Lean Amine Solvent

신 저수계 아민 용매 기반 이산화탄소 포집 공정을 위한 파일럿 스케일 실험을 통한 베이즈 정리 기반의 공정 최적화 및 매개변수 추정

BY

JEONGNAM KIM

August 2019

DEPARTMENT OF CHEMICAL AND BIOLOGICAL ENGINEERING
COLLEGE OF ENGINEERING
SEOUL NATIONAL UNIVERSITY

Ph.D. DISSERTATION

Process Optimization and Parameter Estimation in Pilot Plant Experiments via Bayesian Theorem for the CO_2 Capture Process with a New Water Lean Amine Solvent

신 저수계 아민 용매 기반 이산화탄소 포집 공정을 위한 파일럿 스케일 실험을 통한 베이즈 정리 기반의 공정 최적화 및 매개변수 추정

BY

JEONGNAM KIM

August 2019

DEPARTMENT OF CHEMICAL AND BIOLOGICAL ENGINEERING
COLLEGE OF ENGINEERING
SEOUL NATIONAL UNIVERSITY

Process Optimization and Parameter Estimation in Pilot Plant Experiments via Bayesian Theorem for the CO_2 Capture Process with a New Water Lean Amine Solvent

신 저수계 아민 용매 기반 이산화탄소 포집 공정을 위한 파일럿 스케일 실험을 통한 베이즈 정리 기반의 공정 최적화 및 매개변수 추정

지도교수 이 윤 우

이 논문을 공학박사 학위논문으로 제출함

2019 년 6 월

서울대학교 대학원

화학생물공학부

김 정 남

김정남의 박사 학위논문을 인준함

2019 년 6 월

위 원 장 이 종 민 (인)

부 위 원 장 이 윤 우 (인)

위 원 남 재 욱 (인)

위 원 임 연 철 (인)

위 원 이 웅 (인)

Abstract

The development of new amine solvents without the major drawbacks of conventional amines is crucial to industrial applications of CO_2 capture. This paper presents a water-lean CO_2 capture solvent having a low regeneration energy and low degradation. The water-lean solvent, K_2Sol, is a sterically hindered diamine; because of the hindered amine site, K_2Sol easily forms bicarbonate, resulting in a high absorption capacity. The minimum solvent regeneration energy is obtained using Gaussian process Bayesian optimization (GPBO) and bench-scale pilot plant experiments. GPBO finds the optimal solution using the input and output relationship of experiments; thus, expensive first-principle model construction can be avoided. According to the pilot plant experiment, the optimal regeneration energies of monoethanolamine (MEA) and K_2Sol are 4.3 and 2.8 GJ/t CO2, respectively, indicating that K2Sol requires only 65% of the regeneration energy of MEA. Fewer than 30 experiments are required to nd the optimal pilot plant operation for both the MEA and K_2Sol experiments. The superior properties of K_2Sol in terms of the CO_2 loading, cyclic capacity, regeneration temperature, and degradation is also presented.

Additionally, Bayesian parameter estimation is implemented for the absorber model with K_2Sol, for the process design and the configuration optimization using a commercial process simulator. According to various assumptions, parameter candidates to be used in GSA is selected. The subset including 8 physiochemical parameters served as input variables of the surrogate model. Due to non-linearity of the full model, the surrogate model can not reflect the responses of the full model. The trade-off between the inaccuracy of the sur-

rogate model and the high computation costs of the full model was solved by applying the hybrid model in the final sampling of MCMC. From the parameters posterior distribution, it is presented that a standard Gibbs free energy of HK_2Sol^+ is the most influenceable parameter at the full model and both forward reactions are near equally dominant. Most output responses of a full model with estimated parameters were also located in 95% confidence interval.

Keywords: CO_2 capture, Water-lean amine solvent, Gaussian process Bayesian optimization, Pilot-scale testing, Global sensitivity analysis, Bayesian parameter estimation

Student Number: 2011-21025

Contents

List of Figures

List of Tables

Chapter 1

Introduction

1.1 Research Motivation

Aqueous amine-based post-combustion CO_2 capture processes are known to be one of the most feasible technologies and are considered to be a promising option to meet the Paris Agreement to limit the global temperature increase to below 2 °C [1]. The amine absorption method can be applied to large CO_2 emitting sources by retrofitting existing facilities, and its technological maturity has been demonstrated in many industrial projects. Most of the industrial-applicable CO_2 reactive amine solvents contain a significant amount of water as a cosolvent, and a copious amount of water is inefficiently boiled and recondensed during solvent regeneration [2]. Thus, a high solvent regeneration energy, solvent evaporation, and solvent degradation are inevitable. As a result, a power decrease of more than 30% is expected when a CO_2 capture process is applied, even when state-of-the-art aqueous amine CO_2 capture technology is used [3].

Solvent development and post-combustion CO_2 capture process optimiza-

tion are the two main strategies for mitigating the drawbacks of the aqueous amine-based CO_2 capture process. Regarding solvent development for an aqueous amine-based post-combustion CO_2 capture, a number of amine solvents have been investigated, including blended amines and sterically hindered amines. These amines can have higher cyclic capacities, faster reaction rates, and/or lower heats of absorption, and thus lower regeneration energies and solvent evaporation. Water-lean solvents have attracted much attention recently because they improve the efficiency of solvent regeneration dramatically by lowering the specific heat of the solvent while maintaining chemical reactivity. Several researchers have developed water-lean solvents by replacing the water in conventional amine solvents [e.g., monoethanolamine (MEA), diethanolamine (DEA), and methyl diethanolamine (MDEA)] with organic cosolvents. Song et al. blended MEA with ethylene glycol (EG) and polyethylene glycol instead of water, and the addition of the cosolvents increases the CO_2 solubility and capacity [4]. Guo et al. investigated solvent regeneration energy of MEA or DEA blended with glycol ethers (2-methoxyethanol (2ME) and 2-ethoxyethanol (2EE)). They reported the mixtures of MEA and 2ME/2EE have huge potential to reduce reboiler heat duty as they shows 55% reduction in solvent regeneration energy in lab scale experiments [5]. Similar studies have been performed, for example, on triethanolamine in alcohol [6], DEA in EG [7], and MDEA in methanol [8]. Im et al. also developed sterically hindered amine blends in EG or methanol [9]. These solvents form ammonium alkyl carbonate zwitterion, which can be regenerated at lower temperature than MEA. Note that the organic cosolvents in these studies can act as better CO_2 carriers with a higher solvation effect. However, the high volatility of the cosolvent is an obstacle to industrial application. Mixture of ionic liquids with conventional solvents (i.e., MEA and MDEA) have also drawn attention as CO_2 capture solvent as they

show high absorption capacity, moderate viscosity, and low vapor pressure [10]. However, these solvents have been tested only in lab scale experiment and their high cost can be a potential obstacle for industrial application. Recently, several biphasic absorbent solvent developed having low regeneration energy Wang et. al. introduced MEA/1-propanol aqueous absorbent and the total regeneration energy were reduced by 39.85% [11]. Shen et. al. compared mixture often primary/secondary amines with eight tertiary amines for biphasic solvent and discovered latent heat increases with the tertiary amine's hydrophobicity [12]. A comprehensive review for phase change solvent is available in Zhang et. al [13].

Blasucci et al. introduced reversible ionic liquids as CO_2 binding organic liquids [14]. These amines bind CO_2 through the standard carbamate formation mechanism, forming ionic liquids. Reversible ionic liquids have excellent CO_2 capture capacity and a low regeneration temperature, but they exhibit high viscosity during regeneration. Heldebrant et al. developed low-volatility diamines, which can also be used as reversible ionic liquids [15]. The use of diamines makes it possible to form zwitterionic carbamate, greatly improving the CO_2 uptake capacity compared with ones proposed by Blasucci et al. Heldebrant et al. first introduced alkylcarbonate-derived switchable ionic liquids called CO_2-Binding Organic Liquids (CO_2BOLs) [16]. Although CO_2BOLs have reasonably low solvent regeneration energies, they are not practical for industrial application because of the evaporation losses caused by high vapor pressure. Lail et al. recently introduced and tested reversible ionic liquids known as nonaqueous solvents (NASs) [17]. NASs are carbamate-forming amines having low vapor pressure, low foaming, and reduced water accumulation. NASs also have a low regeneration energy and temperature while maintaining very low viscosities (2.5 to 38 cP) throughout the operating range. The viscosities of NASs, in fact, are

an order of magnitude lower than those of other reversible ionic liquid solvents. A comprehensive review of water-lean amine solvents for CO_2 capture is available in Heldebrant et al. [2].

Optimization of post-combustion CO_2 capture processes is an effective strategy for lowering the solvent regeneration energy and also for finding the optimal operating conditions, solvent concentration, and process configuration. Because the optimal operating conditions of different solvents for minimizing the solvent regeneration energy can differ significantly, it is necessary to compare the solvent performance under each optimal condition for consistent argument. Mores et al. developed a detailed mathematical model of a CO_2 capture process and validated the results using published experimental data [18]. They minimized the capital and operating cost for different CO_2 removal targets and proposed a set of optimal conditions [19]. Rodriguez et al. studied the optimization of a CO_2 capture process using DEA and MDEA mixtures [20]. They presented the minimum total annual cost according to the MDEA concentration in the blended amine. Damartzis et al. used a superstructure model to evaluate combinations of amine solvents and alternative process configurations [21]. They presented the optimal values of process design parameters such as the column stages, column pressure, amine flow rate, and reboiler temperature using solvent-configuration combinations. Oh et al. also applied superstructure optimization method to find the optimal process design and they insist the flue gas splitting shows a significant reduction of energy consumption [22]. Lee et al. also performed superstructure optimization to retrofit an existing post-combustion capture pilot plant [23]. They employed exergy analysis to reduce the number of configurations used in the optimization. They proposed the optimal process configuration by minimizing the thermal energy requirements.

The optimization in these studies requires a process model describing the

chemical and physical behavior of the underlying process. For consistent comparison across various solvent regeneration energies, a rigorous process model should be developed for each solvent to obtain the optimal operating conditions, but model development has enormous energy and cost requirements. Although this type of model evaluation is generally less costly than experiments, building a process model can be very expensive because the physicochemical properties should be included in the process model (e.g., the kinetics of absorption, phase equilibrium between CO_2, CO_2 solubility, and mass transfer). Therefore, numerous experiments are generally conducted *a priori* to develop the process model.

To avoid difficulties of the model construction, several studies reported finding the optimal operating condition using a black-box-model-based (model-free) approach. Process optimization of a pilot plant can be converted into the mathematical problem of finding the optimal solution of "black-box function". When the underlying black-box function is pilot plant operation, evaluation of the black-box model is economically very expensive and generally time consuming; thus, it is required to reduce the number of function evaluation as much as possible. In a related study, Mangalapally et al. evaluated four new solvents and compared them to MEA in a pilot plant [24]. They performed experimental studies with varying the solvent and flue gas flow rates. The optimal solvent flow rate for each solvent was obtained using a sensitivity analysis, which reveals the effect of the operating parameters on the process output even though the physical and chemical properties are not fully specified. They also proposed the most promising solvent. However, the number of experiments increases exponentially as decision variables are added, and the minimum point obtained from sensitivity analysis does not guarantee the optimal solution. Several studies of CO_2 capture process optimization have been conducted using a machine-

learning technique based on the response surface model (RSM) to train the black-box function [25]. However, the reported methodologies are considered to be unsuitable for this system, because at least 100 to 2000 function evaluations are needed to find an optimal point. Sequential design of experiments (SDOE) and the framework for optimization, quantification of uncertainty and surrogates (FOQUS), which makes the test runs maximally informative, were applied recently to the National Carbon Capture Center (NCCC) pilot plant test campaigns in Wilsonville, AL, USA [26]. The output responses were estimated using the surrogate model, and the model parameters were updated using Bayesian inference.

As the alternative methods to avoid difficulties of the model constructions, non-experimental estimation approaches can be employed. Non-expermental methods is classified into several groups; those based on theoretical, semi-theoretical (e.g. statical thermodynamics and quantum mechanics), and empirical relationship (e.g. group contribution methods). In the case of CO_2 capture process, non-experimental methods with empirical relationships are limited because the estimated parameters are inaccurate and the methods do not estimate the reaction relationships. Several researchers implemented the method of continuous molecular targeting-computer-aided molecular design for the solvent selection [27, 28]. But these studies limits only the chemical related to physical absorption to candidates or, the molecular structure that can be analyzed is limited to certain structures. From statistical methods, other researchers calibrated computer models through few experimental data to represent the real system. Konomi et al. developed the Bayesian treed calibraion as an extension of standard Gaussian process calibration methods, and 6 parameters in the computational fluid dynamics (CFD) model were estimated from experimental data of the CO_2 capture process with AX amine based sorbents [29].

Na et al. constructed a rigorous mathematical model of aqueous mineral carbonation kinetics for carbon capture and utilization (CCU) and estimated the parameter posterior distribution using Bayesian parameter estimation from lab-scale experiment data [30]. Theses studies show that the number of parameter candidates is small enough to do not first screening before the parameter estimation, and such methods have not been applied to the CO_2 capture process with aqueous amine solvent.

1.2 Research Objectives

The objective of this thesis is to demonstrate the performance of a new water lean amine solvent from the experimental based optimization and build a process model applied pilot-scale experiment data. The proposed methodology to conduct this study comprises Gaussian process Bayesian optimization (GPBO), which can solve black-box optimization problems by expensive objective function evaluation through a sequential decision theory [31], and Bayesian parameter estimation to find the posterior probability of the parameters that predict the pilot-scale experimental results well.

First, a new sterically hindered water-lean diamine solvent, K_2Sol, is presented. Lab-scale experiments show the superior performance of K_2Sol to 30wt% MEA in water such as rich amine loading, cyclic capacity, degradation resistance and viscosity. Next, pilot-scale experiments are conducted with both K_2Sol and 30 wt% MEA in water to quantitatively assess the new solvent, and systematically optimize its operating conditions using a machine-learning-based optimization technology for the evaluation of its superiority. The optimal operating conditions for each solvent are found using machine-learning-based black-box optimization (i.e., GPBO). GPBO builds a probabilistic surrogate model and

also optimizes it. The additional computational effort of optimization minimizes the number of experiments needed; thus, expensive surrogate model training can be avoided. Finally, physicochemical parameters for a process model development reflecting K_2Sol characteristics are estimated only with pilot-scale experiments data. By using ASPEN Plus, a commercial chemical process simulator, pure components parameters are estimated by the group contribution methods and several assumptions. The subset selection through global sensitivity analysis (GSA) finds parameters candidates that have the most influence on a process model among the remaining parameters such as phase equilibrium binary parameters. After that, ASPEN plus model with these parameters candidates as input variables is developed, then surrogate modeling based on deep neural networks is carried on for the computation load reduction of Bayesian parameter estimation. Bayesian parameter estimation is based on a Markov chain Monte Carlo method and analyzes the posterior inference of each paramters. Applying the estimated parameters to the ASPEN plus model, the CO_2 capture process model using K_2Sol as a solvent is simulated and compared with pilot scale experiments data.

1.3 Outline of the Thesis

The outline of the thesis as follows. In chapter 2, comparison of MEA and K_2Sol in lab-scale experiments is introduced. Chapter 3 introduces the pilot-scale experiments for the verification of K_2Sol performance and the method for an experimental based optimization, Gaussian process Bayesian optimization. Chapter 4 presents the methodologies of parameter estimation from small number of biased experiments and validation results of Bayesian parameter estimation. Chapter 5 is a conclusion of the thesis.

Chapter 2

Performance of A New Water Lean Amine Solvent Compared to MEA in Lab-Scale Experiments

2.1 Introduction

Amine-based absorption process is considered as the most effective approach to remove carbon dioxide (CO_2) in flue gas from power plant and to mitigate greenhouse gas emissions. Although it is a realistic option for practical applications, the major drawbacks such as high energy consumption for CO_2 stripping hinder the extensive implementation of CO_2 capture. Many studies focus on the development of new solvents that have high reaction rate with CO_2 and high CO_2 loading capacity for lower regeneration energy than that of conventional processes. However, a significant improvement on energy consumption is still yet to be achieved.

As an example of traditional amine solvents, primary, such as monoethanolam-

ine (MEA), and secondary amine, like diethanolamine (DEA) has higher reaction rate with CO_2 even at low concentration than tertiary amines, such as methyl diethanolamine (MDEA). On the other hand, the carbamates of unhindered primary and secondary amines cause the reduction of loading capacity compared with tertiary amines and sterically hindered primary amines, such as 2-amino-2-methyl-1-propanol (AMP). Furthermore, deployment of these aqueous amine solvent is limited by their high regeneration temperature. The heat capacity of water which is twice that of the organic solvent partly contributes to the high regeneration temperature [2]. Conversely, if the water content is reduced, an increase of the viscosity interferes with the process operation. Recent studies have proposed alternative amine solvents such as Piperazine, ethylenediamine and ionic liquids have been identified promising options for lowering regeneration energy but other drawbacks, especially in terms of high viscosity and thermal/oxidate degradation, tackle practical applications.

To avoid the drawbacks arising from the use of aqueous alkanolamines, K_2Sol was designed by employing a diamine (DA), 1,1′-[(1-methyl-1,2-ethanediyl) bis(oxy)]bis[2-propanamine], with two hindered primary amino groups. It is expected to facilitate regeneration while affording a high CO_2 absorption rate by introducing a moderate hindrance around the primary amino group. Like other primary amines, including MEA, as shown in figure 2.1, DA would react rapidly with CO_2, forming zwitterionic carbamate species **I**. Upon further absorption of CO_2, the carbamate species can be transformed into bicarbonate species (**II**) in the presence of water.

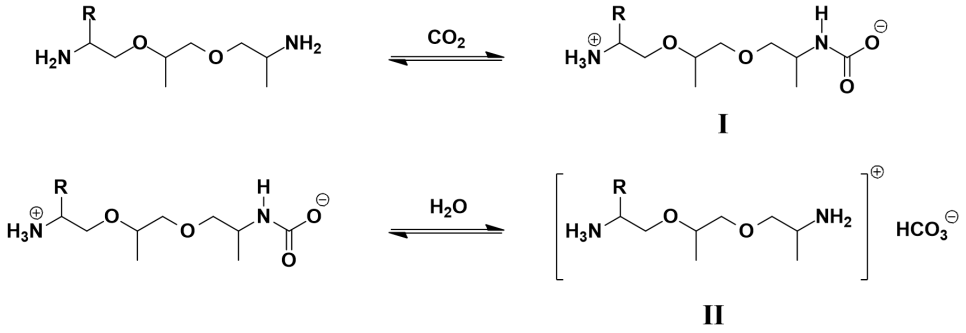

Figure 2.1: Formation of carbamate and bicarbonate species from the interaction of K_2Sol with CO_2.

2.2 Experimental Section

An lab-scale test is conducted to compare the solvent performance of 30 wt% MEA and K_2Sol on rich amine loading, cyclic capacity, heat capacity, viscosity and degradation. MEA was obtained from Green Chemicals Co. (Korea) and used as received. Diamine was obtained from Huntsman (USA). K_2Sol was prepared by dissolving a mixture of 60 wt% DA and 40 wt% water.

The rich amine loading and cyclic capacity of K_2Sol (60 wt% DA) and 30 wt% MEA was measured by ^{13}C NMR spectra. ^{13}C NMR spectra were recorded on a 400 MHz Bruker NMR spectrometer. The thermal stability of K_2Sol and 30 wt% MEA was investigated using a specially designed tube-type bomb reactor in an oven maintained at 120 °C. A diameter of a bomb reactor is 1 in, and a volume of that is 100 ml. The mass of sampling for the stability test is 10 g. To accelerate the possible decomposition, the stability test was conducted with fully CO_2-saturated K_2Sol for 7 days. Decomposition of MEA and K_2Sol was analyzed by ^{1}H NMR spectroscopy and gas chromatography. Viscosity measurements were performed with both fresh and CO_2-saturated samples at 25, 40, and 60 °C using a Viscometer TV-22 (Toki Sangyo Co.). The measurement of heat capacity was carried on using TA Instruments heat flow differential scanning calorimeter(DSC) which model name is DSC Q2000. The liquid samples were prepared within T-zero Aluminum hermetic pan, and sample mass is in the range 10 – 20 mg. To obtain accurate results, the calibration was performed using water and MEA before the heat capacity measurement of diamine.

Figure 2.2: Specially designed tube reactors for the degradation experiments of CO_2 saturated solvents

2.3 Result and Discussion

The formation of the carbonation species **I** and **II** were supported by ^{13}C NMR experiments. As shown in figure 2.3, the carbonyl peak assignable to the zwitterionic carbamate species, **I**, appeared at 163.7 ppm almost exclusively during the early stage of absorption. As absorption proceeded, the carbonyl peak corresponding to the bicarbonate species, **II**, started to grow at 161.4 ppm. Interestingly, the carbonyl peak associated with **I** was shifted slightly upfield compared with that of MEA (δ = 164.5 ppm), suggesting that desorption of CO_2 would be easier from **I** than from the carbamate species of MEA. Although desorption of CO_2 from **II** is expected to occur more slowly than that from the bicarbonate species of 2-amino-2-methyl-1-propanol (AMP), the co-presence of bicarbonate species along with carbamate species would be highly beneficial for enhancing the CO_2 absorption capacity to 1 mol CO_2/mol DA and for reducing the regeneration energy. One interesting feature of K_2Sol is that it contains much smaller amounts of water than conventional alkanolamine-based solvents; thus, the energy consumed by the latent and specific heats of water could be reduced, at least to some extent.

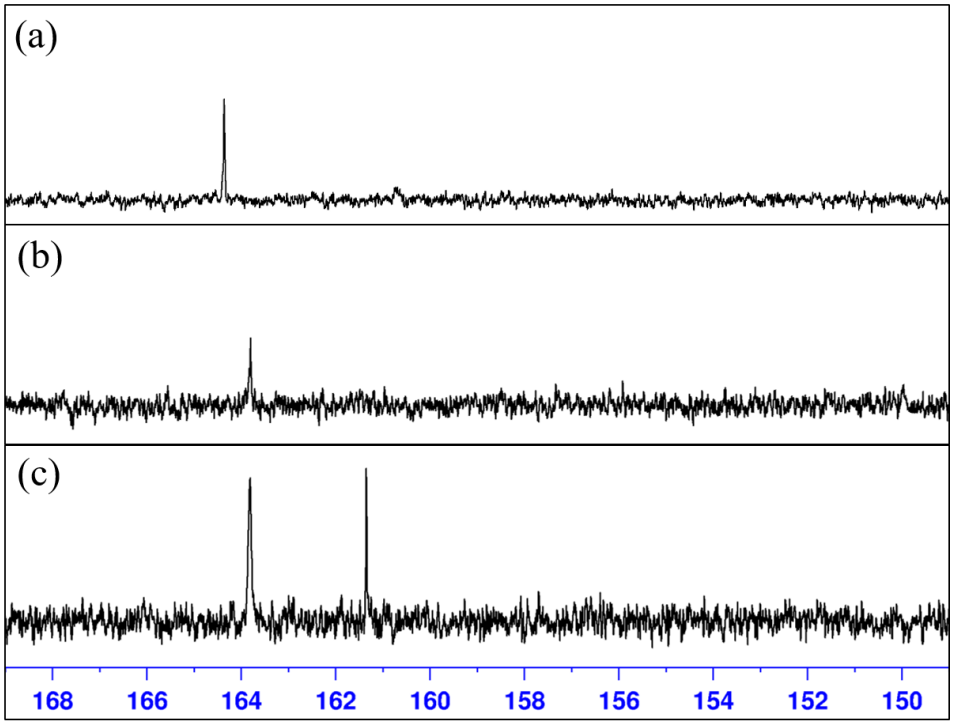

Figure 2.3: ^{13}C NMR spectra of 30wt% MEA at 0.5 mol CO_2/mol MEA and K_2Sol at different CO_2 loadings: a) 0.5 mol CO_2/mol MEA, b) 0.23 mol CO_2/mol K_2Sol, c) 0.82 mol CO_2/mol K_2Sol.

To test the recyclability of K_2Sol, CO_2 (0.1 MPa) was introduced into a closed cell absorber containing K_2Sol at 40 °C and then desorbed at 105 °C under N_2 flow. As shown in figure 2.4, the recycle experiments with K_2Sol clearly demonstrated that the absorbed CO_2 can be almost completely desorbed, allowing the K_2Sol to be recycled without appreciable loss of the initial performance. A cyclic capacity of 124.4 g CO_2/kg K_2Sol (0.9 mol CO_2/mol DA) was maintained constantly up to five cycles. For comparison, absorption/desorption experiments were also conducted with 30 wt% MEA under the same experimental conditions. Unlike the case of K_2Sol, desorption of CO_2 from the CO_2-loaded 30 wt% MEA was far from completion at 105 °C. The CO_2 absorption capacity was found to decrease by 30.8% after the first cycle and decreased further by 2.4% after 5 cycles. The cyclic capacity of 30 wt% MEA was measured as 87.6 g CO_2/kg 30 wt% MEA (0.4 mol CO_2/mol MEA), which is approximately 70% of that achieved using K_2Sol. These results strongly suggest that K_2Sol can be more easily regenerated, leading to reduced energy consumption in the stripper. Moreover, the absorption rate can be calculated from figure 2.4. The initial absorption rates are 25 g CO_2/kg solvent·min for 30 wt% MEA and 30 g CO_2/kg solvent·min for K_2Sol. K_2Sol is about 20% faster than MEA solvent. For CO_2 capture, the absorption rate is an important factor for choosing the size of the absorber and flow rate of the absorbents. Assuming an absorber as a ideal CSTR, size of an absorber could be reduced by about 20% compared to 30wt% MEA.

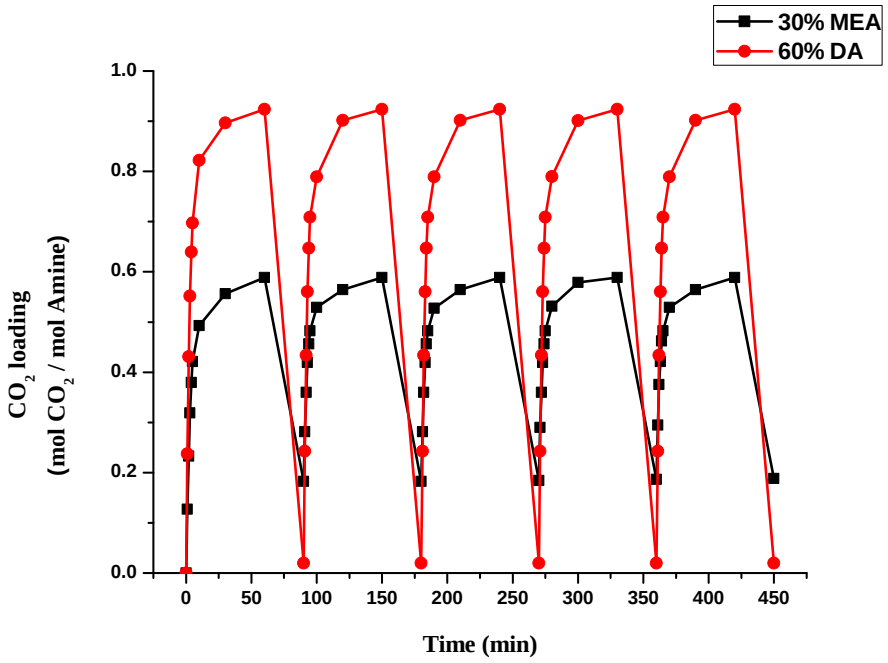

Figure 2.4: CO_2 absorption/desorption cycles of K_2Sol and 30 wt% MEA. In each cycle, CO_2 is absorbed at 40 °C and 0.1 MPa, and desorbed at 105 °C.

Most of the energy consumption in post combustion CO_2 capture process occurs during solvent regeneration. Many studies described that regeneration energy in stripping section accounts for higher than 80% of the entire operating cost [32, 33, 34]. Regeneration energy consists of the heat of desorption (ΔH_d), sinsible heat (q_s), and heat of vaporization (q_v) as shown Eq. 2.1

$$q_r = \Delta H_d + q_s + q_v \tag{2.1}$$

Sensible heat is the heat required to raise the temperature of the saturated amine solvent from the absorption temperature to the desorption temperature. The sensible heat of the amine solvent is determined by heat capacity of the saturated amine solvent. Several studies reported that sensible heat accounts for the largest amount of heat duty [35, 36]. Especially, Sensible heat is significant high in CO_2 capture process using MEA because of high reboiler temperature over 100 °C. Thus, heat capacity of amine solvent is very important for the economical implement of CO_2 capture process.

The heat capacity data for MEA and DA are given in table 2.1, 2.2 and figure 2.5, 2.6. As shown in table 2.1 and figure 2.5, the measured C_p of MEA for temperatures from 30 to 80 °C are well validated with the values of Lee et al. and Chiu et al.. Comparing table 2.1 and 2.2, heat capacity of DA is significantly lower than one of MEA. Moreover, water weight fraction in K_2Sol is lower than 30wt% MEA, so it is expected to significantly reduce a sensible heat of K_2Sol in the application of CO_2 capture process.

Table 2.1: Heat Capacities of MEA

	Heat capacity (C_p) [kJ/kg·K]					
Temp [°C]	Lee et al. [37]	Chiu et al. [38]	Ex.1.	Ex.2.	Ex.3.	Average
30	2.734	2.740	2.722	2.730	2.730	2.727
35	2.767	2.760	2.734	2.742	2.743	2.740
40	2.783	2.780	2.756	2.764	2.764	2.761
45	2.816	2.810	2.774	2.783	2.784	2.780
50	2.832	2.830	2.795	2.806	2.803	2.801
55	2.865	2.860	2.818	2.828	2.824	2.823
60	2.881	2.880	2.842	2.85	2.847	2.846
65	2.914	2.910	2.867	2.877	2.874	2.873
70	2.931	2.930	2.896	2.905	2.903	2.901
75	2.947	2.950	2.923	2.93	2.929	2.927
80	2.980	2.980	2.953	2.957	2.956	2.955

Table 2.2: Heat Capacities of 1,1′-[(1-methyl-1,2-ethanediyl) bis(oxy)]bis[2-propanamine]

Temp [°C]	Heat capacity (C_p) [kJ/kg·K]			
	Ex.1.	Ex.2.	Ex.3.	Average
30	2.134	2.144	2.139	2.139
35	2.141	2.150	2.145	2.145
40	2.152	2.158	2.152	2.154
45	2.160	2.166	2.163	2.163
50	2.169	2.175	2.174	2.173
55	2.181	2.186	2.185	2.184
60	2.191	2.195	2.193	2.193
65	2.204	2.207	2.205	2.205
70	2.216	2.220	2.217	2.218
75	2.228	2.232	2.232	2.231
80	2.242	2.245	2.247	2.245

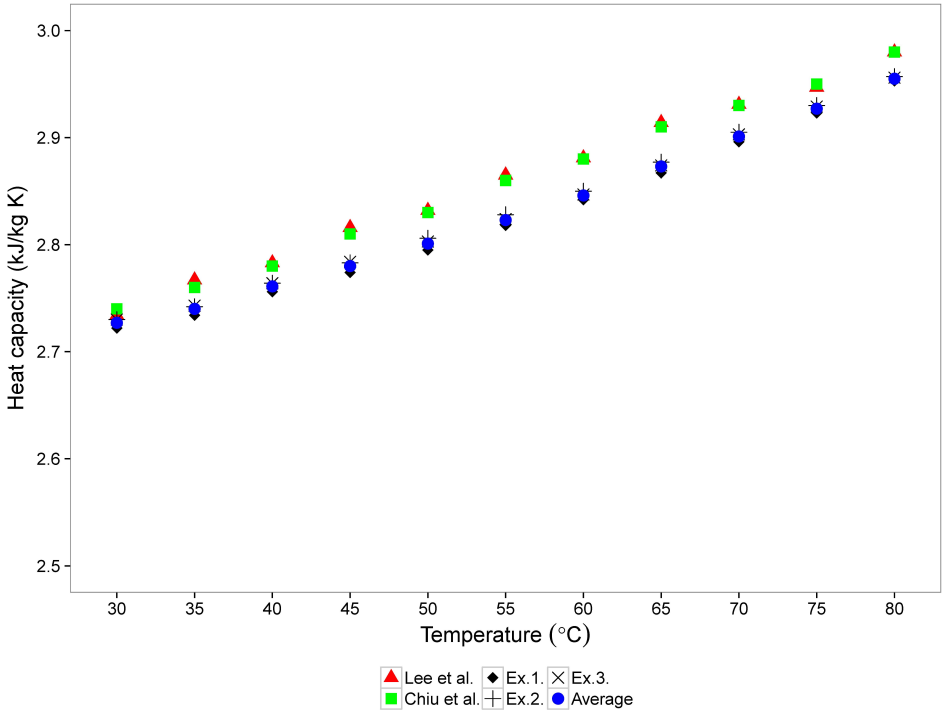

Figure 2.5: Heat capacity of MEA.

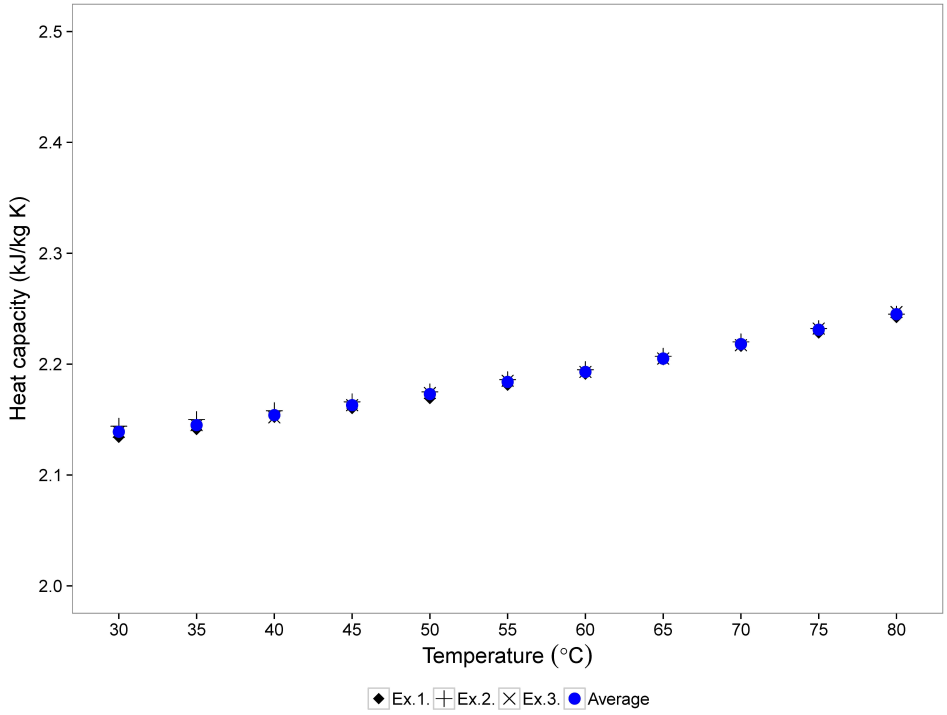

Figure 2.6: Heat capacity of 1,1′-[(1-methyl-1,2-ethanediyl) bis(oxy)]bis[2-propanamine].

The high viscosity have been pointed out as obstacles of commercialization of amine solvents. Aminosilicones and reversible ionic liquid are good examples that have high viscosity. Thus, the industrial application of those solvent is very challenging in spite of their small solvent regeneration energy. Herein, the viscosity of K_2Sol is measured in order to show that K_2Sol has reasonable viscosity throughout the pilot plant operation range as well as low degradation. As shown in figure 2.7, viscosity of K_2Sol is under 140 cP, even at 100 % CO_2 saturated sample, with loading of 1.07 mol CO_2/mol K_2Sol. Also, at $60°C$, viscosities of each loadings are under 24 cP which is order of magnitude lower than that of conventional water lean amine solvent for CO_2 absorption process.

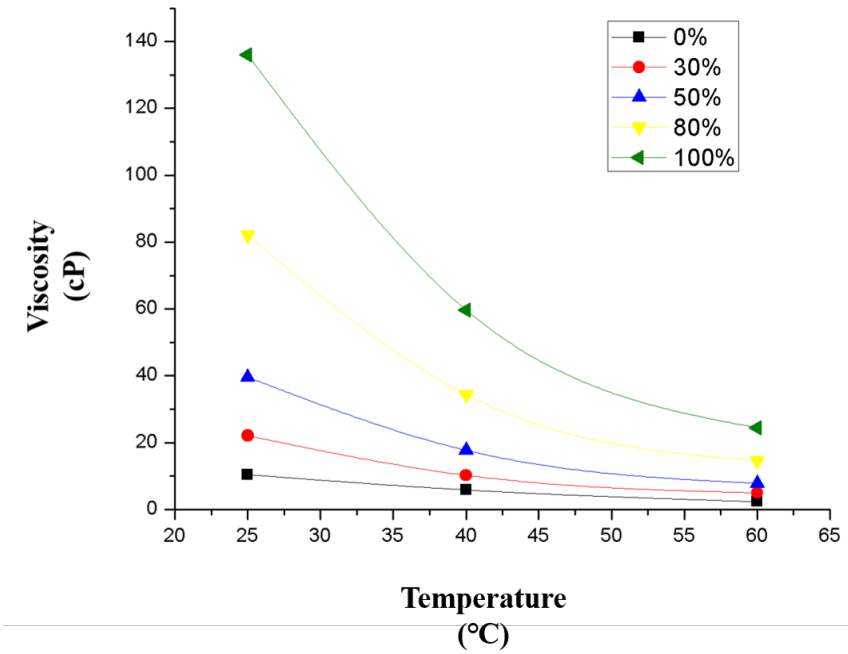

Figure 2.7: Viscosity of K_2Sol relative to absorbed CO_2 concentration and temperature

Degradation of the solvents is also an obstacle for practical application of amine-based solvents. For this reason, degradation experiments are conducted at 120 °C for 2, 7, and 14 days. Before the decomposition tests, 30 g of K_2Sol was fully saturated with CO_2 (124 g CO_2/kg K_2Sol) at room temperature. The CO_2-saturated K_2Sol solvent was divided into three portions, and each portion was charged into a specially designed tube reactor. The tube reactors were stored in an oven maintained at 120 °C for 2, 7, and 14 days, respectively. As shown in figure 2.8, NMR analysis of the CO_2-saturated K_2Sol samples after degradation shows that no noticeable decomposition occurred, clearly demonstrating that K_2Sol is thermally stable at 120 °C for at least 14 days. In contrast, degradation of MEA was evident from the 1H NMR spectra taken after 5, 7, and 14 days. Unknown peaks associated with the degradation of MEA were clearly observed in the range 3.0 – 3.2 ppm.

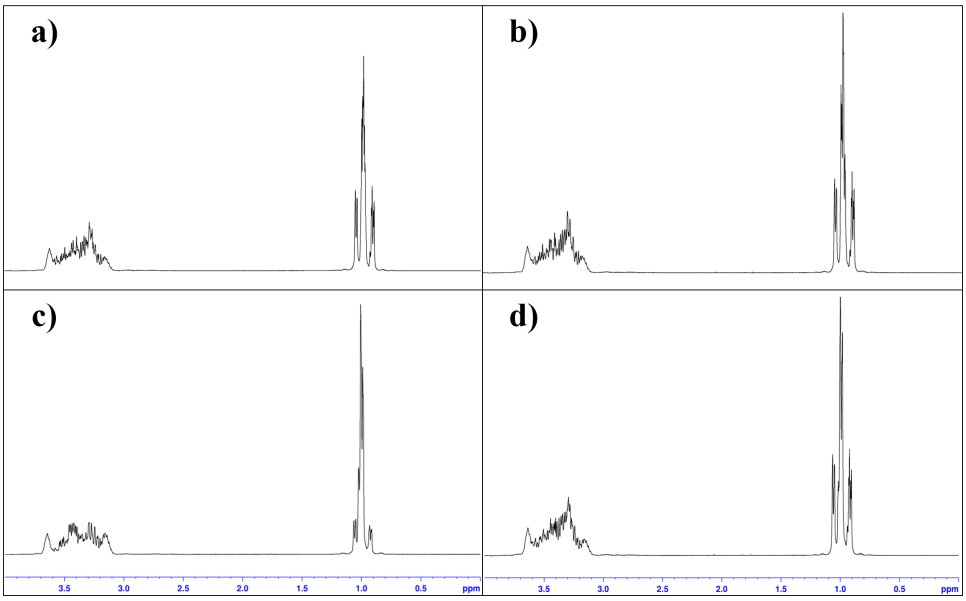

Figure 2.8: ^{1}HNMR spectra of CO_2-saturated K_2Sol before and after degradation experiment at 120 °C: (a) CO_2-saturated, (b) after 2 days at 120 °C, (c) after 7 days at 120 °C, (d) after 14 days at 120 °C.

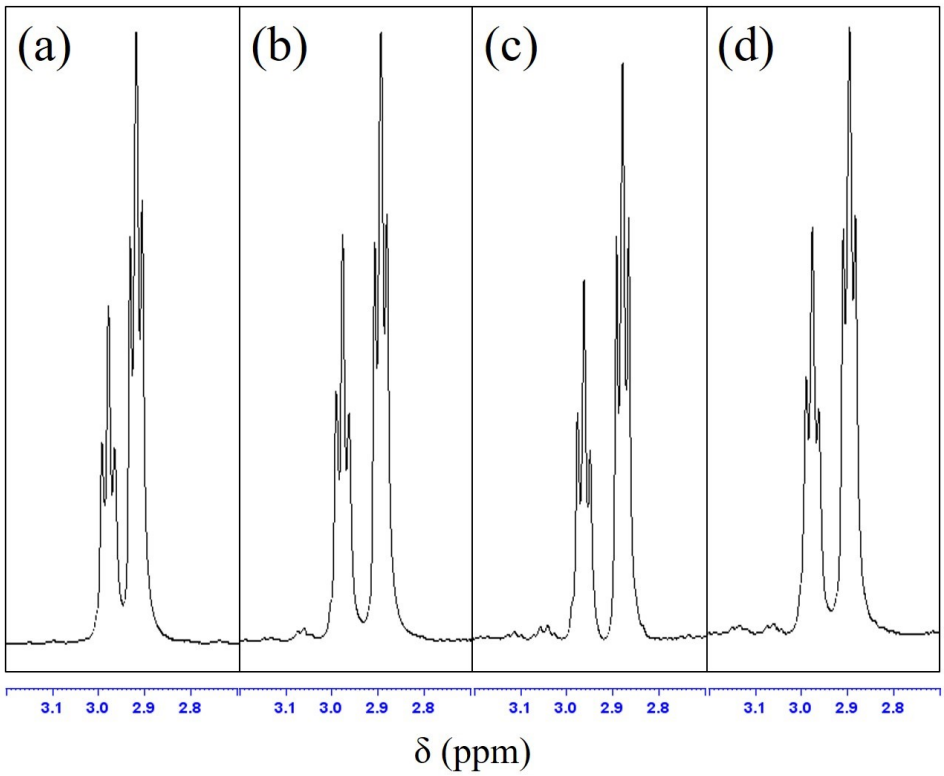

Figure 2.9: ^{1}HNMR spectra of CO_2-saturated MEA before and after degradation experiment at 120 °C: (a) CO_2-saturated 30wt% MEA, (b) after 5 days at 120 °C, (c) after 7 days at 120 °C, (d) after 14 days at 120 °C.

2.4 Conclusion

This chapter proposed the performance of a new water lean amine solvent, K_2Sol, through lab-scale experiments for the application of CO_2 capture process. The objective is to confirm the superiority compared with MEA, which is a traditional amine solvent for CO_2 separation. Rich amine loading, cyclic capacity and heat capacity were measured in order to predict that K_2Sol has lower regneration energy and operating cost, and the measurement of viscosity and degradation resistance is criteria for determine whether process operation has any problems when K_2Sol is applied to CO_2 capture process. High CO_2 loading and cyclic capacity indicate that an absorption rate of K_2Sol in CO_2 capture process is higher than one of MEA, and it is expected that low heat capacity contributes the reduction of sensible heat which accounts for large amounts in regeneration energy. In addition, the outstanding resistance to degradation and low viscosity at each loading indicated that K_2Sol has a competitive advantage in industrial application of CO_2 capture processes.

Chapter 3

Process Optimization of Pilot Scale Experiments for Post Combustion CO_2 Capture Process with A New Water Lean Amine Solvent

3.1 Introduction

Finding an optimal operating condition is very important to assess chemical process and lower its energy consumption and/or operating costs. In CO_2 capture process, many researchers founds an optimal operating conditions and process configuration of CO_2 capture process for lowering regneration energy. several researches find an optimal operating condition through a sensitivity analysis using pilot scale experiments. The sensitivity analysis shows effect of operating parameters on the process output even though the physical and chemical properties are not fully specified. As the related studies, H. P. Mangalapally et al. evaluated the four new solvents and compared to MEA in a pilot plant

[24]. They carried out experimental studies with varying the solvent and flue gas flow rate. The optimal solvent flow rate for each solvent was presented, and they proposed the most promising solvent. However, the number of experiments increases exponentially in addition of decision variables and the minimum point obtained from the sensitivity analysis does not guarantee the optimum solution.

The process optimization is an effective option for finding an optimal operating conditions. Compared to pilot scale experiments with sensitivity analysis, it has a great advantage that it can not only find the operating conditions but also evaluate the alternative process configurations at relatively low cost. Many studies carried on the optimization of CO_2 capture process with various solvents and configurations [18, 20, 21, 39, 23]. However, the process optimization can be applied only if data or parameters reflecting the physiochemical properties are obtained for the development of process model. If they are not enough to build process models, they causes numerous lab-scale experiments, so the development of process model can be more expensive than building pilot-scale test systems.

Gaussian process Bayesian optimization (GPBO) can solve black-box optimization problems by expensive objective function evaluation through a sequential decision theory [31, 40]. This method extracts information from given data and infers a posterior distribution to determine the search point for the next function evaluation or experiment. The criterion for finding the search point can be the greatest information generation or the optimal function value. In addition, GPBO can robustly optimize the black-box function considering the uncertainty, which usually exists in experiments and/or in functions. GPBO has been actively applied in areas such as drug design and robotics [31]. Because of these properties, model-free design of experiments for consistent solvent comparison with an actual CO_2 capture pilot plant within the minimum number of

experiments is possible.

In this chapter, bench-scale pilot experiments are conducted with both K_2Sol and 30 wt% MEA in water to quantitatively assess the new solvent. The optimal operating conditions for each solvent are found using GPBO. GPBO builds a probabilistic surrogate model and also optimizes it. The additional computational effort of optimization minimizes the number of experiments needed; thus, expensive surrogate model training can be avoided.

3.2 Pilot-Scale Experimental Setup

An experimental study is conducted to quantitatively compare the solvent regeneration energy of 30 wt% MEA and K_2Sol. A picture of the pilot plant is shown figure 3.1. figure 3.2 illustrates the experimental setup used in this study. The pilot plant consists mainly of an absorber (C02), stripper (C03) column, and amine heat exchanger (H01). The amine solvent comes into contact with the synthesized flue gas and selectively absorbs CO_2. The CO_2-lean gas is vented to the top of the absorber. The CO_2-rich solvent from the absorber is then sent to the stripper through the residual heat-recovering heat exchanger (HX01) and thermally regenerated in the stripper. The hot CO_2-lean solvent is cooled in HX1 and sent back to the absorber to complete the cycle. Sulzer structured packing (Sulzer BX) is deployed in both the absorber and the stripper to obtain a larger vapor/liquid contact area. Process equipment details are provided in table 3.1. Note that the temperature of the synthesized flue gas, lean amine solvent, and stripper top is adjusted in C01, CW01, and CW02, respectively, using circulators.

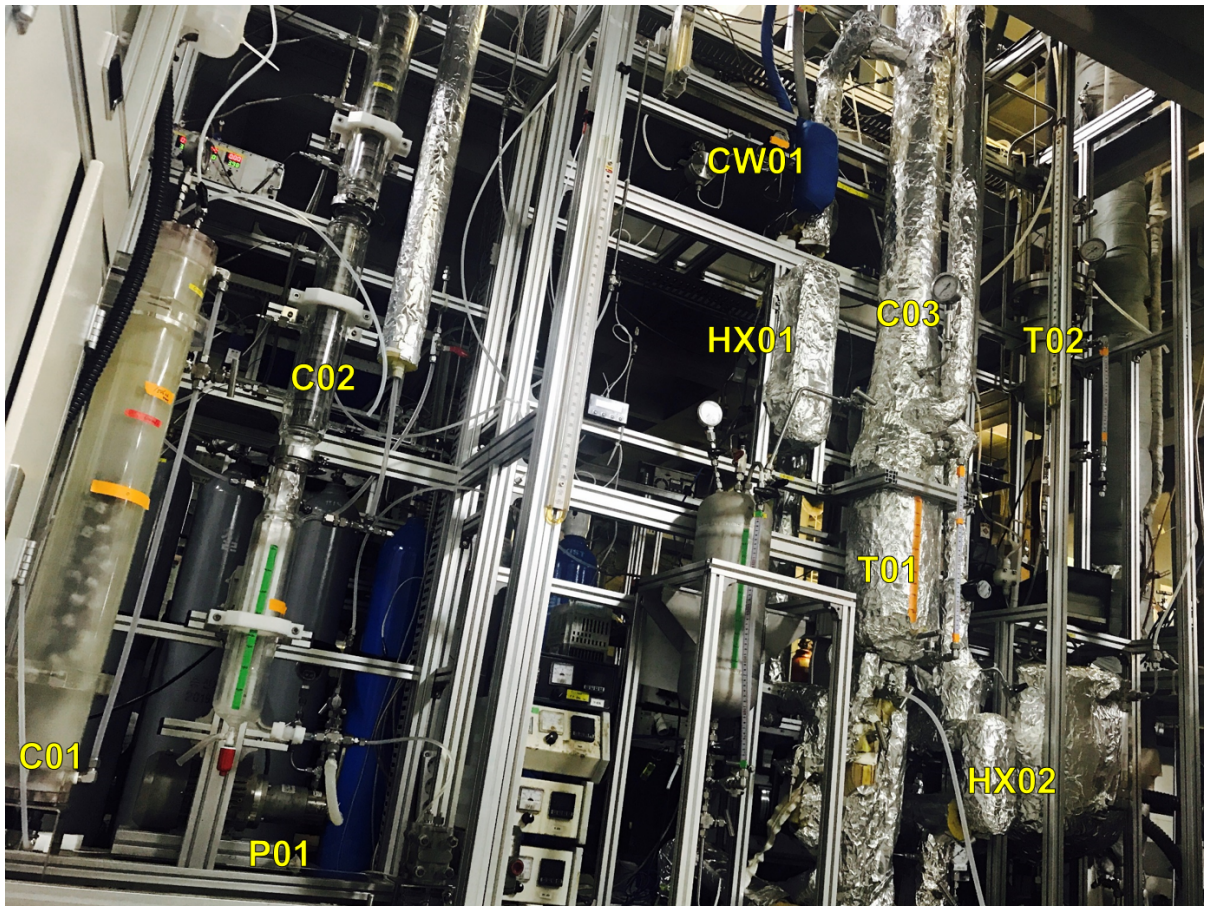

Figure 3.1: Bench-scale pilot plant for CO_2 capture.

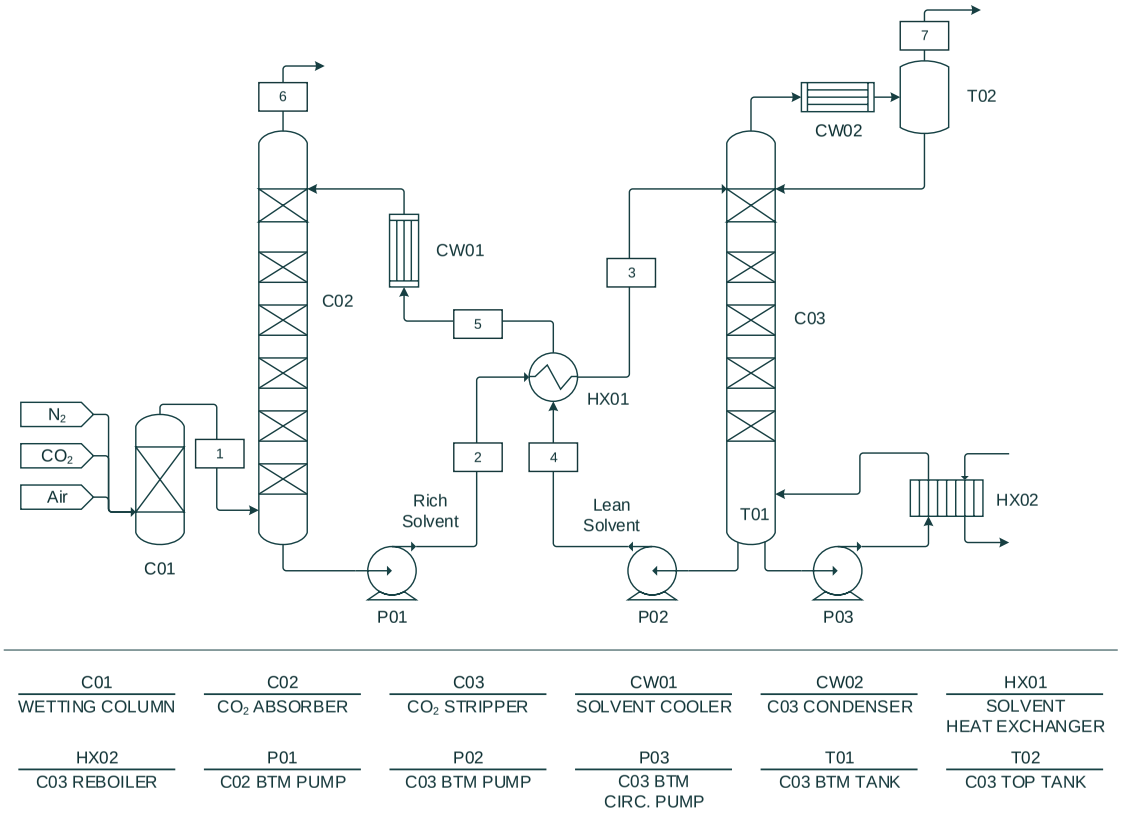

Figure 3.2: Process flow diagram of the bench-scale pilot plant for CO_2 capture.

Table 3.1: Detailed Process Equipment Specification

Equipment	Manufacturer	Specification	Note
Column			
Wetting column [C01]	-	3 in/4 in×890 mmH	
Metal pall ring random packing	-	400 mmH	
Absorber column [C02]	-	2 in×3,110 mmH	
BX gauze packing	Sulzer	2 in×5 mmH×43 ea	
Stripper column [C03]	-	2 in×1,585mmH	
BX gauze packing	Sulzer	2 in×5 mmH×20 ea	
Pump			
Absorber pump [P01]	Micropump Co.	13.9 L/min	Max. flow rate
Stripper pump [P02]	Speck Pumpen Co.	2800 /min	50Hz/Cycles
Reboiler pump [P03]	Micropump Co.	25 L/hr	Max. flow rate
Heat exchanger			
Lean and rich heat exchanger [HX01]	Alfa Laval	70 mmW×200 mmH×2 ea	AlfaNova14
Reboiler [HX02]	Alfa Laval.	70 mmW×200 mmH	AlfaNova14
Condenser			
Stripper condenser [CW01]	Alfa Laval.	70 mmW×200 mmH	AlfaNova14
Stripper to absorber condenser [CW02]	Alfa Laval.	70 mmW×200 mmH	AlfaNova14
Tank			
Stripper bottom tank [T01]	-	6 in× 400mmH	
Make-up tank [T02]	-	12 in× 200mmH	
Probe			
CO_2 gas probe	MRU Inst., INC.	Range : 0 − 40 vol%	Optima7
		Measured error : ±0.3 abs or 5%	For absorber
Wet gas meter	Sinagawa Co.	Range : 4 − 1200 L/hr	W-NK-2B
			For stripper
Temperature thermometer	ETI Ltd.	Range : -200 − 200 °C	Ref-Plus
Circulator			
CW01	Lab. Companion	Target temperature : 0 °C	RW-1040G
CW02	Lab. Companion	Target temperature : 40 °C	RW-1025G

The liquid-to-gas (L/G) ratio and stripper pressure are chosen as process variables for process optimization. The flue gas flow rate is fixed at 1.2 m^3/h; thus, the L/G ratio can be adjusted by changing the circulating amine flow rate. The liquid flow rate is controlled using a Siemens gear pump (P01). The stripper column pressure is adjusted using a back-pressure regulator (BPR). The temperature of the columns, vent gas CO_2 concentration, and gas volume flow rate of the absorber and stripper is measured. Thermocouples are located at 200 mm intervals starting at the top of the column to check the temperature profile of the absorber; seven are located in the stripper, and one of them measures the reboiler temperature. The vent gas concentration is measured using an Optima 7 CO_2 gas probe. The gas volume flow is measured using a Yokogawa wet gas meter. The amine concentration in the CO_2 absorbent is analyzed by gas chromatography (6890N, Agilent). The gas chromatograph is equipped with an RTX Amine capillary column (30 m, 0.25 mm, 1.0 mm, Restek) and a thermal conductivity detector with helium as the carrier gas. Quantitative analysis is performed using pyrazine as an internal standard, and the mass fraction is calibrated. The CO_2 loading was determined by a total organic carbon analyzer (TOC, Shimadzu) using an inorganic carbon detector. For confirmation, the ^1H and ^{13}C NMR (Brucker) chemical shift difference was calibrated and used. To ensure steady-state operation, the amine solvent is completely circulated at least five times, and the change in the temperature profile and CO_2 concentration of the absorber and stripper is checked. Once the system reached the steady state, the lean and rich amine solvents are sampled and analyzed for the measurement of their concentration and CO_2 loading. Note that the MEA and K_2Sol operations ran for 130 and 180 h, respectively.

Table 3.2: Operating conditions of the bench-scale pilot plant for CO_2 capture.

Parameter	Data
Feed gas flow rate [Nm^3/h]	1.2
Feed gas composition [mol%]	
CO_2	15
N_2	65
Air	20
L/G ratio [L/Nm^3]	2.5–7
Stripper pressure [bar]	1–3

3.3 Optimization Methodology

Optimization of the water-lean solvent process is a complicated task, not only because the system is highly nonlinear and nonconvex, but also because the parameters required for building the first-principle model are missing. Here, Bayesian optimization is used to optimize the expensive black-box function "pilot plant experiment." Because our surrogate model should be in continuous spaces, Gaussian processes are used to model the unknown function. Bayesian optimization also builds surrogate models using input and output data, and the additional computation for constructing the surrogate models minimizes the number of evaluations needed to find the optimal solution.

Optimization of the water-lean solvent CO_2 capture process can be formulated as a nonlinear programming problem, $minf(x)$, where x is a vector consisting of two continuous variables (i.e., the gas-to-liquid ratio and stripper pressure). For the function $f(x)$ representing the CO_2 capture process on a domain χ, the goal is to find the minimizer of $f(x)$:

$$x^* = \underset{x \in \chi \subset \mathbb{R}^2}{argmin}\, f\,(x) \tag{3.1}$$

where the assumption is that the experimental system is a black-box model that can provide as an output the solvent regeneration energy. Thus, the optimizer of the problem can be obtained sequentially as experiments are performed by using information from the previous data. In this study, the Thompson sampling efficient multiobjective optimization (TSEMO) algorithm proposed by Bradford et al. is modified for the CO_2 capture experiment [41]. The methodology and validation are described in detail in sections 3.1 and 3.2.

3.3.1 Gaussian process Bayesian optimization

The surrogate model describing the CO_2 capture process is built using a Gaussian process model. The Gaussian process model can provide the distribution of unknown points using a mean function and a covariance function. The regeneration energy of the CO_2 capture system, y, is then described by Eq. (3.2).

$$y \sim GP(m(x), k(x, x')) \tag{3.2}$$

The mean function of Eq. (3.2) is set to zero to simplify the calculation. The prior is then specified by a positive semidefinite kernel function, $k(x, x')$. Here, the stationary Matérn 3 kernel is used at this study,

$$k_{v=3}(x, x') = \sigma_f^2(1 + \sqrt{3}r)\exp(-\sqrt{3}r) + \sigma_n^2\delta(x, x') \tag{3.3}$$

where σ_f and σ_n represent the variance of the output and the noise of the observation, respectively. The Euclidean distance, r, can be calculated using Eq. (3.4).

$$r = \sqrt{(x - x')\lambda(x - x')^T} \tag{3.4}$$

$$w = [\sigma_f, \sigma_n, \lambda],\ w_i \sim \mathcal{N}(\mu_i,\, \sigma_i^2). \tag{3.5}$$

Note that a scaling variable λ for the input length scale is introduced; thus, the covariance function is calculated on the anisotropic length scale [41]. Eq. (3.2) can be fully specified once the parameters σ_f, σ_n, and λ are determined. It is assumed that these parameters have independent Gaussian distributions.

The prior distribution expressed by Eq. (3.2) describes the properties of the underlying function (i.e., the CO_2 capture process), but it does not reflect observations from the CO_2 capture experiment. The inference of the prior on the posterior distribution over parameter w can be calculated using Bayes rule.

$$p(w \mid data) \ \propto\ p(data \mid w) \times p(w) \tag{3.6}$$

The appropriate value of w is estimated using the MAP estimate. By taking the log of the right-hand side of Eq. (3.6), the optimization problem for finding the parameters can be formulated as follows.

$$w_{MAP} = \underset{w}{argmin} \log MAP(w) \tag{3.7}$$

The optimization problem of Eq. (3.7) is solved using the DIviding hyper-RECTangles (DIRECT) algorithm [42]. 100 evaluations is used as the DIRECT algorithm termination criterion. More detailed explanations of the derivation of the MAP estimate and equations are available in Bradford et al. [41]. The predictive output distribution of the CO_2 capture process is given from a training data set of n points $X = \{x_1, \cdots, x_n\}$ and the corresponding observation set $Y = \{y_1, \cdots, y_n\}$

$$f(x) \sim GP(m(x), k(x, x') \mid X, Y) \tag{3.8}$$

with

$$m(x) \mid X, Y = \sum(x, X) \sum{}^{-1} y \tag{3.9}$$

$$k(x, x') \mid X, Y = k(x, x') - \sum(x, X) \sum{}^{-1} \sum(x, X)^T \tag{3.10}$$

where $\sum = [k(x_i, x_j)]_{n \times n}$, and $\sum(x, X) = [k(x, x_1), \cdots, k(x, x_n)]$.

The goal of this study is to find an optimal operating condition of the CO_2 capture process x^* with a posterior distribution of $p(x^* \mid X, Y)$. The conditional distribution of the optimal operating condition is approximated using Thompson sampling [43].

$$p(x^* \mid X, Y) = p(f(x^*) = \underset{x \in \chi}{min} f(x) \mid X, Y) \tag{3.11}$$

The distribution of the optimizer can be approximated using the spectral sampling method proposed by Bradford et al. [41]. In their formulation, the covariance function $k(x, x')$ can be approximated by the following inner product:

$$k(x, x') \approx \xi(x)^T \xi(x) \tag{3.12}$$

where $\xi(x) = \sqrt{2\alpha/M}cos(Wx + b)$. M represents the number of Monte Carlo samples, and W is sampled from $p(w)$, which is proportional to the Fourier dual of the stationary Kernel function, Eq. (3.3). Similarly, b is also sampled from $\mathcal{U}(0, 2\pi)$. 2000 Monte Carlo sampling is conducted for probability matching. The approximated kernel function, Eq. (3.12), allows us to express the Gaussian process prior using a linear model, where θ is also a Gaussian distribution.

$$f(x) = \xi(x)^T\theta \tag{3.13}$$

Eq. (3.13) then approximates the Gaussian posterior distribution with the following mean function, m, and covariance function, V [44].

$$\begin{aligned} m &= (Z^TZ + \sigma_n^2 I)^{-1}Z^T y \\ V &= (Z^TZ + \sigma_n^2 I)^{-1}\sigma_n^2 \end{aligned} \tag{3.14}$$

where $[Z]_i = \xi(x_i)$ is made up of stacked random vectors of ξ evaluated at the inputs of the data. Therefore, the approximated posterior $f(x)$ in Eq. (3.11) in the ith experiment is given by $f_i(x) = \xi_i(x)^T\theta_i$, where $\theta_i \sim \mathcal{N}(m_i, V_i)$. The constructed acquisition function is optimized using a genetic algorithm [45]. The solver options of a genetic algorithm includes a maximum of 100 generations and a maximum population size of 150. The optimization terminates at either a function tolerance of 10^{-6} or 10 consecutive stall generations.

3.3.2 Performance test of optimization method

Although GPBO has been applied to many science and engineering problems, it has rarely been used in chemical process optimization. To validate the performance of the algorithm, a process model is optimized by GPBO and a genetic algorithm. The performance of the algorithm is evaluated in terms of model evaluation and the objective function value. Aspen Plus V10 is used to

build a rate-based aqueous MEA CO_2 capture process model based on experimental data. The rigorous rate-based reactive distillation model can precisely describe the mass transfer and reactions within the absorber and stripper. The phase equilibrium is calculated using the electrolyte nonrandom two-liquid (e-NRTL); thus, a rigorous flash calculation is performed for each unit operation.

The objective function of the process model optimization can be written as

$$\begin{aligned} &\text{minimize } g(P, \dot{f}_{sol}) + \gamma a(P, \dot{f}_{sol})^2 \\ &1 < P < 3 \\ &2 < \dot{f}_{sol} < 6 \end{aligned} \tag{3.15}$$

where $g(\cdot)$ represents the regeneration energy of the solvent, P is the operation pressure of the stripper, and $\dot{f}_{sol}$ is the absorber bottom pump flow rate of the solvent. γ and $a(P, \dot{f}_{sol})$ are penalty parameter (10^7) and penalty function which checks the convergence of simulation. Depending on whether the process simulation converges without error, objective function assigns zero or a large positive value as $a(P, \dot{f}_{sol})$. Because P and $\dot{f}_{sol}$ are independent, and $g(\cdot)$ is a nonlinear function calculated by the process simulator model, the problem is an unconstrained, bounded, and nonlinear optimization problem. Note that Eq. (3.15) has tighter bounds than that of the experiment because the optimum operating condition for MEA is well identified in many literatures. The genetic algorithm and GPBO are performed 5 times each, and the minimum of the results is determined as the optimization results.

Table 3.3 shows that the genetic algorithm and GPBO have similar objective function values. In fact, the same L/G ratio is obtained from both optimizations, where the optimal pressure differs by 4%. Note that the objective function value from GPBO is even lower than that from the genetic algorithm. The function evaluation of the proposed algorithm is less than 2% of that of

the genetic algorithm. The acquisition function constructed using Eq. (3.14) reflects the underlying CO_2 capture process well around the optimizer; thus, expensive function evaluation can be minimized. Further, the genetic algorithm randomly evaluates a large number of populations to select promising offspring. The solutions of both optimizations do not guarantee the global optima. However, the results in Table 3.3 indicate that the proposed algorithm can obtain a near-optimal solution with a relatively small amount of evaluation, thus possibly reducing the number of experiments when it is applied to find the optimal operating conditions for the real process.

Table 3.3: Optimization result of Aspen Plus MEA CO_2 capture model using a genetic algorithm and GPBO proposed in this study.

	Genetic algorithm	This study
L/G [L/Nm^3]	4.3	4.3
Pressure [bar]	1.31	1.26
Regen. energy [GJ/t CO_2]	3.96	3.92
# function evaluation	1500	20

3.4 Result and Discussion

Figure 3.3 shows the convergence results of optimization during experiments. For both MEA and K_2Sol, the optimal conditions were found with relatively few pilot plant evaluations. The K_2Sol experiment is terminated at the end of the 28th experiment, and the MEA experiment is ended after 21 tests. Note that GPBO is terminated when the same points are consecutively recommended three time by the algorithm. In the case of MEA, the regeneration energy of optimization result is relatively higher than that reported in other literature. Because of the relatively small size of the pilot plant, the regeneration energy is more sensitive to the heat loss of the entire equipment than other studies. This effect caused relatively high regeneration energy, but it is decided that the results were close to the near optima in the light of several research case and operational experience.

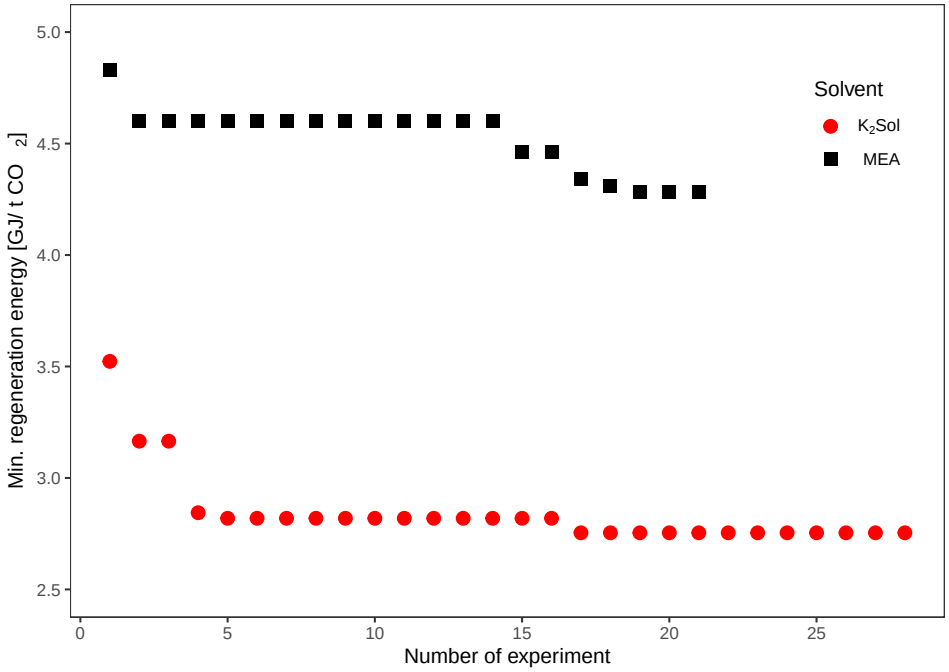

Figure 3.3: Convergence results of experiments with MEA and K_2Sol.

The mass balance of the pilot plant is analyzed from two different criteria to verify that operation reached the steady state. Once the temperature profile of the pilot plant reached a steady value, first, the CO_2 concentration at the absorber gas outlet is measured, and the CO_2 capture rate is calculated. Then, the CO_2 flow rate from the stripper is also measured and balanced with the gas flow rate from the absorber. Figure 3.4 describes the deviation of the regenerated CO_2 flow rate measured by these two methods. As indicated in the figure, most of the deviation between the two measurements lies within $\pm 5\%$. The initial four tests differed by more than -5%. However, GPBO can still find the optimal operation conditions for K_2Sol operation because it accounts for the noise of the observations, which is minimized as the number of experiments increases.

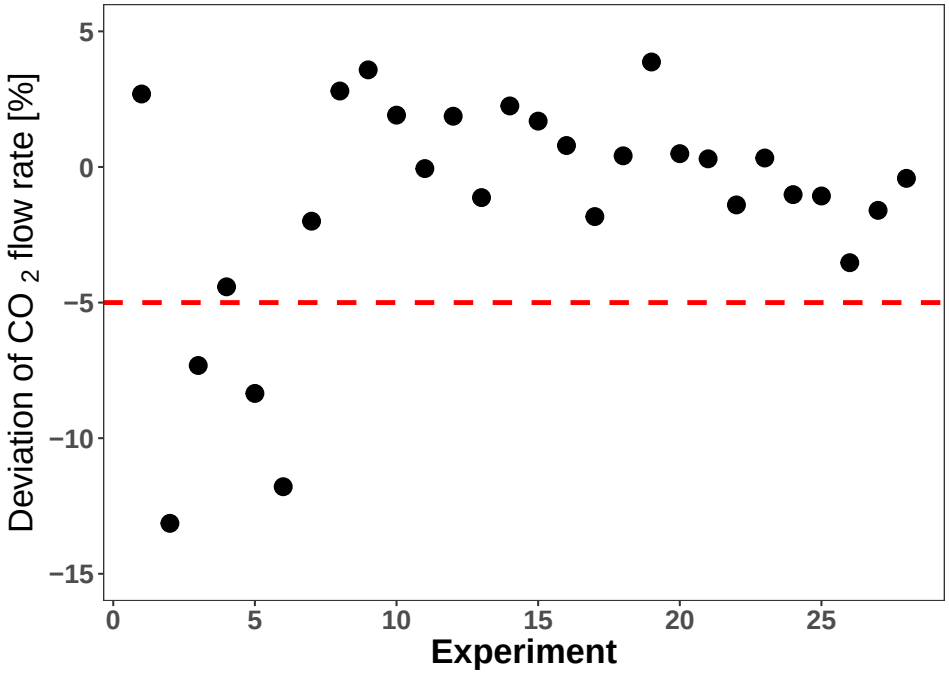

Figure 3.4: Difference between CO_2 flow rate calculated using the concentration of the treated gas and the approximate value measured at the stripper.

Table 3.4 compares the regeneration energies of 30 wt% MEA and K_2Sol under the optimal operating conditions. The heat and material balance are presented in table 3.5 The minimum regeneration energy of K_2Sol is 2.8 GJ/t CO_2, which is 65% of that of MEA. The optimal operating condition appears at atmospheric pressure and an L/G ratio of 5.67 L/Nm^3. The measured rich and lean loadings of K_2Sol are 124.69 and 77.64 g CO_2/kg K_2Sol under the optimal operating condition. The higher working capacity of K_2Sol can be ascribed largely to the unique property of the DA contained in the solvent. As stated above, DA, the major component of K_2Sol, is a diamine with two primary amino groups per molecule. For this reason, DA can interact with CO_2 relatively quickly, forming a 1:1 CO_2 adduct, the zwitterionic carbamate species, as shown in figure 2.1. Moreover, the amino groups of DA are moderately hindered; thus, the stability of the resulting CO_2 adduct of DA is slightly lowered, facilitating regeneration of DA from its CO_2 adduct. The heat of CO_2 absorption in an amine-based solvent generally decreases with increasing CO_2 loading in the solvent. Therefore, it is desirable to use a solvent with higher CO_2 absorption capacity. In this context, K_2Sol can be considered a promising alternative to conventional alkanolamine-based solvents because it is prepared using a moderately hindered primary diamine with a high absorption rate and capacity as well as easy regenerability

Table 3.4: Comparison of optimal results for 30 wt% MEA and K_2Sol.

	30 wt% MEA	K_2Sol
Regeneration energy	4.3	2.8
(GJ/t CO_2, $g(P, \dot{f}_{sol})$)		
Pressure	1.29	1
(bar , P)		
L/G ratio	4.52	5.67
(L/Nm^3, –)		
Solvent flow rate	5.42	6.80
(L/h, $\dot{f}_{sol}$)		
CO_2 regeneration rate	80	80
(%, –)		

Table 3.5: Heat and Material Balance for the optimum operating condition

Stream Name		1	2	3	4	5	6	7
Temperature	°C	34.05	37.13	79.83	87.10	37.21	21.35	21.35
Pressure	Bar	1	1	1	1	1	1	1
Flow rate	l/min	21.24	0.1204	0.1204	0.1204	0.1204	17.36	2.56
Loading	g_{CO_2}/kg_{K_2SOL}		124.69	124.69	77.64	77.64		
CO2 Conc.	mol%	14.9					2.95	
DA fraction	wt%		60.38	60.38	61.06	61.06		

Figure 3.5 compares the temperature profiles in the 30 wt% MEA and K_2Sol experiments. The absorber temperature profile in figure 3.5a shows that the CO_2 absorption is not maximized for K_2Sol within the column, although K_2Sol has quite a low regeneration energy, whereas 30 wt% MEA exhibits a typical absorption temperature profile. The location of the bulge indicates the column availability for solvent absorption of CO_2 [46]. The temperature at the bottom of the column should be similar to the gas inlet temperature when the column height is sufficient. The column bottom temperature for 30 wt% MEA operation is close to the gas inlet temperature, indicating an adequate absorber size. However, the bottom temperature for K_2Sol operation is 10 °C higher than that of 30 wt% MEA. In addition, the uniform temperature for each column height shows that K_2Sol uptakes CO_2 uniformly along most of the packing height. The result suggests slower CO_2 mass transfer in K_2Sol, thus more CO_2 can be absorbed when a sufficiently large absorber was used in these experiments. If the absorber tower is optimally designed for K_2Sol, the optimum regeneration energy can become lower than our result because the absorption capacity is maximized.

Figure 3.5b shows the temperature profile for 30 wt% MEA and K_2Sol in the stripper. The reboiler temperature of K_2Sol is 93 °C, which is 20 °C lower than that of 30 wt% MEA. The lower reboiler temperature means that the partial pressure of water in the stripper is lower than that in 30 wt% MEA operation. The regeneration energy is the sum of the heat of desorption, sensible heat, and heat of vaporization. The heat of vaporization is expressed as [35, 36]

$$q_v = \Delta H_{v,\mathrm{H_2O}} \cdot \frac{p_{\mathrm{H_2O}}}{p_{\mathrm{CO_2}}} \tag{3.16}$$

where $\Delta H_{v,\mathrm{H_2O}}$ is the enthalpy of H_2O vaporization, and $p_{\mathrm{H_2O}}$ and $p_{\mathrm{CO_2}}$ are the partial vapor pressures of H_2O and CO_2, respectively. The low water par-

tial pressure indicates a lower heat of evaporation and eventually leads to a reduction in the regeneration energy. In addition, a low-grade heat source can be used for solvent regeneration, making the K_2Sol process more economical than that of 30 wt% MEA.

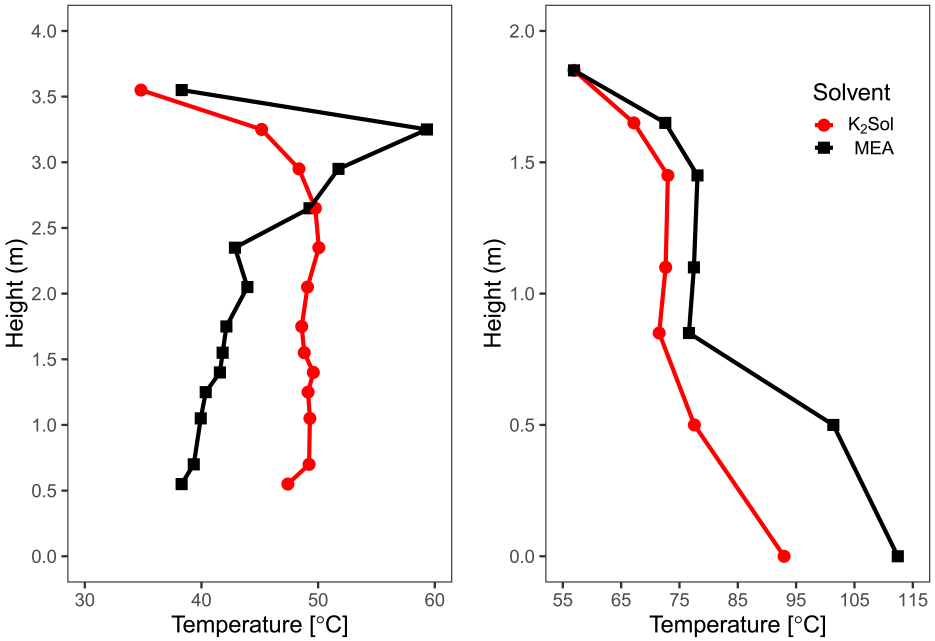

(a) Absorber temperature profile

(b) Stripper temperature profile

Figure 3.5: Comparison of temperature profiles of MEA (a) and K_2Sol (b).

Table 3.6 compares the regeneration energy obtained in this study with those in previous studies. Recall, however, that direct comparison is somewhat difficult because the regeneration energy is known to depend strongly on the plant design. For this reason, the regeneration energy of K_2Sol was compared directly with that of 30 wt% MEA measured in the same test unit. The relative regeneration energy of K_2Sol with respect to that of MEA is the lowest among the reported values except for that of NASs by Lail et al. [17], which is 53% of that of MEA. Although this value is lower than that of our study, their pilot plant had alternative process configurations, including absorber intercooling and stripper interheating. These process improvements greatly reduced the regeneration energy [47, 48]. The pilot plant used in our study has no advanced configurations. Applying advanced process configurations such as stripper interheating can enhance the performance of K_2Sol. Consequently, K_2Sol is expected to be highly competitive commercially for post-combustion CO_2 capture.

Table 3.6: Comparison of regeneration energy from different studies.

Source	Amine	GJ/t CO_2	As compared with MEA	Remark
Mimura et al. (1997) [49]	MEA 30%	3.8		
	KS-1, KS-2	3.0	79%	Hinderd amine
Knudsen et al.(2009) [50]	MEA 30%	3.6		
	Castor 1	3.8	106%	
	Castor 2	3.5	97%	
Ogawa et al. (2009) [51]	MEA 30% (sim.)	4.4		
	AMP (sim.)	3.7	86%	
	TS-1	2.9	66%	
Schneider and Schramm (2011) [52]	Siemens AAS	2.7		Amino acid salt
Managalapally and Hasse (2011) [53]	MEA 30%	3.8		
	AMP 28%, PZ 17%	3.0	79%	
	EDA 32%	3.5	92%	
Brúder et al. (2012) [54]	DMMEA/MAPA 3M/2M	3.8		
Esmaeili and Roozbehani (2014) [55]	MEA 30%	3.6		Hindered amine
	ACOR100	2.7	75%	
Lail et al. (2014) [17]	MEA 30%	4.0		Alternative configuration
	NASs	2.1	53%	(Interheating with absorber intercooling)
This study	MEA 30%	4.3		
	K_2Sol	2.8	65%	**Hindered amine**

3.5 Conclusion

This chapter highlighted the evaluation of the new solvent K_2Sol for post-combustion CO_2 capture processes. A bench-scale pilot experiment was conducted to find the optimal operating conditions with the minimum regeneration energy. GPBO is employed to avoid the need for expensive experiments.

The superior performance of K_2Sol was analyzed in terms of the differences in rich amine loading, cyclic capacity, column temperature profile, and degradation. The results indicate that K_2Sol is economical more favorable for industrial application. The low regeneration energy, amine vapor pressure, and reboiler temperature can make the K_2Sol process less costly. In addition, the outstanding resistance to degradation and low viscosity at each loading indicated that K_2Sol has a competitive advantage in industrial application of CO_2 capture processes. The optimal regeneration energy of K_2Sol was found to be 2.8 GJ/t CO_2 at L/G = 5.67 L/Nm^3 and operation at atmospheric pressure.

Because the column design and process configuration are not optimized for K_2Sol, further efforts are needed to evaluate K_2Sol completely. To design the optimal CO_2 capture process for K_2Sol, the model development of the solvent properties is essential. Stochastic techniques using data from this study or parameter estimations from additional laboratory-scale experiments will make this possible. An advanced process design based on a model of the solvent properties will maximize the performance of K_2Sol and further reduce the regeneration energy.

Chapter 4

Bayesian Parameter Estimation for the CO_2 Capture Process with A New Water Lean Amine Solvent

4.1 Introduction

Chemical process simulation is a very attractive tool because it facilitates the designs of chemical processes, the process optimization, and analysis of process dynamic characteristics. Regardless of whether a commercial process simulator is used or not, the process model must be developed, and it requires data and/or parameters to represent various chemicals and physical chemistry phenomena as a necessity. For example, in the carbon dioxide capture process, the process model requires data and parameters for amine solvents which include not only pure component parameters and phase equilibrium parameters but also those of reaction kinetics and aqueous species. When designing the CO_2 capture process with a newly developed solvent, numbers of lab-scale experiments should be planned to estimate the parameters, resulting in expensive

costs and unpredictable time-consuming.

If any conditions causes in that experiments cannot be determined and data on physicochemical property is required, many researchers employed some non-experimental estimation approaches [56]. To overcome the lack of experimental data, many researches developed various estimation methods to provide missing data. Non-experimental methods is classified into several groups; those based on theoretical, semi-theoretical (e.g. statical thermodynamics and quantum mechanics), and empirical relationship (e.g. group contribution methods). They can be estimated various physicohemical properties of chemicals (e.g. enthalpy and entropy of vaporization, liquid heat capacity and flash temperature) without additional experiments. The parameter estimation using only chemical structures without any other input data is a powerful and economical option compared with the accomplishments of all experiments required. However, the types of physicochemical properties that can be estimated are limited, and the relatively low estimation accuracy often do not reflect actual phenomena except for some organic compounds.

This chapter introduces a method to estimate physicochemical parameters using non-experimental methods from only pilot-scale experiments data. Figure 4.1 shows the procedure of parameter estimation. First, the CO_2 capture process model is developed using ASPEN Plus, which is a commercial process simulator. The parameters that can be estimated by molecular structure are calculated by group contribution methods, and non-estimated parameters serve as input variables of the process model. Global sensitivity analysis(GSA) is employed to confirm how each parameter has an identifiable influence on the output response of full model. Subset selection is conducted to determine the value of parameters which have less influential than others from GSA results. Using rigorous model in parameter estimation causes the computation

load and convergence problems, so surrogate modeling is carried on through sampling with latin hypercube methods, and deep neural network technique. Bayesian parameter estimation based on a Markov chain Monte Carlo method is conducted to analyze the posterior inference of each parameters. Applying the estimated parameters to the ASPEN plus model, the CO_2 capture process model using K_2Sol as a solvent is simulated and compared with pilot scale experiments data.

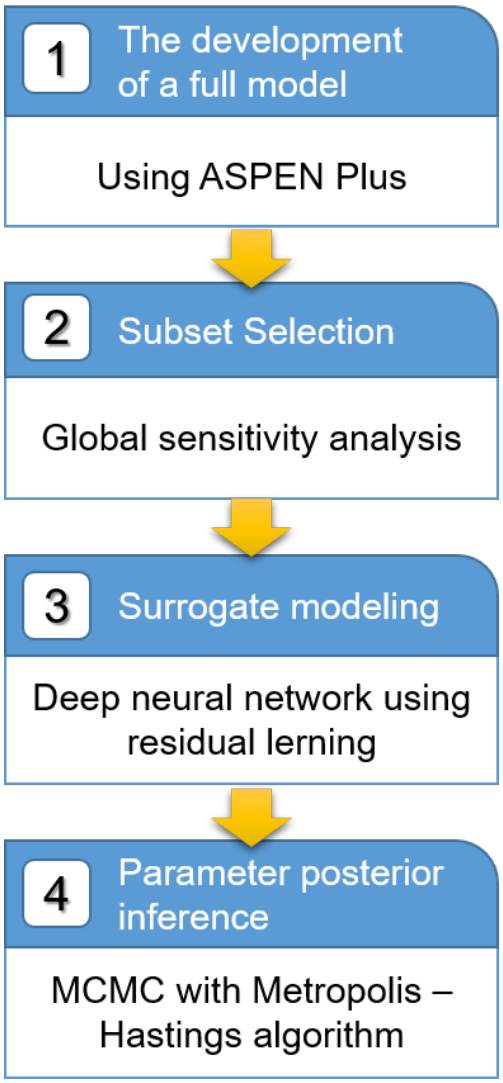

Figure 4.1: Procedure of parameter estimation

4.2 Model Description

The amine based CO_2 capture process model requires various physicochemical properties of amine solvent. Process model with hypothetic compounds should generally include its pure component parameter and binary parameters with other chemicals. Furthermore, process model in chemical reaction, like CO_2 capture process, also requires parameters of reaction kinetic and data about intermediate products. Finding the suitable value of parameters to validate the entire process output is very difficult. In this chapter, the target of modeling is limited to the absorber in CO_2 capture pilot plant for this reason.

In chapter 3, the pilot-scale experiment of CO_2 capture process with K_2Sol is conducted. The measurement of vent gas CO_2 concentration and gas volume flow rate from the absorber is performed in stream 6 of figure 3.2. The concentration and CO_2 loading of lean and rich amine were measured at stream 2 and 5. After the calculation of CO_2 mass balance in an absorber, eight experiment data with a difference between the CO_2 amount removed from flue gas and one absorbed by rich amine solvent as less than $\pm 10\%$ are selected.

It is assumed that the compositions of flue gas is constant. The absorber model has three input variables; mass flow rate determined L/G ratio, amine weight fraction and CO_2 loading of lean amine in stream 5. Output responses include absorber temperature profiles, treated gas volume flow rate and CO_2 mole fraction of stream 5. Thermocouples of an absorber were unevenly located at 15 to 25cm intervals. The values of temperature profiles are recalculated by linear interpolation so that the output response were equally spaced by 30 cm. Table 4.1 and 4.2 show specific information of selected experiments data.

Table 4.1: Experiments data for Bayesian parameter estimation

Name	Unit					
No.			1	4	15	17
Pressure	bar		2.3	1.27	1	1
L/G ratio	L/Nm^3		5.37	3	2.62	5.67
Lean flow	g/min		104.3	61.06	50.60	110.8
Lean Conc.	wt%		58.41	55.37	58.31	61.06
Lean loading	g/kg		85.84	62.15	62.15	77.64
Lean (Amine)	mol %		10.92	10.00	11.10	12.07
Lean (water)	mol %		82.13	85.14	83.79	81.29
Lean (CO_2)	mol %		6.943	4.856	5.115	6.638
Absorber T	°C	1	37.61	41.60	44.59	34.82
		2	46.16	54.64	53.84	45.16
		3	45.17	49.65	47.96	48.36
		4	46.86	48.56	43.87	49.76
		5	47.96	46.56	39.37	50.06
		6	46.81	45.82	38.09	49.09
		7	47.00	46.01	37.47	48.59
		8	47.26	46.56	38.73	49.33
		9	46.68	44.93	37.86	49.22
		10	46.52	43.89	36.81	49.25
Vent gas flow	L/min		18.67	18.28	16.04	17.39
Vent gas CO_2	mol %		6.550	4.640	5.510	2.950
Vent gas T	°C		27.41	24.07	19.85	21.35

Table 4.2: Experiments data for Bayesian parameter estimation (Cont.)

Name	Unit					
No.			26	31	33	38
Pressure	bar		2.78	1	1	1
L/G ratio	L/Nm^3		4.96	6.14	4.73	3.35
Lean flow	g/min		96.89	119.97	92.33	64.57
Lean Conc.	wt%		66.16	64.25	67.23	67.96
Lean loading	g/kg		112.3	80.26	81.04	75.11
Lean (Amine)	mol %		14.01	13.48	15.00	15.49
Lean (water)	mol %		75.70	79.23	77.19	77.11
Lean (CO_2)	mol %		10.29	7.285	7.817	7.403
Absorber T	°C	1	35.71	35.51	35.61	40.60
		2	44.76	44.46	52.24	57.13
		3	44.78	48.66	51.55	52.64
		4	45.27	52.16	53.26	52.46
		5	45.46	52.96	53.25	50.76
		6	44.43	52.06	52.36	49.58
		7	44.12	52.07	52.17	49.59
		8	44.29	52.65	52.98	49.92
		9	44.44	52.75	53.15	48.82
		10	44.55	52.88	52.78	47.63
Vent gas flow	L/min		19.03	17.61	17.94	18.18
Vent gas CO_2	mol %		7.180	2.300	2.980	3.930
Vent gas T	°C		26.98	26.62	27.75	26.75

ASPEN Plus V10.0 was used for the absorber modeling of CO_2 capture process. Group contribution methods is used to estimate pure component parameters of K_2Sol (e.g. critical temperature and pressure, saturated vapor pressure, Gibbs free energy and heat of formation). In chapter 2, heat capacity of liquid state K_2Sol is estimated, however this values can not be employed in ASPEN Plus because applying experiment results causes error with parameters estimated by group contribution methods. Electrolyte non-random two-liquid model (e-NRTL) was employed to predict thermodynamic mixtures properties between K_2Sol and other components. It is assumed that only the first term and second terms of water-K_2Sol binary parameters are meaningful. Electrolyte-molecule or electrolyte pair parameters and the temperature dependency of the dielectric constant is set the default values recommended by ASPEN Plus.

The reaction of CO_2 with various amines is generally described by the zwitterion mechanism, proposed by Caplow [57] and reintroduced by Dankwerts [58]. This sugeests two-step mechanism of the reaction between CO_2 and an amine; the formation of a zwitterion as an intermediate and carbamate formation caused by the deprotonation zwiterrion by a base. Although the zwitterion mechanism can well explain CO_2-an amine reaction kinetics, this has some uncertainty, that the exact form of the zwiterrion is not entirely known [59]. Furthermore, several studies reports that the zwiterrion mechanism can not predict kinetic rate constants of aqueous amine mixtures. ASPEN Plus also supports reactions with zwitterion only in equilibrium reactions.

The termolecular mechanism is considerable candidate mechanism which can be applied to the reaction of CO_2 and various amines. The termolecular mechanism, proposed by Crooks and Donellan, suggests that an amine reacts simultaneously with one molecule of CO_2 and a base [60]. The single step reaction

proceeds, it can be shown as follows

$$CO_2 + AmH\cdots B \rightleftharpoons AmCOO^{-}\cdots BH^{+} \tag{4.1}$$

If H_2O, OH^{-}, AmH are the dominating bases, the forward reaction rate for the termolecular mechanism is given by

$$r = [k_{H2O}(H_2O) + k_{OH-}(OH^{-}) + k_{AmH}(AmH)](AmH)(CO_2) \tag{4.2}$$

In aqueous solution, if the water is the dominant base, Eq. 4.2 can be rewritten by

$$r = k_{H2O}(H_2O)(AmH)(CO_2)=\hat{k}(AmH)(CO_2) \tag{4.3}$$

where $\hat{k}=k_{H2O}(H_2O)$. When the most dominant base is an amine, the reaction rate represent to an equation for second order of amine concentration

$$r = k_{AmH}(CO_2)(AmH)^2 \tag{4.4}$$

when the contribution of water for reaction is competitive with that of an amine, Eq. 4.2 is changed by

$$r = [k_{H2O}(H_2O) + k_{AmH}(AmH)](AmH)(CO_2) \tag{4.5}$$

Whether water or diamine itself is a dominant base is not clear in CO_2 capture process using K_2Sol. The reaction rate by water and that by diamine may be competitive, so this may be the reason why temperature profile of the absorber with K_2Sol under optimal operating conditions was different from typical absorber temperature profile of CO_2 capture process in figure 3.5a. In this study, It is assumed that the contribution of diamine is comparable to that of water. As with the CO_2 capture process model for MEA in ASPEN Plus, a reaction model is employed in an absorber model regardless of an chemical

equilibrium model. The reaction model includes the reaction of CO_2 with OH^- and CO_2 with K_2Sol of which reaction rates is calculated by the power law expressions. Other reactions is assumed with chemical equilibrium reactions, and those equilibrium constants are calculated from the standard Gibbs free energy change. It is assumed that all reactions proceed in liquid phase due to the limits of ASPEN Plus model. Table 4.3 shows the input information of reaction model for an absorber.

Table 4.3: The input information of reaction model for an absorber in ASPEN Plus

No.	Reaction type	Stoichiometry
1	Equilibrium	$HK_2Sol^+ + H_2O \rightleftharpoons K_2Sol + H_3O^+$
2	Equilibrium	$2\,H_2O \rightleftharpoons H_3O^+ + OH^-$
3	Equilibrium	$HCO_3^- + H_2O \rightleftharpoons CO_3^{2-} + H_3O^+$
4	Kinetic	$CO_2 + OH^- \longrightarrow HCO_3^-$
5	Kinetic	$HCO_3^- \longrightarrow CO_2 + OH^-$
6	Kinetic	$K_2Sol + CO_2 + H_2O \longrightarrow K_2SolCOO^- + H_3O^+$
7	Kinetic	$K_2SolCOO^- + H_3O^+ \longrightarrow K_2Sol + CO_2 + H_2O$
8	Kinetic	$2\,K_2Sol + CO_2 \longrightarrow K_2SolCOO^- + HK_2Sol^+$
9	Kinetic	$K_2SolCOO^- + HK_2Sol^+ \longrightarrow 2\,K_2Sol + CO_2$

An absorber model was based on **RadFrac** distillation model in ASPEN Plus. It is assumed that a calculation of distillation model is used to an equilibrium method. The packing type of an actual absorber is Sulzer matal gauze packing, type BX. Its economical load range is presented in F factor from 1 to 2.5 $\sqrt{\text{Pa}}$, and height of a theoretical plate (HETP) is 0.1 – 0.3 m in this range [61]. Although an actual HETP lays under this lower bounds, HETP in an absorber model is assumed to be 0.3m considering also the convergence of a full model.

Input of residence time in each stage is essential for the calculation of reactive distillation model when it is considered as an equilibrium model. If the packed column does not include the reactions, liquid hold-up is calculated by the Froude number and pressure drop through an irrigated bed [62]. The liquid hold-up and residence time is calculated by actual pressure drop at pilot-scale test. As a calculation result, it takes 1.25 minutes for the liquid to pass through an absorber. Since the time taken for the liquid to fall to the bottom at the top of an absorber is actually longer than the calculated value, the residence time of each stage set 12 seconds in consideration of the viscosity difference due to the reaction.

From the above assumptions, an absorber model should have additional 16 parameters including phase equilibrium parameters and data of reaction kinetics. By linking MATLAB and ASPEN Plus, the function model is built to calculate output responses with remaining parameters and operating conditions as input variables, and the function model was used in the next step, global sensitivity analysis and Bayesian parameter estimation. Table 4.4 shows the specification of input variables, output responses of an absorber model. Specification of remaining paramters is introduced in chapter 4.3.1 with a range of parameters used in global sensitivity analysis.

Table 4.4: Specification of input variables, output responses of an absorber model

Variable Type	Abbreviation	Description
Input variables	x_1	Lean amine mass flow rate
	x_2	CO_2 mole fraction of lean amine
	x_3	Water mole fraction of lean amine
	x_4	K_2Sol mole fraction of lean amine
	x_5	Temperature of vent gas
Output Responses	y_{1-10}	1st – 10th stage temperature of an absorber model
	y_{11}	Volume flow rate of vent gas
	y_{12}	CO_2 mole fraction of vent gas

4.3 Bayesian Inference using Surrogate Models and Hybrid Models

4.3.1 Parameter subset selection using global sensitivity analysis

Due to the possibility of unidentifiability of model parameters in the full process, global sensitivity analysis (GSA) is the important step to select the parameter subset. The variance-based global sensitivity indices of 8 kinetic parameters and 8 thermodynamics parameters is calculated by Fourier amplitude sensitivity testing (FAST) [63, 64], which ranges the parameters in order of sensitivity. Unlike the local sensitivity analysis, GSA can globally decompose the variance of each parameters over search space. The local sensitivity and the global sensitivity can be extremely different where the relationship between output responses and parameters is non-linear. Thus, GSA is appropriate to find what parameters more contribute to output responses over total range of search space. Although it is difficult to identify the best parameter subset before conducting the parameter estimation, the 8 parameters are extracted over 16 parameters without loss the consistency because the parameters in this subset have extremely larger sensitivity than the others. The list and the search space of each parameter are listed in Table 4.5.

Table 4.5: The prior range for the parameter $\boldsymbol{\theta}$

Parameter	Abbreviation	Unit	Min.	Max.	Description
A_{ij}	θ_1	–	-10	10	NRTL binary parameter of H_2O and K_2Sol
A_{ji}	θ_2	–	- 10	10	NRTL binary parameter of H_2O and K_2Sol
B_{ij}	θ_3	–	- 2000	2000	NRTL binary parameter of H_2O and K_2Sol
B_{ji}	θ_4	–	- 2000	2000	NRTL binary parameter of H_2O and K_2Sol
$\Delta_f H^{\infty,25°C}_{K_2Sol^+}$	θ_5	kJ/mol	- 800	-300	Standard formation enthalpy of K_2Sol^+
$\Delta_f G^{\infty,25°C}_{K_2Sol^+}$	θ_6	kJ/mol	- 300	0	Standard formation Gibbs free energy of K_2Sol^+
$\Delta_f H^{\infty,25°C}_{K_2SolCOO^-}$	θ_7	kJ/mol	- 800	-300	Standard formation enthalpy of $K_2SolCOO^-$
$\Delta_f G^{\infty,25°C}_{K_2SolCOO^-}$	θ_8	kJ/mol	- 500	0	Standard formation Gibbs free energy of $K_2SolCOO^-$
k^6_a	θ_9	–	10^5	10^{10}	Pre exponential factor of reaction 6
k^7_a	θ_{10}	–	10^{15}	10^{20}	Pre exponential factor of reaction 7
k^8_a	θ_{11}	–	10^5	10^{10}	Pre exponential factor of reaction 8
k^9_a	θ_{12}	–	10^{15}	10^{20}	Pre exponential factor of reaction 9
E^6_a	θ_{13}	cal/sec	$10^{3.5}$	10^5	Activation energy of reaction 6
E^7_a	θ_{14}	cal/sec	$10^{3.5}$	10^5	Activation energy of reaction 7
E^8_a	θ_{15}	cal/sec	$10^{3.5}$	10^5	Activation energy of reaction 8
E^9_a	θ_{16}	cal/sec	$10^{3.5}$	10^5	Activation energy of reaction 9

4.3.2 Posterior inference with surrogate models and hybrid models

Main objective of our study is to infer the parameter posterior inference under pilot plant experimental data sets. Even though the dimension of parameter set is reduced, there are several numerical problems to perform the posterior inference using full process simulation model directly. The characteristics of the full model are that computational cost is expensive, the convergence rate of full range of the design space is low, and the correlation between parameters and output responses are highly nonlinear, which makes difficult to formulate the surrogate model to substitute the original full model. Altogether, hybrid model which exploits the deep neural network surrogate model is employed to evaluate the error covariance matrix and optimal step size from iterative sampling algorithm and to substitutes the diverged output responses from full model.

The full model of an absorber includes 5 design variables ($\mathbf{x}$) and 12 output responses ($\mathbf{y}$) for 8 experiments. Each finite set of design variable $\{\mathbf{x}^{(1)}, \cdots, \mathbf{x}^{(M)}\}$ consists of mass flow rate of lean amine, mass fraction of lean amine, and lean amine CO_2 loading as $\mathbf{x} = (\dot{m}_{\text{lean}}, w_{\text{lean}}, \alpha_{\text{lean}})$, respectively. Since it is assumed that the case that $\mathbf{y}$, which is multiple response $\{\mathbf{y}_1, \cdots, \mathbf{y}_D\}$, are in steady state, $\mathbf{y}_d$ is scalar. $\mathbf{y}_{1-10}$ measure temperature of an absorber (HETP: 0.3 m), $\mathbf{y}_{11}$ measures volume flow rate of treated gas, and $\mathbf{y}_{12}$ measures CO_2 mole fraction of treated gas. Single experiment contains a data set as $\{\mathbf{x}^{(m)}, \mathbf{y}_d^{(m)}\}$, where m represents the number of experiments and d means the number of output responses. In our problem, M equals 8 and D equals 12, where $m = 1, \cdots, M$ and $d = 1, \cdots, D$.

Let $\mathbf{f}(\mathbf{x}, \boldsymbol{\theta})$ be a rigorous model which is stated in chapter 4.2. Model can predict $\mathbf{y}_{\text{model}}$ using $\mathbf{x}$ and a specific set of model parameters $\boldsymbol{\theta}$. Herein, it has K-dimensional parameter vector $\boldsymbol{\theta}$, where K is 16. In 4.3.1, however, the $\boldsymbol{\theta}$ is re-

duced as parameter subset $\hat{\boldsymbol{\theta}} = (A_{ij}, A_{ji}, B_{ij}, B_{ji}, \Delta_f H^{\infty,25^\circ\mathrm{C}}_{\mathrm{K_2SolCOO^-}}, \Delta_f H^{\infty,25^\circ\mathrm{C}}_{\mathrm{K_2Sol^+}}, \Delta_f G^{\infty,25^\circ\mathrm{C}}_{\mathrm{K_2SolCOO^-}}, \Delta_f G^{\infty,25^\circ\mathrm{C}}_{\mathrm{K_2Sol^+}}, k^6_\mathrm{a}, k^7_\mathrm{a}, k^8_\mathrm{a}, k^9_\mathrm{a}, E^6_\mathrm{a}, E^7_\mathrm{a}, E^8_\mathrm{a}, E^9_\mathrm{a})$, which changes K as 8. The model-plant miss match, lack of experiment data, and unknown disturbances may affects the discrepancy between $\mathbf{y}$ and $\mathbf{y}_{\mathrm{model}}$. To compensate the uncertainty between $\mathbf{y}$ and $\mathbf{y}_{\mathrm{model}}$, a multivariate Gaussian distribution error $\boldsymbol{\epsilon}$ is applied, with covariance matrix Σ [65, 66, 30].

$$\boldsymbol{\epsilon} = \mathbf{y} - \mathbf{f}(\mathbf{x}, \boldsymbol{\theta}) \sim \mathcal{N}(\mathbf{0}, \Sigma). \tag{4.6}$$

If extracting the derivative information from the model is difficult (black-box) and model is expensive to perform large sampling, several previous studies tried to substitute the rigorous model to simple surrogate model $\tilde{\mathbf{f}}(\boldsymbol{\theta})$ such as a quadratic hypersurface fitting [65, 66, 30].The design variables can be marginalized as,

$$\mathbf{f}(\mathbf{x}, \boldsymbol{\theta}) \approx \tilde{\mathbf{f}}(\boldsymbol{\theta}), \tag{4.7}$$

at surrogate model if the surrogate models are generated at each experiment set. However, the significant limitation of this method is that regression fails if the relationship between parameters and model has highly nonlinear or discrete transitions. If the parameter estimation is performed using the wrong surrogate model, output responses reconstructed by the estimated parameters and the rigorous model may be undesirable. There are also several problems with MCMC sampling using the rigorous model. First, the iterative algorithm used to determine the $\hat{\Sigma}$ and the optimal MCMC step size needs huge sampling (10^4 scale) which is computationally costly if the rigorous model is used. Also, searching through a wide range of parameter search space leads convergence problem at the rigorous model. This causes a dilemma in the calculation of likelihood that which parameters are better, 1) well converged in all eight experiments but poor estimation performance or 2) some divergence at one or two experimental

sets with better estimation performance.

Here, the systematic framework is introduced to solve the problems using hybrid models (Figure 4.2). First, to maximize the regression performance of the surrogate, a deep neural network based surrogate model was applied to achieve a low mean squared error of 30% versus quadratic hypersurface fitting. Iterative sampling method was performed using the surrogate model to directly estimate Σ and appropriate step size for MCMC sampling from data and inference distribution over $\boldsymbol{\theta}$. Since Σ and step size do not change the global optimal peak of the posterior distribution obtained from the final MCMC sampling, this process is a preliminary task to find the most feasible Σ and the step size for the effective sampling. In the case of final MCMC sampling, hybrid model is introduced. It uses the rigorous model for converged case and the surrogate model for not converged case like

$$\mathbf{y}_{\text{model}} = \begin{cases} \mathbf{f}(\mathbf{x}, \boldsymbol{\theta}), & \text{for } \mathbf{f}(\mathbf{x}, \boldsymbol{\theta}) \text{ converged} \\ \tilde{\mathbf{f}}(\boldsymbol{\theta}), & \text{for } \mathbf{f}(\mathbf{x}, \boldsymbol{\theta}) \text{ not converged} \end{cases} \tag{4.8}$$

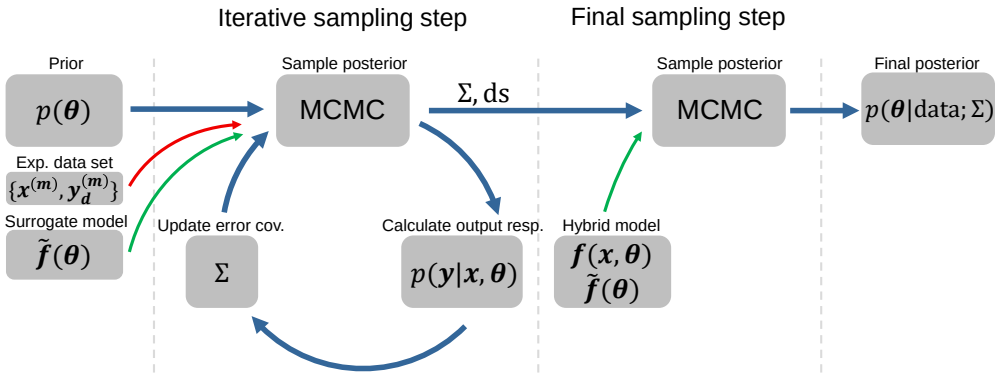

Figure 4.2: A graphical representation of Bayesian inference for hybrid model(rigorous and surrogate) under iterative sampling algorithm

This type of hybrid model can provide the most acceptable value to replace the likelihood for not converged cases, so it is much more stable than a fixed penalty value.

To construct the posterior distribution $\mathcal{P}(\boldsymbol{\theta})$ over the parameters $\boldsymbol{\theta}$, the method to evaluate the Bayes rule should be formulated,

$$\mathcal{P}(\boldsymbol{\theta}) \equiv p(\boldsymbol{\theta}|\text{data}) \propto p(\text{data}|\boldsymbol{\theta}) \cdot p(\boldsymbol{\theta}), \tag{4.9}$$

where $p(\boldsymbol{\theta})$ is the prior distribution over parameters and $p(\text{data}|\boldsymbol{\theta})$ is likelihood. It is assumed that the prior distribution is uniform in bounded and unconstrained search area. After iterative sampling step, Σ is localized around its true value for each dataset, log likelihoods of multiple dataset can be reduced as,

$$p(\text{data}|\boldsymbol{\theta}) = \prod_{m=1}^{M} \prod_{d=1}^{D} \int d\Sigma_{m,d}\, p(\{\mathbf{x}^{(m)}, \mathbf{y}_d^{(m)}\}|\boldsymbol{\theta}, \Sigma_{m,d})\, p(\Sigma_{m,d}) \tag{4.10}$$

$$\approx \prod_{m=1}^{M} \prod_{d=1}^{D} p((\mathbf{x}^{(m)}, \mathbf{y}_d^{(m)})|\boldsymbol{\theta}, \Sigma_{m,d}) \tag{4.11}$$

Thus, the log likelihoods can be calculated by product all log likelihoods of each combination of experiment and output response. The MCMC sampling using Metropolis-Hastings algorithm[67] is conducted and the $\mathbf{y}_{\text{model}}$ evaluation for each set of experiment is parallelized. Further detailed information and theoretical background of the Bayesian inference used in this paper is given in [30] and vanilla code is available in GitHub: https://github.com/ jihyunbak/BayesChemEng.

4.3.3 Deep neural network surrogate model methods

As described in Chapter 4.3.2, the surrogate model was developed and used for interactive sampling step during the posterior inference calculation.

Although the surrogate model which substitutes ASPEN Plus full model is inaccurate due to highly non-linearity of the correlation between parameters and output responses, using only full model causes expensive computational costs and suffers from unpredictable convergence rate problems. Thus, the surrogate model is applied to iterative sampling step, and serves as a penalty function of hybrid model during final sampling step.

In this study, deep neural network methods using residual learning is conducted[68]. Deep residual learning methods was proposed for better learning network as easy as stacking more layers. Addition of more layers for a suitably prediction often causes higher training error. Such **degradation** problems is not raised by overfitting. The degradation by saturated accuracy presents that most of systems are not easy to model using deep neural network methods. A residual learning block fit the residual, $F(x)$, between the desired output mapping function, $H(x)$, and input, x. If an identity mapping were optimal, the learning objective is fixed by that the residual is close to zero, so the optimization of residual mapping is easier than that of the original, unreferenced mapping. It is expected that deep residual learning methods predicts output responses better than other methods.

Deep Network Designer in MATLAB is used for the surrogate modeling. The number of sampling per experiment was 10,000. Of these, only 70% of the converged samples were used for the surrogate modeling, and the rest are used for validation. Adaptive moment estimation (Adam) was used as the network training solver. Training options include that; max number of epoch is 1,000, initial learn rate is 0.1, value of validation frequency is 30, mini-batch size is 64, and others are set to default options. The network mapping consisted of 4 fully connected layers, which three of have an output size of 10, and another has an output size of 12, and 3 leakyRelu layers shown as Figure 4.3.

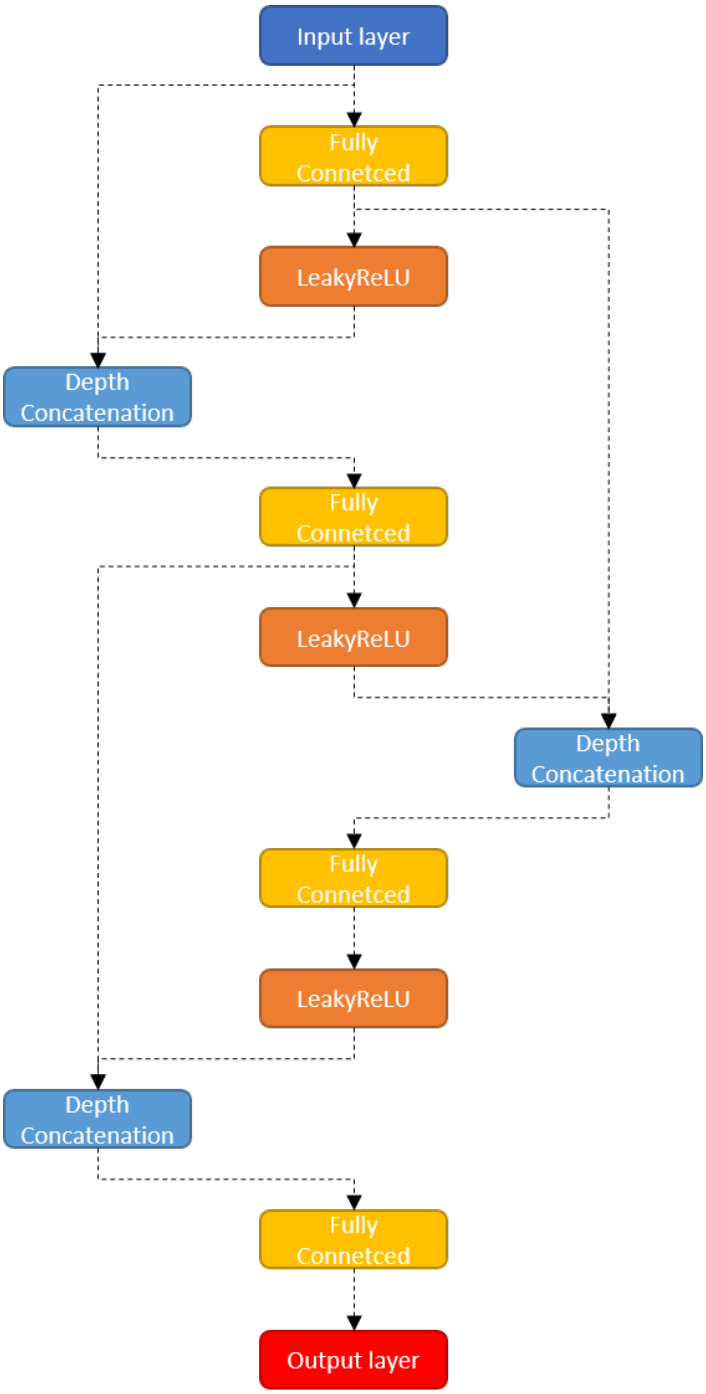

Figure 4.3: Network mapping of the surrogate model

4.4 Results and Discussion

Figure 4.4 and Table 4.6 shows sensitivity indices of the global sensitivity analysis. 16 parameters with 2 input variables, which are mass flow rate and CO_2 mole fraction of lean amine, were included in the global sensitivity analysis. 16,621 samples were performed from FAST methods, and non-converged samples is set to output any specific values. The larger the sensitivity index, the greater influence of the parameter on the output responses.

In Figure 4.4 and Table 4.6, standard formation Gibbs free energy of HK_2Sol^+, θ_6, contributes most ot the overall output responses. Of the hypothetical chemicals for which some parameter values are not specified, only the cation in aqueous intermediates participates in the equilibrium reactions in Table 4.3. Using enthalpy and Gibbs free energy of standard formation, an absorber model in ASPEN Plus calculates heat of reactions and equilibrium constants. Because of that, if θ_6 has an inadequate value, equilibrium constants of reaction 1 in Table 4.3 is abnormally calculated, so an absorber model does not converge well due to mass balance and/or charge balance error. Samples with θ_6 in the upper bound, whose an absolute value is close to zero, converged well over 50%, however temperature of each stage is close to room temperature, and CO_2 is not absorbed at all. This indicates that posterior of θ_6 can be in the range of values where the model does not converge well.

In reaction parameters, activity energy of the forward reactions contributes CO_2 mole faction and volume flow rate of vent gas, and one of the backward reactions contributes temperature profiles of an absorber. This result is reasonable because the forward reactions are CO_2 absorption reaction and the backword reactions are expected to be an endothermic reaction. Since the activation energy enters the exponential term in the reaction rate equation, pre-exponential

factors would not contribute to activation energies as much. Other than that, θ_2 and θ_4 contribute CO_2 mole faction and volume flow rate of vent gas, and θ_2 contributes some to temperature profiles.

From these results, 8 parameters are selected by Bayesian parameter estimation; 3 NRTL parameters, standard formation Gibbs free energy of HK_2Sol^+, and the activation energy of reactions. Table 4.7 shows the specification of the parameters predetermined by GSA.

Table 4.6: Specification of global sensitivity analysis results

$\times 10^{-3}$

	θ_1	θ_2	θ_3	θ_4	θ_5	θ_6	θ_7	θ_8	θ_9
y_1	2.276	1.792	0.787	0.394	0.822	82.35	0.44	0.748	0.644
y_2	2.499	2.068	0.888	0.485	0.800	92.19	0.393	0.684	0.554
y_3	2.577	2.158	0.915	0.497	0.758	97.63	0.38	0.679	0.529
y_4	2.632	2.247	0.923	0.504	0.714	102.2	0.368	0.685	0.525
y_5	2.675	2.338	0.928	0.512	0.673	106.4	0.357	0.694	0.530
y_6	2.705	2.424	0.932	0.519	0.639	110.0	0.347	0.704	0.540
y_7	2.722	2.492	0.934	0.525	0.618	112.8	0.338	0.714	0.552
y_8	2.718	2.499	0.936	0.516	0.611	114.5	0.331	0.729	0.555
y_9	2.664	2.317	0.945	0.436	0.634	114.6	0.326	0.763	0.539
y_{10}	2.239	1.430	0.867	0.230	0.704	112.9	0.285	0.884	0.573
y_{11}	5.323	35.16	2.350	11.38	0.746	71.61	0.842	0.456	4.786
y_{12}	4.753	28.73	2.257	8.578	0.843	89.98	0.831	0.431	4.773

	θ_{10}	θ_{11}	θ_{12}	θ_{13}	θ_{14}	θ_{15}	θ_{16}	x_1	x_2
y_1	1.560	1.225	0.868	4.918	30.77	8.401	10.67	0.524	1.635
y_2	1.618	1.126	0.859	3.767	31.39	6.295	11.28	0.504	1.816
y_3	1.654	1.073	0.864	2.999	31.66	5.101	11.69	0.486	1.786
y_4	1.671	1.032	0.874	2.333	31.66	4.154	11.96	0.477	1.725
y_5	1.677	1.001	0.884	1.798	31.50	3.412	12.14	0.473	1.662
y_6	1.676	0.984	0.890	1.414	31.25	2.881	12.25	0.471	1.606
y_7	1.672	0.978	0.896	1.165	30.98	2.541	12.31	0.470	1.557
y_8	1.673	0.977	0.903	1.037	30.81	2.386	12.35	0.459	1.521
y_9	1.687	0.970	0.914	1.002	30.74	2.377	12.32	0.403	1.477
y_{10}	1.766	0.904	0.85	1.143	30.95	2.501	11.56	0.397	1.242
y_{11}	0.838	6.633	0.471	49.74	5.656	69.76	0.980	1.236	13.32
y_{12}	0.891	7.212	0.505	53.38	4.100	73.97	0.671	0.434	9.150

Table 4.7: Specification of the parameters predetermined by GSA

Parameters	B_{ij}	$\Delta_f H^{\infty,25^\circ C}_{K_2Sol^+}$	$\Delta_f H^{\infty,25^\circ C}_{K_2SolCOO^-}$	$\Delta_f G^{\infty,25^\circ C}_{K_2SolCOO^-}$	$\log(k_a^6)$	$\log(k_a^7)$	$\log(k_a^8)$	$\log(k_a^9)$
Unit	–	kJ/mol	kJ/mol	kJ/mol	–	–	–	–
Value	-865.2	-635.8	-414.9	-390.5	6.251	19.68	6.710	16.18

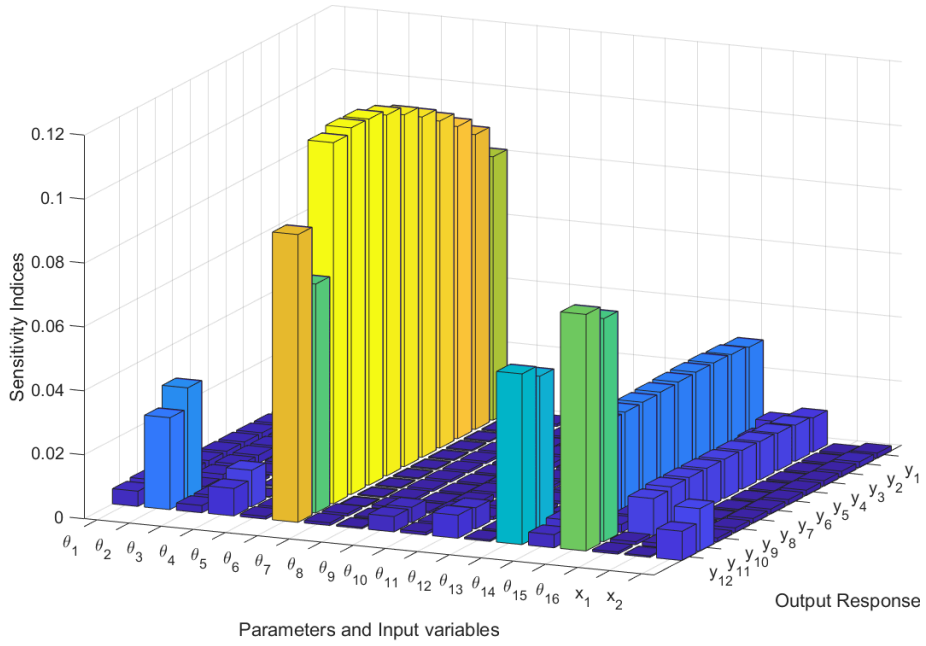

Figure 4.4: Sensitivity indices of global sensitivity analysis

Table 4.8 and Table 4.5 – 4.12 show the validation results between actual output responses and predicted values of surrogate models. Surrogate models predict temperature profiles relatively well, however validation results presents that they can not identify the correlation between output responses of vent gas and parameters. For the parameter estimation, the coefficient of determination, R^2, should be near to one, but validation results are far less than that. Since an absorber model in ASPEN Plus has a high non-linearity so that output responses is vigorously shaken even with very small changes in parameters, it is impossible to build a surrogate model that fully reflects a full model. As mentioned in chapter 4.3.2, reflecting this result, surrogate models is employed for iterative sampling during Bayesian parameter estimation, and serve as a penalty function of a hybrid model for final sampling.

Table 4.8: $\mathbf{R}^2$ of surrogate model

	y_1	y_2	y_3	y_4	y_5	y_6	y_7	y_8	y_9	y_{10}	y_{11}	y_{12}
Ex. 1	0.952	0.954	0.952	0.949	0.948	0.948	0.948	0.947	0.948	0.950	0.742	0.724
Ex. 2	0.954	0.953	0.954	0.954	0.954	0.953	0.953	0.954	0.955	0.953	-0.813	0.822
Ex. 3	0.928	0.946	0.949	0.952	0.953	0.954	0.954	0.953	0.949	0.937	0.066	0.345
Ex. 4	0.958	0.955	0.953	0.952	0.952	0.951	0.950	0.950	0.951	0.955	0.619	0.800
Ex. 5	0.938	0.940	0.941	0.941	0.943	0.942	0.941	0.941	0.941	0.937	0.569	0.762
Ex. 6	0.947	0.944	0.943	0.943	0.943	0.943	0.942	0.942	0.942	0.941	0.368	0.775
Ex. 7	0.959	0.959	0.958	0.957	0.957	0.957	0.956	0.955	0.954	0.947	0.061	0.798
Ex. 8	0.954	0.960	0.961	0.961	0.961	0.961	0.961	0.961	0.961	0.954	0.791	0.828

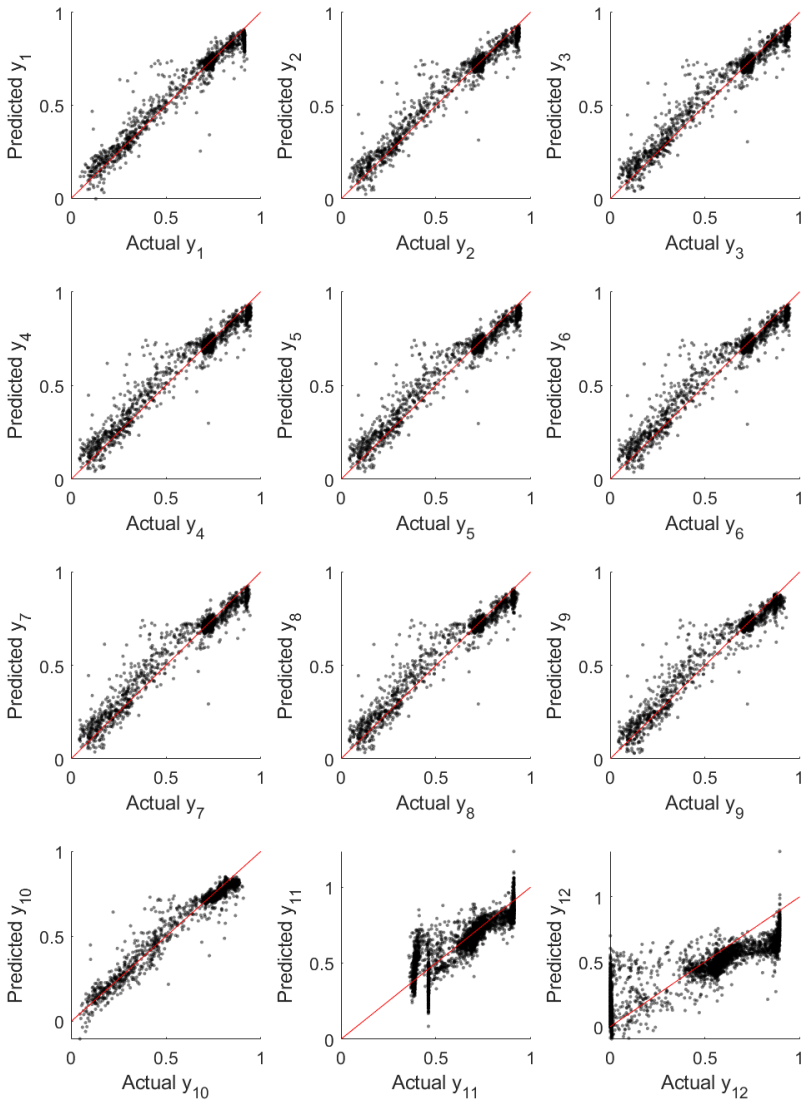

Figure 4.5: Validation result of 1st experiment surrogate model

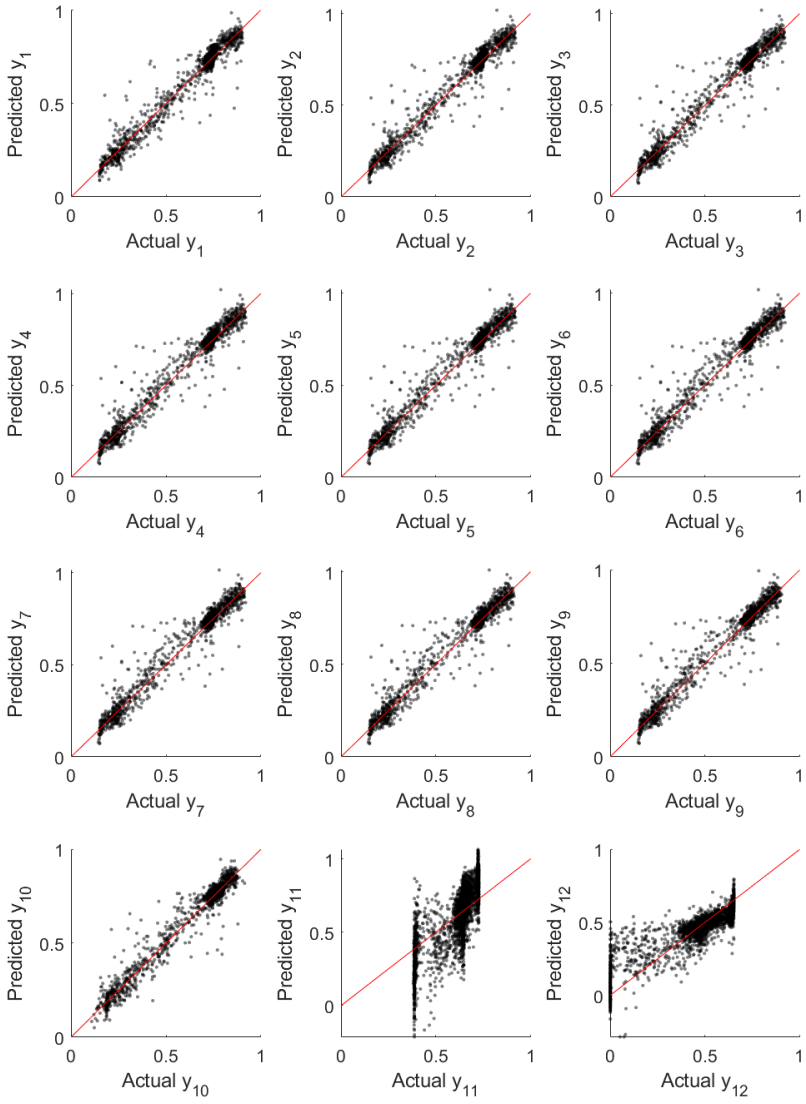

Figure 4.6: Validation result of 2nd experiment surrogate model

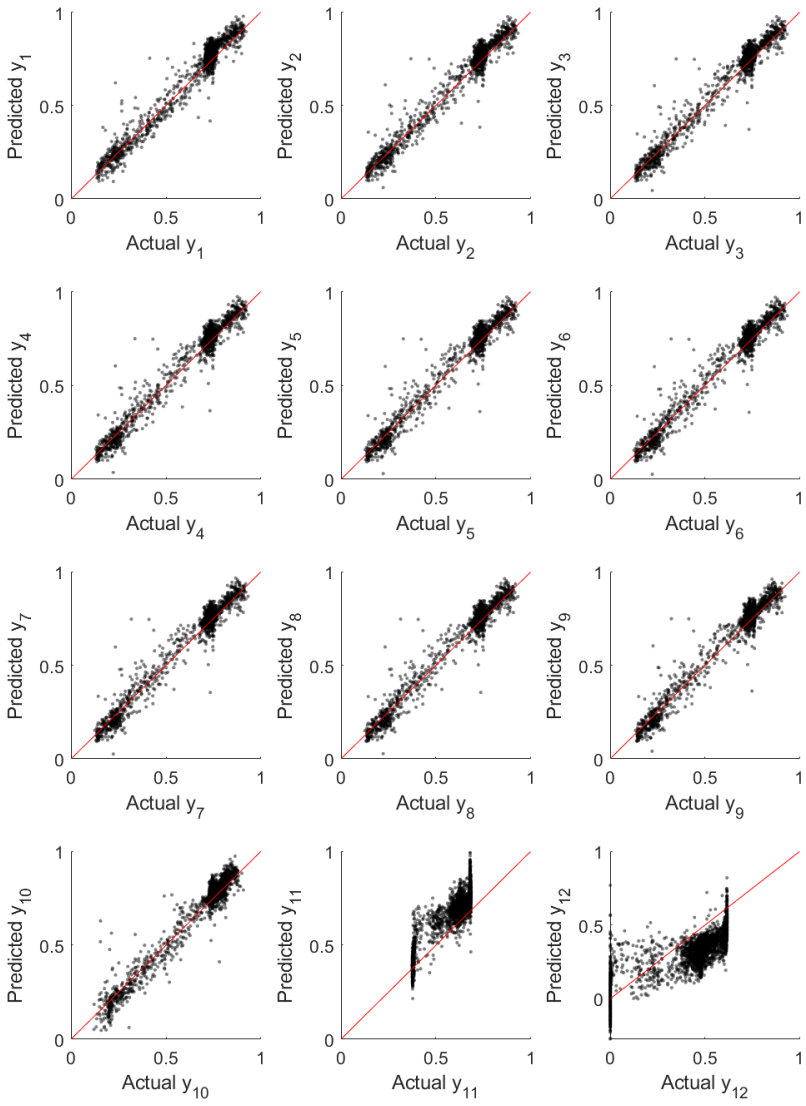

Figure 4.7: Validation result of 3rd experiment surrogate model

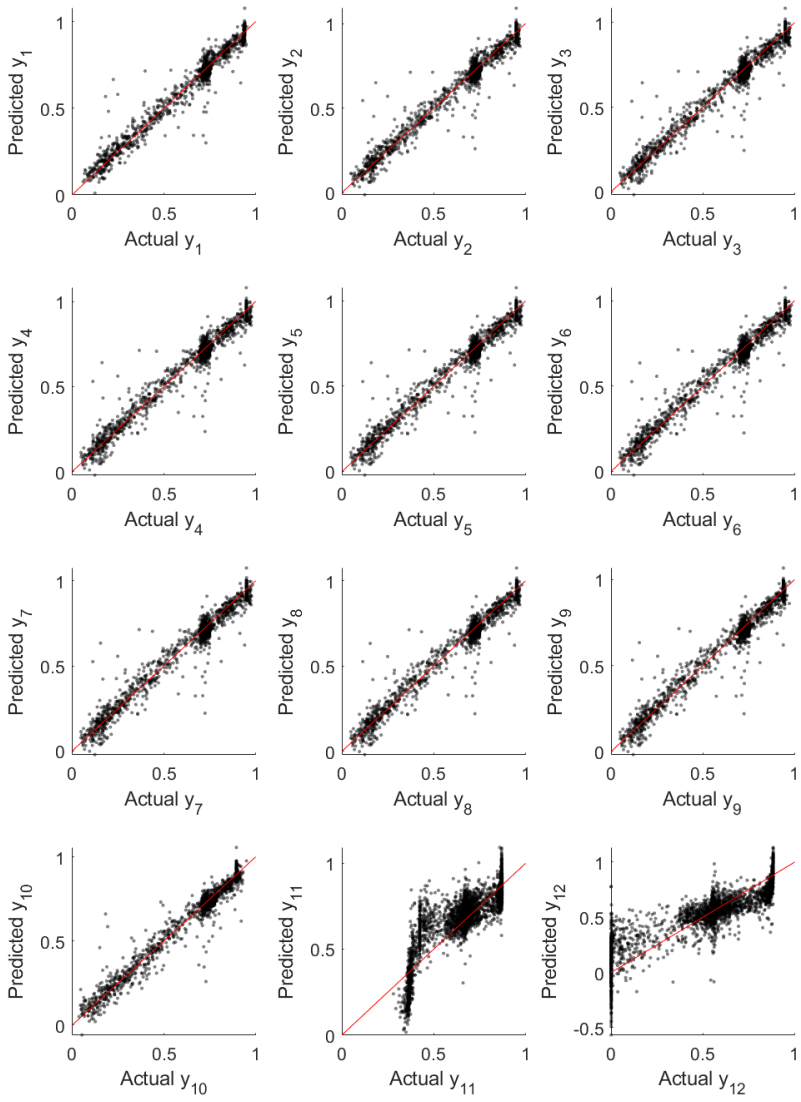

Figure 4.8: Validation result of 4th experiment surrogate model

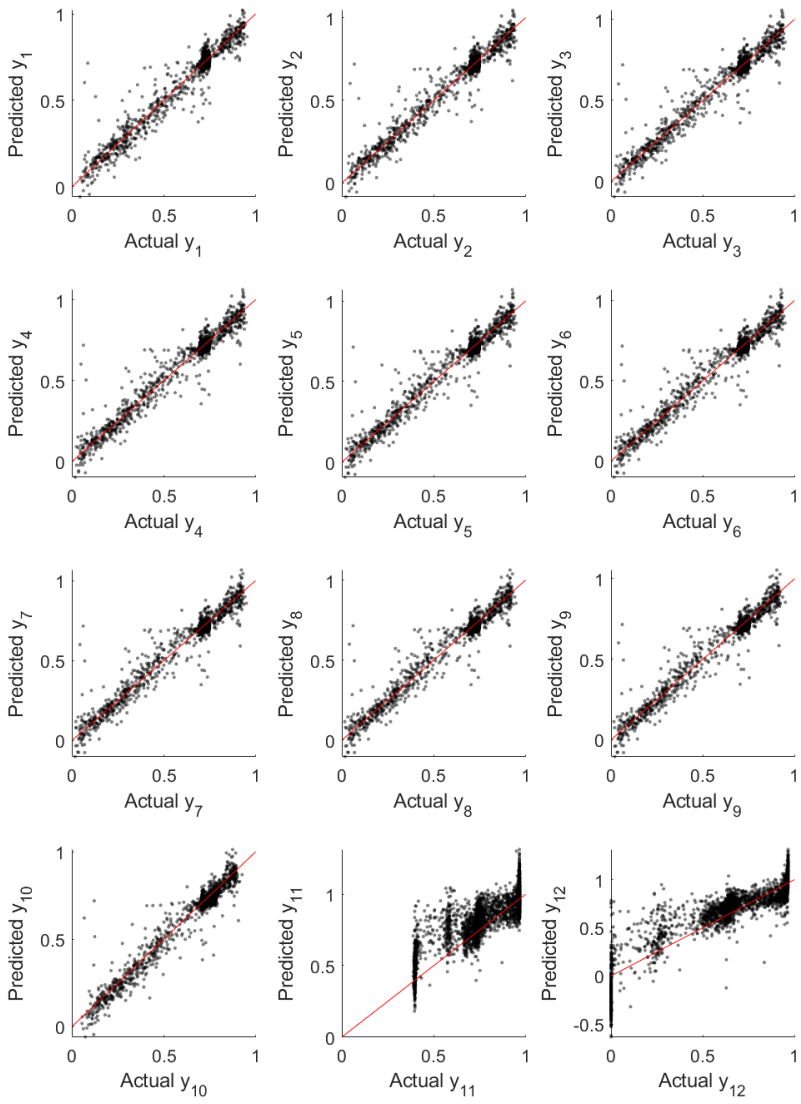

Figure 4.9: Validation result of 5th experiment surrogate model

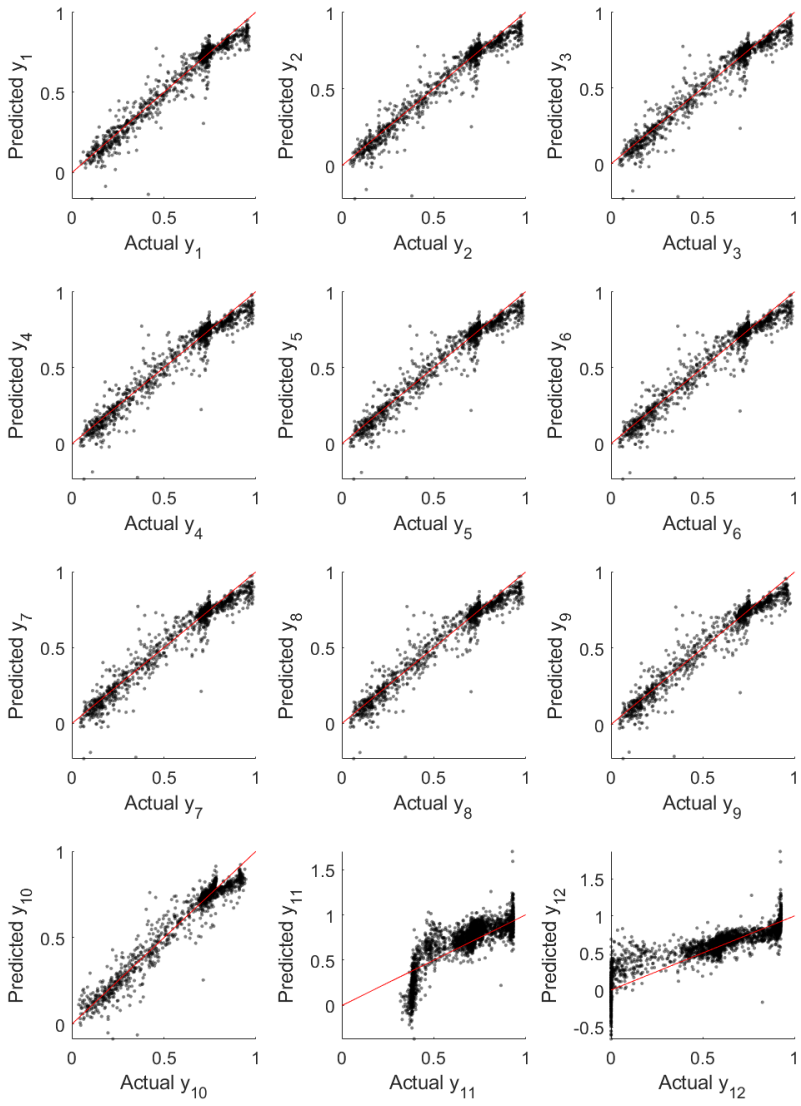

Figure 4.10: Validation result of 6th experiment surrogate model

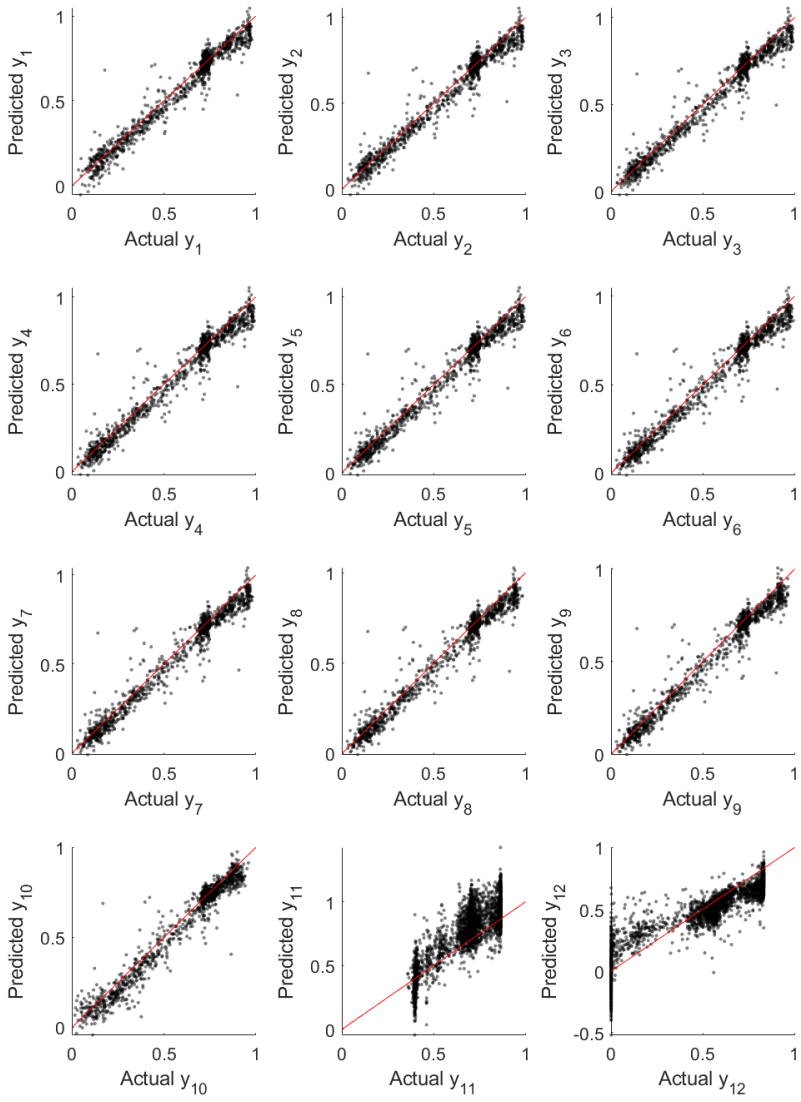

Figure 4.11: Validation result of 7th experiment surrogate model

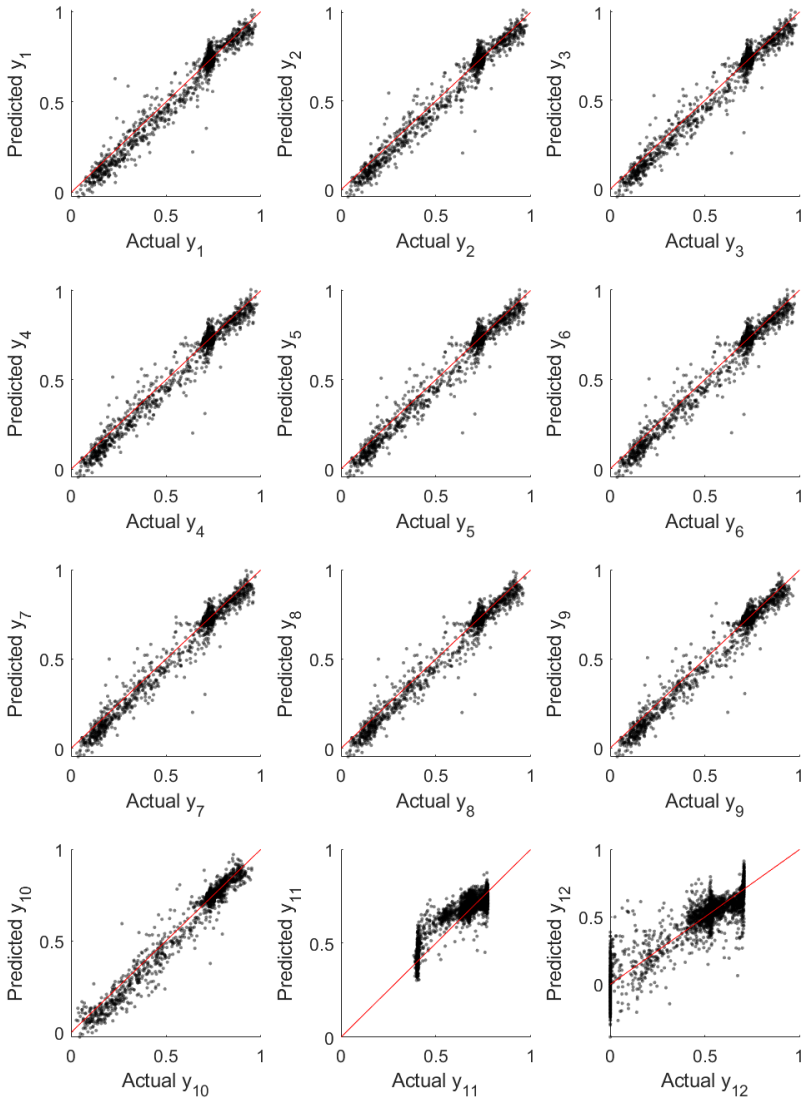

Figure 4.12: Validation result of 8th experiment surrogate model

To accelerating the acceptance rate of Markov chain Mote Carlo (MCMC), the exploration level, tempering, is higher than the default value during final sampling. Unlike iterative sampling steps, the acceptance rate of MCMC is indicated less than 1% at default tempering setting. Setting tempering to 250, the acceptance rate of final sampling points to 6.533%. Figure 4.13 shows the posterior distribution of normalized parameters. As predicted by GSA results, Figure 4.4, standard formation Gibbs free energy of the cation is located to the specific local range about 0.3. When the normalized value of $\Delta_f G^{\infty,25^\circ\mathrm{C}}_{\mathrm{K_2Sol^+}}$ is below to 0.5, a full model of ASPEN Plus generally does not converge well. Regardless of the full model convergence rate, if $\Delta_f G^{\infty,25^\circ\mathrm{C}}_{\mathrm{K_2Sol^+}}$ has not its specific value, about 0.3, an absolber temperature profile has absurd values of less than -100°C or more than 100°C, or indicates same values as room temperature.

Since the activation energy of two forward reactions has similar mean value, it is expected that both water and diamine itself contribute the absorption kinetics as a dominant base. Although their specific values are higher than the activation energy of traditional amines, such as MEA or AMP, it seems that interpreting the contribution of each parameter is no problem, since pre-exponential factors of reactions predefined from GSA results may cause relatively high value of this result. Table 4.9 presents mean value of final sampling parameters.

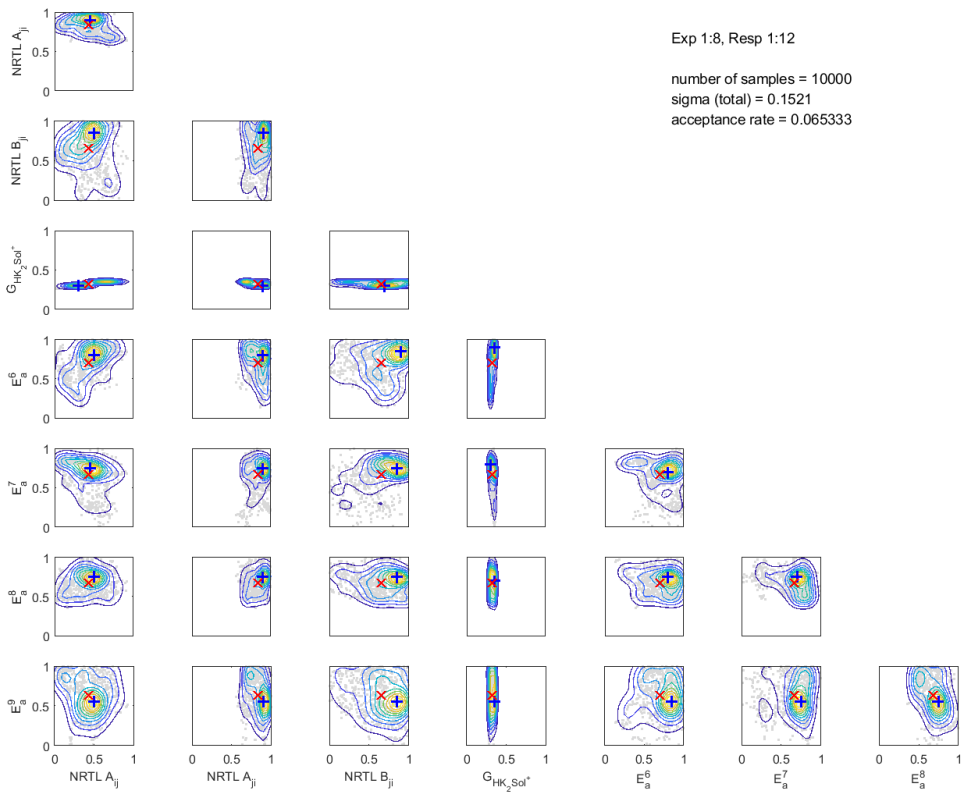

Figure 4.13: Posterior distribution of parameters

Table 4.9: Mean value of final sampling parameters

Parameters	A_{ij}	A_{ji}	B_{ji}	$\Delta_f G^{\infty,25^\circ\mathrm{C}}_{\mathrm{K_2Sol^+}}$	$\log(E^6_\mathrm{a})$	$\log(E^7_\mathrm{a})$	$\log(E^8_\mathrm{a})$	$\log(E^9_\mathrm{a})$
Unit	–	–	–	kJ/mol	cal/sec	cal/sec	cal/sec	cal/sec
Value	-1.440	6.725	629.8	-204.4	4.555	4.501	4.517	4.453

Figure 4.14 – 4.21 presents validation results of each experiment which compare nominal values, mean values of a full model, and actual values. Through the standard deviation values obtained by MCMC sampling, an absorber model is simulated in the range of 90% confidence in the normal distribution. In Figure 4.14 – 4.21, blue area of temperature profile plot and error bars of other plots indicate 95% confidence level of simulation results, and gray area of temperature profile points to 75% confidence level of simulation results.

Validation results of the absorber temperature profile indicate that the actual values is included in the 95% confidence interval in most experiments. In each experiment, the first stage temperature of an full model is generally higher than that of actual experiments. Top stage of an absorber can not reach an equilibrium state of reaction, and it takes time for the temperature to rise from the absorption reaction. In comparison, an absorber model built by equilibrium stage methods consider that each stage reach an equilibrium state. This is a common response in most of CO_2 capture process model using traditional amine solvent, using an equilibrium stage distillation model.

Temperature profiles of some experiments is not located in 75% confidence interval. They include experiment of no.4, 15, and 38.The commonality of these experiments is that the L/G ratio is close to 3 L/Nm^3 or less. In chapter 4.2, one of the modeling assumptions is that the residence time of each stage is 12 seconds. However, the lower L/G ratio, the higher residence time than expected, because high CO_2 loading compared with high amine flow rate causes rise in viscosity and differential pressure that an absorber can not afford. In actual pilot-scale test, experiments of low L/G ratio has the high failure. The absorber model with common amine solvents cannot also reflect the bulge in traditional temperature profile of an absorber relatively well, if the equilibrium methods is used.

Among the output responses of a full model, volume flow rate and CO_2 mole fraction fluctuate sharply with relatively small changes in the parameters. The results of surrogate model validation show that in the case of CO_2 mole fraction, the converged results are clearly divided into a part close to zero and a part above a specific value. According to very small changes of parameters, all of CO_2 in flue gas is absorbed by lean amine, or vent gas includes most CO_2 of feed streams. Because the correlation between vent gas conditions and parameters has the very stiff relationship, predicting the conditions of vent gas well is very difficult. Moreover, the composition of flue gas is measured, but that of feed gas passing through wetting column is not measured. Since the model assumes that flue gas is saturated with arbitrary amounts of water, the feed gas of an full model is likely to be different from the amount of actual experiments. Despite of these difficulties, volume flow rate and CO_2 mole fraction of vent gas is included in the 95% confidence interval at most of experiments.

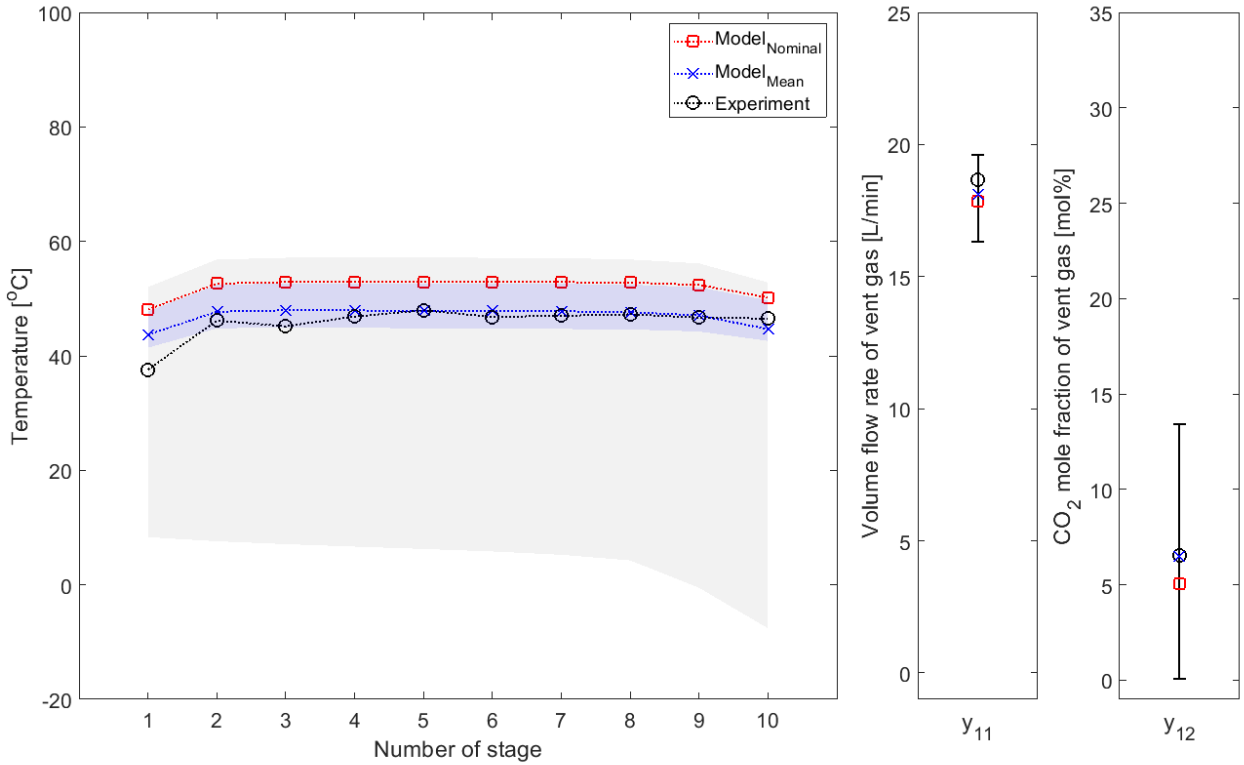

Figure 4.14: Validation results of experiment no. 1

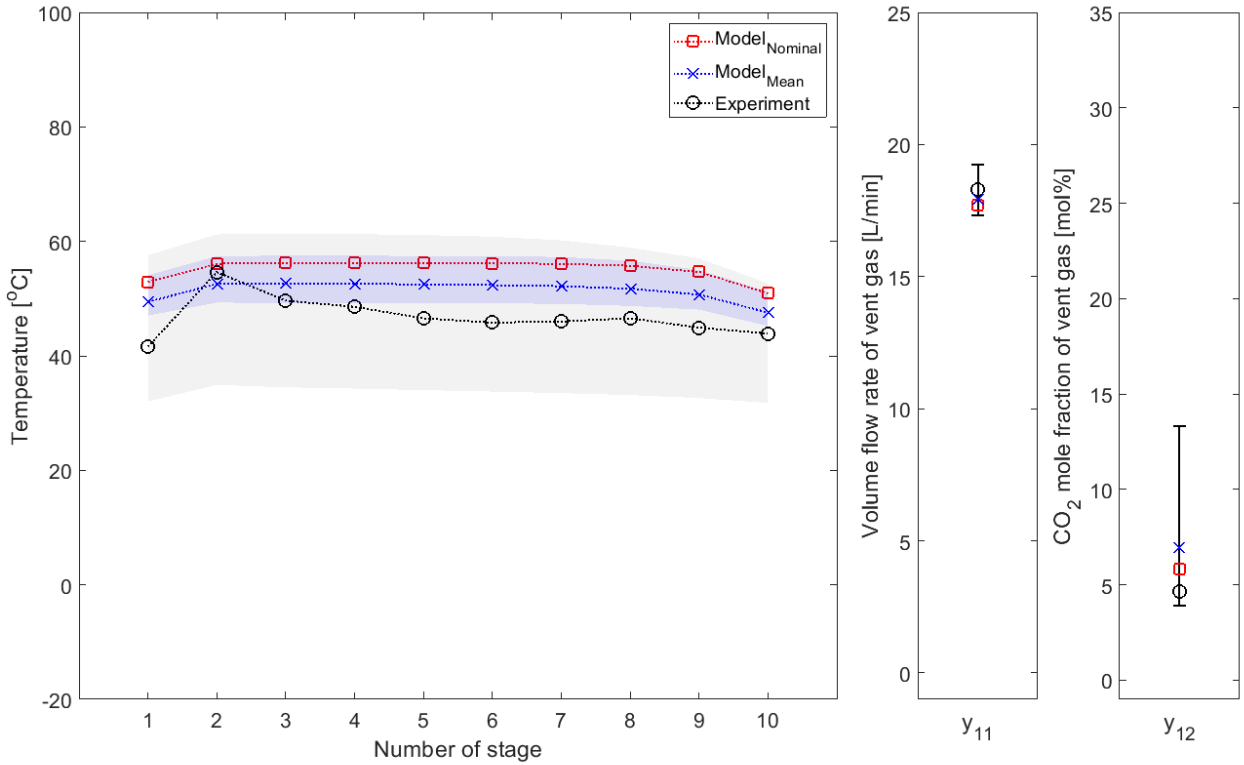

Figure 4.15: Validation results of experiment no. 2

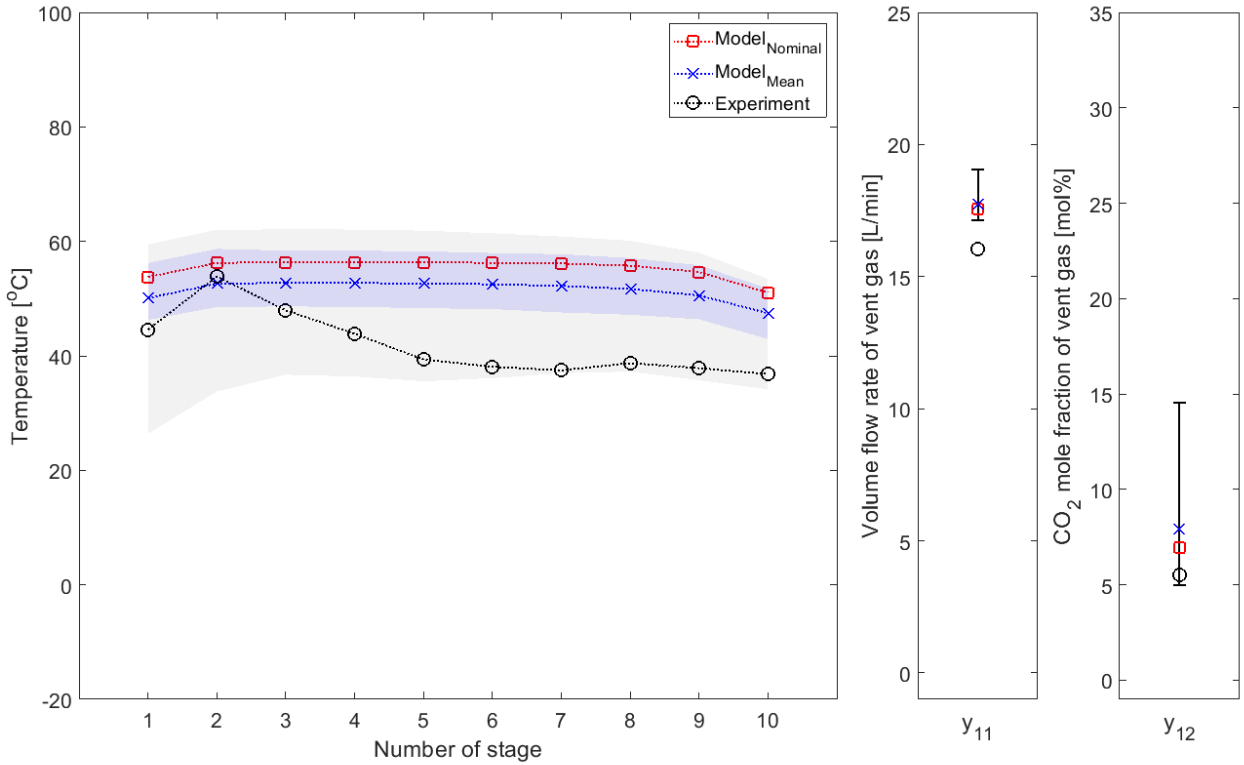

Figure 4.16: Validation results of experiment no. 3

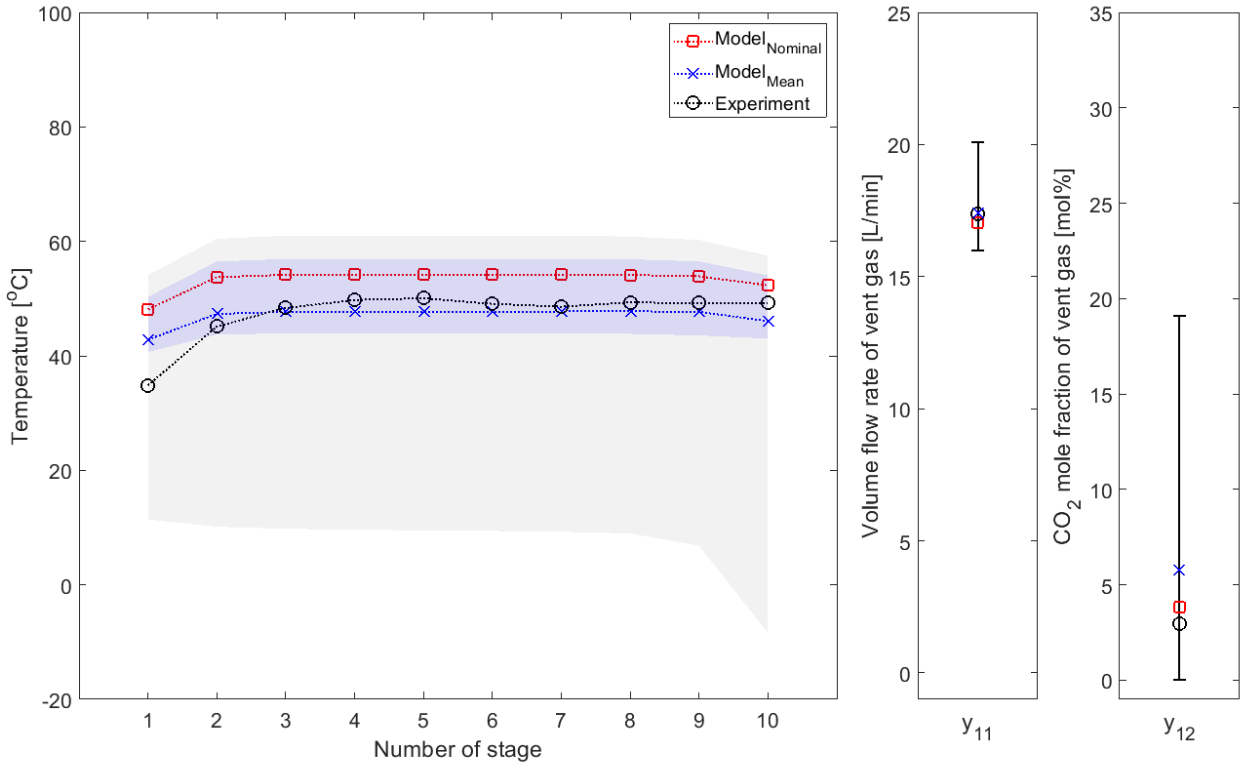

Figure 4.17: Validation results of experiment no. 4

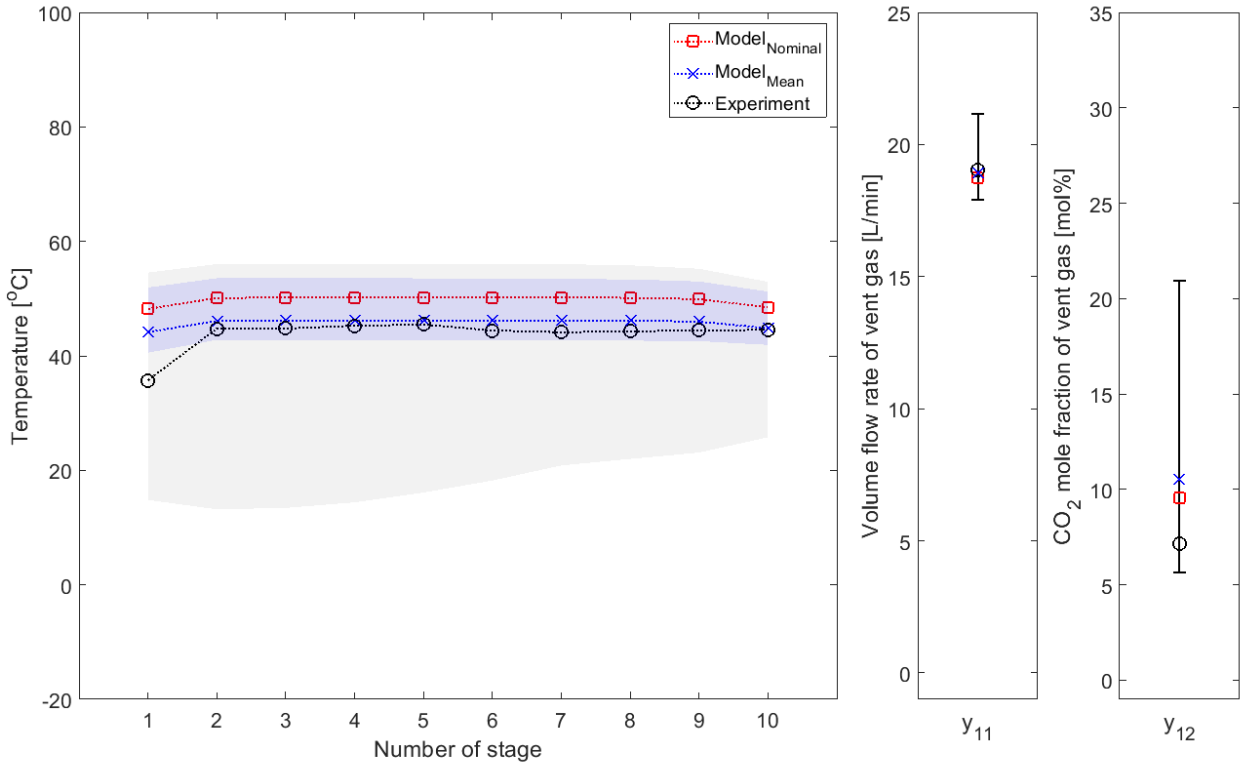

Figure 4.18: Validation results of experiment no. 5

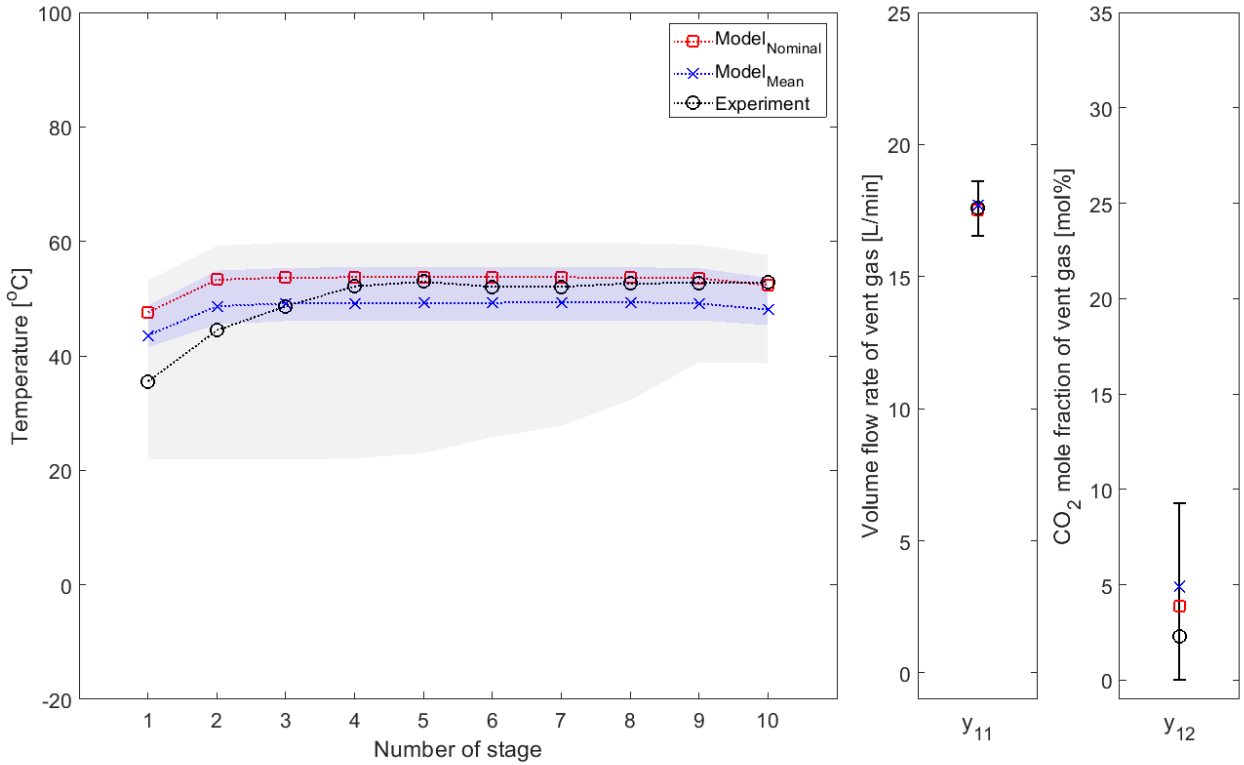

Figure 4.19: Validation results of experiment no. 6

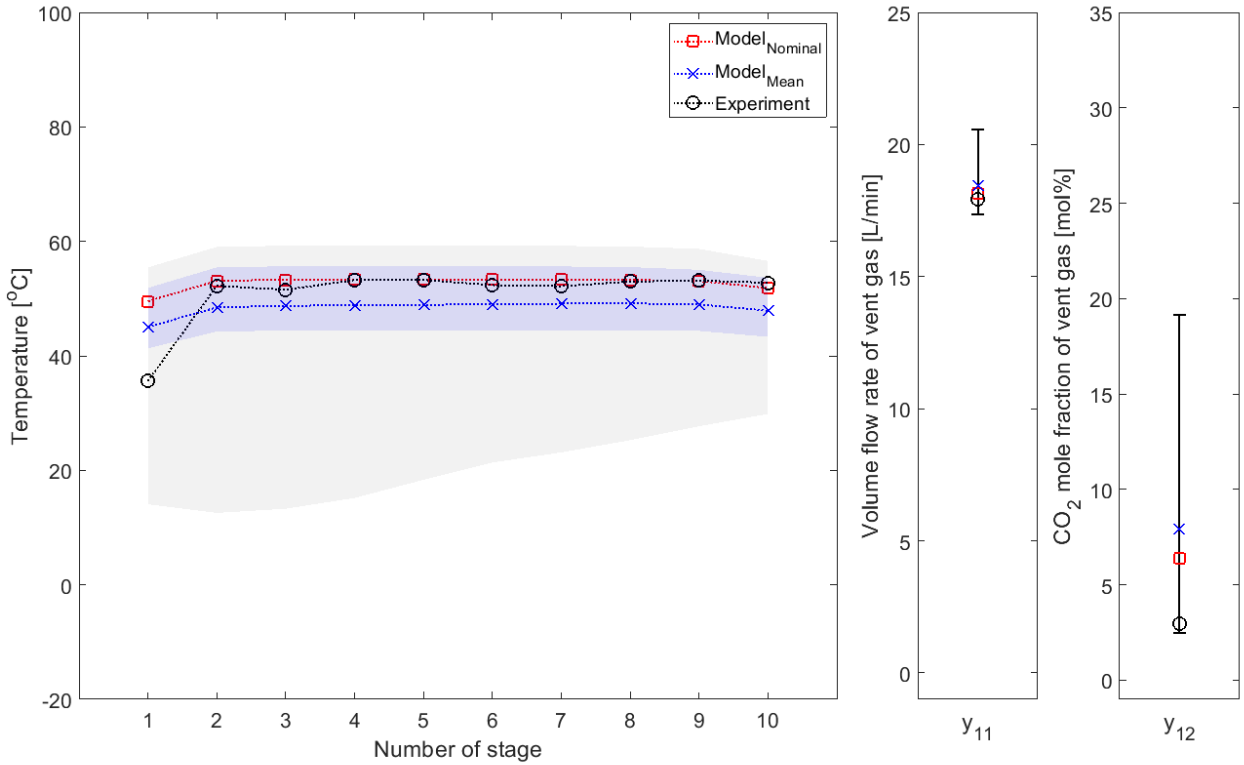

Figure 4.20: Validation results of experiment no. 7

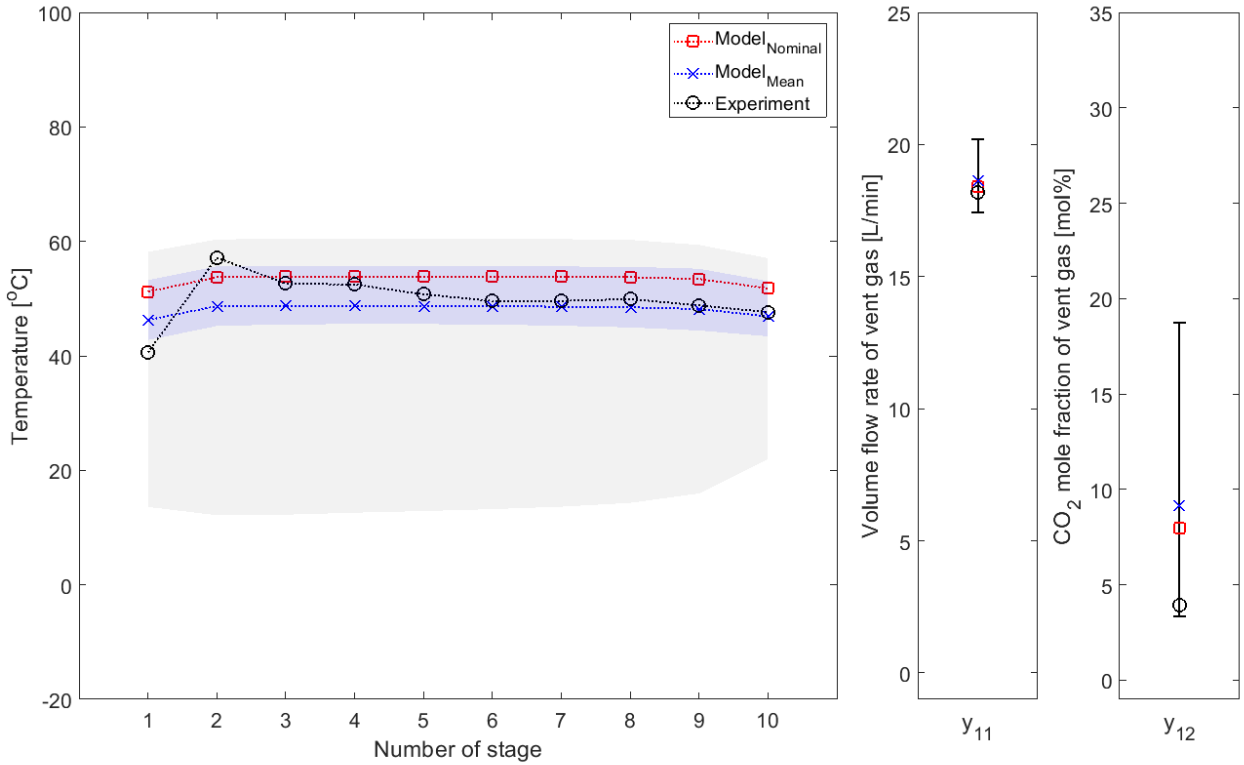

Figure 4.21: Validation results of experiment no. 8

The flash calculation is conducted to evaluate the regeneration energy calculated by a full model with estimated parameters. For the full model of 17th experiment, rich amine stream heats up to the actual temperature of lean-rich heat exchanger, 87.1 °C. The heated stream is firstly separated by the flash tank, then its liquid stream heats up again to the actual reboiler temperature, 92.9°C. The regeneration energy is calculated by the heat duty of 2nd flash tank. From the experimental results in Chapter 3.4, it is predicted that the number of stripper stages with K_2Sol would be smaller than that with MEA. In addition, considering that the reboiler temperature is lower than the water boiling point, it is reasonable to calculate the regeneration energy with the above assumption, although its value differs from the regeneration energy of actual experiments. In the case of MEA, the liquid stream above the bottom stage of a stripper heats up to the reboiler temperature in ASPEN Plus model with the optimal condition, 109.3 °C. Table 4.10 shows the comparison of the solvent performance calculated by ASPEN Plus full model with estimated parameters. The regeneration energy of K_2Sol is less than half of that with MEA. The results of amine loading are well reflected in the prediction of cyclic capacity in Chapter 2.

Table 4.10: Comparison of the solvent performance in the ASPEN Plus full model.

	30 wt% MEA	K_2Sol
Regeneration energy (GJ/t CO_2)	4.15	1.98
Rich amine loading (mol CO_2/ mol Amine)	0.54	0.81
Lean amine loading (mol CO_2/ mol Amine)	0.37	0.28

4.5 Conclusion

Bayesian parameter inference using Hybrid model is applied to the parameter estimation for the CO_2 absorber model with K_2Sol in ASPEN Plus. Pure component parameters is defined by group contribution methods, and it is assumed that CO_2 and K_2Sol react by the termolecular reaction mechanism. Subset selection is conducted by global sensitivity analysis, then 8 parameters, which reflect output responses well, serve as input variables of the surrogate model and the hybrid model. The surrogate model reflecting a full model is developed by deep neural network with residual learning. Using Markov chain Monte Carlo with Metropolis–Hastings algorithm, the posterior of parameters is constructed from pilot-scale experiments data based on Bayesian theorem.

It is indicated from GSA that standard formation Gibbs free energy of the cation is the most contributing parameter throughout all of output responses because of reaction kinetics. The importance of aqueous standard formation Gibbs free energy is reaffirmed from the posterior distribution of parameters, and it is noticed that both the forward reaction may happen equally because of a similar value between the activation energy of them. Since the pilot-scale tests was not for parameter estimation or design of experiments, sample data of experiments were biased. Nevertheless, most output responses of a full model with estimated parameters are located in 95% confidence interval. From the validation results, this chapter presents that the model parameters for a commercial process simulator can be estimated from a small number of experiments by Bayesian parameter estimation method.

Chapter 5

Concluding Remarks

Amine-based absorption process is considered as the most effective approach to remove carbon dioxide (CO_2) in flue gas from power plant and to mitigate greenhouse gas emissions. Although it is a realistic option for practical applications, the major drawbacks such as high energy consumption for CO_2 stripping hinder the extensive implementation of CO_2 capture. Many studies focus on the development of new solvents that have high reaction rate with CO_2 and high CO_2 loading capacity for lower regeneration energy than that of conventional processes. However, a significant improvement on energy consumption is still yet to be achieved. Recent studies have proposed alternative amine solvents such as Piperazine, ethylenediamine and ionic liquids have been identified promising options for lowering regeneration energy but other drawbacks, especially in terms of high viscosity and thermal/oxidate degradation, tackle practical applications.

This study presents a new water-lean amine-based solvent, K_2Sol designed employing a diamine with two hindered primary amino groups. K_2Sol possess

favorable properties suitable for a CO_2 capture solvent in terms of CO_2 absorption rate and capacity, thermal stability, viscosity, and regeneration. After the confirmation of its superior performance, pilot plant operation is conducted in order to identify the operability, steady state regeneration energy, and thermal stability. The machine learning based optimization method, Gaussian process Bayesian optimization, guided us to find optimum operation point for K2Sol even without constructing a expensive first principle model. According to the pilot plant experiment, the optimum regeneration energy of MEA and K_2Sol respectively shows 4.3 and 2.8 GJ/tCO_2 indicating that K_2Sol requires only 65% of regeneration energy of MEA. In addition to that, reboiler temperature below water boiling point showed that the stripper with K_2Sol can be operated with a low-quality heat source, so K_2Sol is economically superior to MEA even using the same thermal energy.

Additionally, Bayesian parameter estimation is implemented for the absorber model with K_2Sol, for the process design and the configuration optimization using a commercial process simulator. According to various assumptions, parameter candidates to be used in GSA is selected. The subset including 8 physiochemical parameters served as input variables of the surrogate model. Due to non-linearity of the full model, the surrogate model can not reflect the responses of the full model. The trade-off between the inaccuracy of the surrogate model and the high computation costs of the full model was solved by applying the hybrid model in the final sampling of MCMC. From the parameters posterior distribution, the result of analysis presents an influence of standard Gibbs free energy at the full model and that both forward reactions are near equally dominant. Most output responses of a full model with estimated parameters were also located in 95% confidence interval.

The future work which further develops this study is categorized into two

groups: First, additional lab-scale experiments are required to estimate exact values about reaction kinetic. Although this study presented the posterior distribution of reaction parameters, these values was overestimated because of pre-exponential factor predefined by GSA. If the rigorous model, such as rate-based distillation model, is necessary, an accurate heat of reaction and kinetic constants will be required. Secondly, the implementation of Bayesian parameter estimation is extended to the whole CO_2 capture process model with K_2Sol including the stripper. In this study, the model that simultaneously considered a stripper and an absorber showed a low convergence rate of 3% before the subset selection. Based on in this study results, the model which reflect whole CO_2 pilot experiment should be developed by Bayesian parameter estimation from the narrow range of candidates.

Appendix A

Information of diamine

Table A.1: Predicted data of diamine

Systematic name	1,1'-[1,2-Propanediylbis(oxy)]di(2-propanamine)
Molecular Formula	$C_9H_{22}N_2O_2$
Average mass	190.283 Da
SMILES	CC(COCC(C)OCC(C)N)N
Density:	1.0±0.1 g/cm^3
Boiling Point:	275.0±20.0 °C at 760 mmHg
Vapour Pressure:	0.0±0.6 mmHg at 25°C
Enthalpy of Vaporization:	51.3±3.0 kJ/mol
Flash Point:	115.4±15.5 °C
Index of Refraction:	1.459
Molar Refractivity:	54.2±0.3 cm^3
Polar Surface Area:	71 Å^2
Polarizability:	21.5±0.5 10-24cm^3
Surface Tension:	34.3±3.0 dyne/cm
Molar Volume:	198.3±3.0 cm^3

Appendix B

Details of approximation spectral sampling

If a stochastic function is stationary process, its covariance are characterized by the property of being non-negative definite, and its covariance function are Fourier-transforms of their *spectral distributions*. The spectral distribution function is characterized by the symmetry, monotonicity, and boundedness property.

According to Bochner's theorem, a weakly stationary kernel function is positive definite, and hence a covariance function, if and only if there exist real function $S(w)$ which is non-decreasing, right, continuous, and bounded such that

$$k(x - x') \equiv k(\tau) = \int_{-\infty}^{\infty} S(w) e^{iw^T \tau} dw \tag{B.1}$$

where $\tau = x - x'$, and $S(w)$ is the spectral density function which is the Fourier dual of k.

$$S(w) = \frac{1}{(2\pi)^d} \int k(\tau) e^{-iw^T \tau} d\tau \tag{B.2}$$

$S(w)$ has the symmetry property, $S(w) = S(-w)$, and Euler's identity, $e^{\pm ix} = \cos x \pm i\sin x$, is used,

$$k(\tau) = \int_{-\infty}^{0} S(w)e^{iw^T\tau}dw + \int_{0}^{\infty} S(w)e^{iw^T\tau}dw \tag{B.3}$$

$$= \int_{0}^{\infty} S(w)e^{-iw^T\tau}dw + \int_{0}^{\infty} S(w)e^{iw^T\tau}dw \tag{B.4}$$

$$= \mathbb{E}_{S(w)} \cos(w^T\tau) \tag{B.5}$$

$$= \alpha\, \mathbb{E}_{p(w)} \cos(w^T\tau) \tag{B.6}$$

The spectral density function $S(w)$ is normalized to a probability density $p(w) = S(w)/\alpha$ where $\alpha = \int S(w)dw$.

For any constant offset $a \in \mathbb{R}$, $\int_0^{2\pi} \cos(a + 2b)db = 0$. As a result, for b uniformly distributed between 0 and 2π, the right side of the above equation changes as follows,

$$k(x - x') = \alpha\, \mathbb{E}_{p(w)} \cos(w^Tx - w^Tx') + \mathbb{E}_{p(b)} \cos(w^Tx + w^Tx' + 2b) \tag{B.7}$$

$$= \alpha\, \mathbb{E}_{p(w,b)} \left[\cos(w^Tx + b - w^Tx' - b) + \cos(w^Tx + w^Tx' + 2b)\right] \tag{B.8}$$

$$= 2\alpha\, \mathbb{E}_{p(w,b)}[\cos(w^Tx + b)\cos(w^Tx' + b)] \tag{B.9}$$

$$= \frac{2\alpha}{m}\mathbb{E}_{p(\mathbf{W},\mathbf{b})}[\cos(\mathbf{W}\mathbf{x} + \mathbf{b})^T\cos(\mathbf{W}\mathbf{x}' + \mathbf{b})] \tag{B.10}$$

where $[\mathbf{W}]_i \sim p(w)$ and $[\mathbf{b}]_i \sim p(b)$. Eq.(B.9) is derived from the sum of angles formula, and Eq. (B.10) is the result of averaging m weight and phases. If $\xi(x) = \sqrt{2\alpha/m}cos(Wx + b)$, the kernel function, k, can be approximated by the inner product of these equation, $k(x, x') \approx \xi(x)^T\xi(x')$.

Bibliography

[1] T Jayaraman and Tejal Kanitkar. The paris agreement. *Economic and Political Weekly*, 51(3), 2016.

[2] David J Heldebrant, Phillip K Koech, Vassiliki-Alexandra Glezakou, Roger Rousseau, Deepika Malhotra, and David C Cantu. Water-lean solvents for post-combustion CO_2 capture: fundamentals, uncertainties, opportunities, and outlook. *Chemical reviews*, 117(14):9594–9624, 2017.

[3] Jinjoo An, Ung Lee, Jaeheum Jung, and Chonghun Han. Parametric optimization for power de-rate reduction in the integrated coal-fired power plant with carbon capture and storage. *Industrial & Engineering Chemistry Research*, 54(18):5062–5076, 2015.

[4] Jae-Hoon Song, Sung-Bum Park, Ji-Ho Yoon, Huen Lee, and Kew-Ho Lee. Solubility of carbon dioxide in monoethanolamine+ ethylene glycol+ water and monoethanolamine+ poly (ethylene glycol)+ water at 333.2 k. *Journal of Chemical & Engineering Data*, 42(1):143–144, 1997.

[5] Hui Guo, Chenxu Li, Xiaoqin Shi, Hui Li, and Shufeng Shen. Nonaqueous amine-based absorbents for energy efficient CO_2 capture. *Applied Energy*, 239:725–734, 2019.

[6] E Sada, H Kumazawa, Y Ikehara, and ZQ Han. Chemical kinetics of the reaction of carbon dioxide with triethanolamine in non-aqueous solvents. *The Chemical Engineering Journal*, 40(1):7–12, 1989.

[7] Martin H Oyevaar, H Jan Fontein, and K Roel Westerterp. Equilibria of carbon dioxide in solutions of diethanolamine in aqueous ethylene glycol at 298 k. *Journal of Chemical and Engineering Data*, 34(4):405–408, 1989.

[8] Amr Henni and Alan E Mather. Solubility of carbon dioxide in methyldiethanolamine+ methanol+ water. *Journal of Chemical and Engineering Data*, 40(2):493–495, 1995.

[9] Jinkyu Im, Sung Yun Hong, Youngeun Cheon, Jeesun Lee, Je Seung Lee, Hoon Sik Kim, Minserk Cheong, and Hoseok Park. Steric hindrance-induced zwitterionic carbonates from alkanolamines and CO_2: highly efficient CO_2 absorbents. *Energy & Environmental Science*, 4(10):4284–4289, 2011.

[10] Min Xiao, Helei Liu, Hongxia Gao, Wilfred Olson, and Zhiwu Liang. CO_2 capture with hybrid absorbents of low viscosity imidazolium-based ionic liquids and amine. *Applied Energy*, 235:311–319, 2019.

[11] Rujie Wang, Shanshan Liu, Lidong Wang, Qiangwei Li, Shihan Zhang, Bo Chen, Lei Jiang, and Yifeng Zhang. Superior energy-saving splitter in monoethanolamine-based biphasic solvents for CO_2 capture from coal-fired flue gas. *Applied Energy*, 242:302–310, 2019.

[12] Yao Shen, Chenkai Jiang, Shihan Zhang, Jun Chen, Lidong Wang, and Jianmeng Chen. Biphasic solvent for CO_2 capture: Amine property-performance and heat duty relationship. *Applied energy*, 230:726–733, 2018.

[13] Shihan Zhang, Yao Shen, Lidong Wang, Jianmeng Chen, and Yongqi Lu. Phase change solvents for post-combustion CO_2 capture: Principle, advances, and challenges. *Applied Energy*, 239:876–897, 2019.

[14] Vittoria Blasucci, Cerag Dilek, Hillary Huttenhower, Ejae John, Veronica Llopis-Mestre, Pamela Pollet, Charles A Eckert, and Charles L Liotta. One-component, switchable ionic liquids derived from siloxylated amines. *Chemical Communications*, (1):116–118, 2009.

[15] David J Heldebrant, Phillip K Koech, M Trisha C Ang, Chen Liang, James E Rainbolt, Clement R Yonker, and Philip G Jessop. Reversible zwitterionic liquids, the reaction of alkanol guanidines, alkanol amidines, and diamines with CO_2. *Green Chemistry*, 12(4):713–721, 2010.

[16] David J Heldebrant, Clement R Yonker, Philip G Jessop, and Lam Phan. Organic liquid CO_2 capture agents with high gravimetric CO_2 capacity. *Energy & Environmental Science*, 1(4):487–493, 2008.

[17] Marty Lail, Jak Tanthana, and Luke Coleman. Non-aqueous solvent (nas) CO_2 capture process. *Energy Procedia*, 63:580–594, 2014.

[18] Patricia Mores, Nicolas Scenna, and Sergio Mussati. A rate based model of a packed column for CO_2 absorption using aqueous monoethanolamine solution. *International Journal of Greenhouse Gas Control*, 6:21–36, 2012.

[19] Patricia Mores, Néstor Rodríguez, Nicolas Scenna, and Sergio Mussati. CO_2 capture in power plants: Minimization of the investment and operating cost of the post-combustion process using mea aqueous solution. *International Journal of Greenhouse Gas Control*, 10:148–163, 2012.

[20] Nestor Rodríguez, Sergio Mussati, and Nicolas Scenna. Optimization of post-combustion CO_2 process using dea–mdea mixtures. *Chemical engineering research and design*, 89(9):1763–1773, 2011.

[21] Theodoros Damartzis, Athanasios I Papadopoulos, and Panos Seferlis. Process flowsheet design optimization for various amine-based solvents in post-combustion CO_2 capture plants. *Journal of Cleaner Production*, 111:204–216, 2016.

[22] Se-Young Oh, Michael Binns, Habin Cho, and Jin-Kuk Kim. Energy minimization of mea-based CO_2 capture process. *Applied energy*, 169:353–362, 2016.

[23] Ung Lee, Jannik Burre, Adrian Caspari, Johanna Kleinekorte, Artur M Schweidtmann, and Alexander Mitsos. Techno-economic optimization of a green-field post-combustion CO_2 capture process using superstructure and rate-based models. *Industrial & Engineering Chemistry Research*, 55(46):12014–12026, 2016.

[24] Hari Prasad Mangalapally, Ralf Notz, Norbert Asprion, Georg Sieder, Hugo Garcia, and Hans Hasse. Pilot plant study of four new solvents for post combustion carbon dioxide capture by reactive absorption and comparison to mea. *International Journal of Greenhouse Gas Control*, 8:205–216, 2012.

[25] Aroonsri Nuchitprasittichai and Selen Cremaschi. Optimization of CO_2 capture process with aqueous amines a comparison of two simulation–optimization approaches. *Industrial & Engineering Chemistry Research*, 52(30):10236–10243, 2013.

[26] Frits Byron Soepyan, Christine M Anderson-Cook, Joshua C Morgan, Charles H Tong, Debangsu Bhattacharyya, Benjamin P Omell, Michael S

Matuszewski, K Sham Bhat, Miguel A Zamarripa, John C Eslick, et al. Sequential design of experiments to maximize learning from carbon capture pilot plant testing. In *Computer Aided Chemical Engineering*, volume 44, pages 283–288. Elsevier, 2018.

[27] Marina Stavrou, Matthias Lampe, André Bardow, and Joachim Gross. Continuous molecular targeting–computer-aided molecular design (comt–camd) for simultaneous process and solvent design for co2 capture. *Industrial & Engineering Chemistry Research*, 53(46):18029–18041, 2014.

[28] Athanasios I Papadopoulos, Sara Badr, Alexandros Chremos, Esther Forte, Theodoros Zarogiannis, Panos Seferlis, Stavros Papadokonstantakis, Amparo Galindo, George Jackson, and Claire S Adjiman. Computer-aided molecular design and selection of co 2 capture solvents based on thermodynamics, reactivity and sustainability. *Molecular Systems Design & Engineering*, 1(3):313–334, 2016.

[29] Bledar A Konomi, Georgios Karagiannis, Kevin Lai, and Guang Lin. Bayesian treed calibration: an application to carbon capture with ax sorbent. *Journal of the American Statistical Association*, 112(517):37–53, 2017.

[30] Jonggeol Na, Seongeon Park, Ji Hyun Bak, Minjun Kim, Dongwoo Lee, Yunsung Yoo, Injun Kim, Jinwon Park, Ung Lee, and Jong Min Lee. Bayesian inference of aqueous mineral carbonation kinetics for carbon capture and utilization. *Industrial & Engineering Chemistry Research*, 0(ja):null, 0.

[31] Zoubin Ghahramani. Probabilistic machine learning and artificial intelligence. *Nature*, 521:452, 2015.

[32] Douglas Aaron and Costas Tsouris. Separation of CO_2 from flue gas: a review. *Separation Science and Technology*, 40(1-3):321–348, 2005.

[33] Raphael Idem, Malcolm Wilson, Paitoon Tontiwachwuthikul, Amit Chakma, Amornvadee Veawab, Adisorn Aroonwilas, and Don Gelowitz. Pilot plant studies of the CO_2 capture performance of aqueous mea and mixed mea/mdea solvents at the university of regina CO_2 capture technology development plant and the boundary dam CO_2 capture demonstration plant. *Industrial & engineering chemistry research*, 45(8):2414–2420, 2006.

[34] Amit Chakma. CO_2 capture processes—opportunities for improved energy efficiencies. *Energy conversion and management*, 38:S51–S56, 1997.

[35] Jochen Oexmann, Alfons Kather, Sebastian Linnenberg, and Ulrich Liebenthal. Post-combustion CO_2 capture: chemical absorption processes in coal-fired steam power plants. *Greenhouse Gases: Science and Technology*, 2(2):80–98, 2012.

[36] Chikezie Nwaoha, Raphael Idem, Teeradet Supap, Chintana Saiwan, Paitoon Tontiwachwuthikul, Wichitpan Rongwong, Mohammed Jaber Al-Marri, and Abdelbaki Benamor. Heat duty, heat of absorption, sensible heat and heat of vaporization of 2–amino–2–methyl–1–propanol (amp), piperazine (pz) and monoethanolamine (mea) tri–solvent blend for carbon dioxide (CO_2) capture. *Chemical Engineering Science*, 170:26–35, 2017.

[37] LL Lee. Thermodynamic models for natural gas sweetening fluids. *Annual report to the Gas Research Institute, University of Oklahoma, Norman, OK*, 1994.

[38] Li-Feng Chiu, Hsiao-Fen Liu, and Meng-Hui Li. Heat capacity of alkanolamines by differential scanning calorimetry. *Journal of Chemical & Engineering Data*, 44(3):631–636, 1999.

[39] Ung Lee, Alexander Mitsos, and Chonghun Han. Optimal retrofit of a CO_2 capture pilot plant using superstructure and rate-based models. *International Journal of Greenhouse Gas Control*, 50:57–69, 2016.

[40] Donald R. Jones, Matthias Schonlau, and William J. Welch. Efficient global optimization of expensive black-box functions. *Journal of Global Optimization*, 13(4):455–492, Dec 1998.

[41] Eric Bradford, Artur M Schweidtmann, and Alexei Lapkin. Efficient multiobjective optimization employing gaussian processes, spectral sampling and a genetic algorithm. *Journal of Global Optimization*, 71(2):407–438, 2018.

[42] Mattias Björkman and Kenneth Holmström. Global optimization using direct algorithm in matlab. 1999.

[43] José Miguel Hernández-Lobato, Matthew W Hoffman, and Zoubin Ghahramani. Predictive entropy search for efficient global optimization of black-box functions. In *Advances in neural information processing systems*, pages 918–926, 2014.

[44] Adrián Pérez-Suay, Julia Amorós-López, Luis Gómez-Chova, Valero Laparra, Jordi Muñoz-Marí, and Gustau Camps-Valls. Randomized kernels for large scale earth observation applications. *Remote Sensing of Environment*, 202:54–63, 2017.

[45] David E Goldberg. Genetic algorithms in search. *Optimization, and MachineLearning*, 1989.

[46] Finn Andrew Tobiesen, Hallvard F Svendsen, and Olav Juliussen. Experimental validation of a rigorous absorber model for CO_2 postcombustion capture. *AIChE Journal*, 53(4):846–865, 2007.

[47] Mehdi Karimi, Magne Hillestad, and Hallvard F Svendsen. Investigation of intercooling effect in CO_2 capture energy consumption. *Energy Procedia*, 4:1601–1607, 2011.

[48] David H Van Wagener and Gary T Rochelle. Stripper configurations for CO_2 capture by aqueous monoethanolamine and piperazine. *Energy Procedia*, 4:1323–1330, 2011.

[49] Tomio Mimura, Hidenobu Simayoshi, Taiichiro Suda, Masaki Iijima, and Sigeaki Mituoka. Development of energy saving technology for flue gas carbon dioxide recovery in power plant by chemical absorption method and steam system. *Energy Conversion and Management*, 38:S57–S62, 1997.

[50] Jacob N Knudsen, Jørgen N Jensen, Poul-Jacob Vilhelmsen, and Ole Biede. Experience with CO_2 capture from coal flue gas in pilot-scale: Testing of different amine solvents. *Energy Procedia*, 1(1):783–790, 2009.

[51] Takashi Ogawa, Yukio Ohashi, Susum u Yamanaka, and Kiyoshi Miyaike. Development of carbon dioxide removal system from the flue gas of coal fired power plant. *Energy Procedia*, 1(1):721–724, 2009.

[52] Rüdiger Schneider and Henning Schramm. Environmentally friendly and economic carbon capture from power plant flue gases: The siemens postcap

technology. In *1st Post Combustion Capture Conference*, pages 17–19. United Arab Emirates, 2011.

[53] Hari Prasad Mangalapally and Hans Hasse. Pilot plant experiments for post combustion carbon dioxide capture by reactive absorption with novel solvents. *Energy Procedia*, 4:1–8, 2011.

[54] Peter Brúder, Farshid Owrang, and Hallvard F Svendsen. Pilot study—CO_2 capture into aqueous solutions of 3-methylaminopropylamine (mapa) activated dimethyl-monoethanolamine (dmmea). *International Journal of Greenhouse Gas Control*, 11:98–109, 2012.

[55] Hamid Esmaeili and Behrooz Roozbehani. Pilot-scale experiments for post-combustion CO_2 capture from gas fired power plants with a novel solvent. *International Journal of Greenhouse Gas Control*, 30:212–215, 2014.

[56] Zdenka Kolska, Milan Zabransky, and Alena Randova. Group contribution methods for estimation of selected physico-chemical properties of organic compounds. In *Thermodynamics-Fundamentals and Its Application in Science*. IntechOpen, 2012.

[57] Michael Caplow. Kinetics of carbamate formation and breakdown. *Journal of the American Chemical Society*, 90(24):6795–6803, 1968.

[58] PV Danckwerts. The reaction of CO_2 with ethanolamines. *Chemical Engineering Science*, 34(4):443–446, 1979.

[59] Parkash D Vaidya and Eugeny Y Kenig. Termolecular kinetic model for CO_2-alkanolamine reactions: An overview. *Chemical Engineering & Technology*, 33(10):1577–1581, 2010.

[60] John E Crooks and J Paul Donnellan. Kinetics and mechanism of the reaction between carbon dioxide and amines in aqueous solution. *Journal of the Chemical Society, Perkin Transactions 2*, (4):331–333, 1989.

[61] Sulzer Chemtech. Structured packings for distillation, absorption and reactive distillation. *Sulzer Chemtech*, 2010.

[62] J Stichlmair, JL Bravo, and JR Fair. General model for prediction of pressure drop and capacity of countercurrent gas/liquid packed columns. *Gas Separation & Purification*, 3(1):19–28, 1989.

[63] R. I. Cukier, C. M. Fortuin, K. E. Shuler, A. G. Petschek, and J. H. Schaibly. Study of the sensitivity of coupled reaction systems to uncertainties in rate coefficients. i theory. *The Journal of Chemical Physics*, 59(8):3873–3878, 1973.

[64] Flavio Cannavó. Sensitivity analysis for volcanic source modeling quality assessment and model selection. *Computers & Geosciences*, 44:52 – 59, 2012.

[65] Sebastian Mosbach, Andreas Braumann, Peter L. W. Man, Catharine A. Kastner, George P. E. Brownbridge, and Markus Kraft. Iterative improvement of bayesian parameter estimates for an engine model by means of experimental design. *Combustion and Flame*, 159(3):1303–1313, 2012.

[66] Catharine A. Kastner, Andreas Braumann, Peter L. W. Man, Sebastian Mosbach, George P. E. Brownbridge, Jethro Akroyd, Markus Kraft, and Chrismono Himawan. Bayesian parameter estimation for a jet-milling model using metropolis-hastings and wang-landau sampling. *Chemical Engineering Science*, 89:244–257, 2013.

[67] Nicholas Metropolis, Arianna W. Rosenbluth, Marshall N. Rosenbluth, Augusta H. Teller, and Edward Teller. Equation of state calculations by fast computing machines. *The Journal of Chemical Physics*, 21(6):1087–1092, 1953.

[68] Kaiming He, Xiangyu Zhang, Shaoqing Ren, and Jian Sun. Deep residual learning for image recognition. *CoRR*, abs/1512.03385, 2015.

초록

습식 아민을 이용한 이산화탄소 포집 공정의 상용화를 위해서는 높은 재생 에너지를 비롯한 기존 아민 용매의 단점을 극복한 신 용매의 개발이 필수적이다. 본 연구에서는 이러한 단점을 극복한 신 저수계 아민 용매, K_2Sol, 을 제안한다. K_2Sol은 입체장애 구조를 가지는 디아민으로 구성되어 있으며, 아민 사이트의 장애구조로 인해 중탄산염을 쉽게 만들어 내며, 이로 부터 높은 흡수 용량을 가질 것으로 기대된다. 실험실 규모의 테스트를 통해 K_2Sol의 이산화탄소 흡수능력, 열용량, 열화내구성, 이산화탄소 흡수능에 따른 점도 등을 측정하였고, 이를 30wt% MEA의 성능과 비교하여 이산화탄소 포집 공정의 용매로서 우월한 성능을 가짐을 입증하였다.

이후 실험실 규모의 테스트 결과로부터, 이산화탄소 포집 공정에서 K_2Sol의 성능을 검증하기 위해 최적 재생 에너지를 측정하기 위한 파일럿 스케일의 실험을 시행하였다. 파일럿 스케일의 실험의 비용과 시간 소모를 최소화하기 위해 해당 실험에 가우시안 프로세스 베이지안 최적화 기법 (GPBO) 을 적용하여 최저의 재생에너지를 찾는 최적 운전 조건을 찾았다. GPBO는 공정의 제일원리 모델 (First principle model) 없이 실험의 입력변수와 출력반응의 관계를 통해 근사 수학 모델을 만들어 최적해를 찾는다. 적은 횟수의 평가로 블랙박스 모델의 국부 최적값을 찾는데 용이하기 때문에, 파일럿 스케일 실험과 같은 높은 비용의 실험에 적절하다. 파일럿 플랜트 실험 결과 30wt% MEA의 최적 재생에너지가 4.3 GJ/t CO_2, K_2Sol의 최적 재생에너지가 2.8 GJ/t CO_2로 MEA 대비 65% 수준의 낮은 재생에너지를 보였다. GPBO를 통해 최적 운전조건을 찾는데 각각 30회가 안되는 실험이 수행되었다. 또한 K_2Sol을 이용한 이산화탄소 포집공정의 리보일러의 온도가 물의 끓는 점보다 낮은 것으로부터 낮은 수준의 열량으로 운전이 가능하므로 30wt% MEA 대비 경제적임을 입증했다.

마지막으로 파일럿 스케일 실험의 데이터만으로 상용 시뮬레이터를 이용한 공정 모델을 개발하기 위해 전역 민감도 분석과 베이지안 매개변수 추정법을 K_2Sol을 이용한 흡수탑 모델에 적용하였다. 몇 가지의 가정을 통해, K_2Sol의 순물질 매개변수를 group contribution method를 통해 추정하였고, K_2Sol와 이산화탄소의 반응은 termolecular reaction mechanism으로 가정하였다. 이로부터 남은 16개의 파라메터를 이용하여 전역 민감도 분석을 시행하였고, 흡수탑 모델의 출력반응에 기여를 제일 많이 하는 8개의 파라메터를 선정하였다. 이 8개의 파라메터를 입력 변수로 하는 수학대리모델을 잔여학습기법을 기반으로 한 딥러닝 기법을 통해 개발하고, 개발된 수학대리모델과 기존 ASPEN Plus 모델을 기반으로 한 하이브리드 모델을 이용하여 베이지안 매개변수 추정법을 적용하였다. 그 결과, K_2Sol 수용액의 양이온의 형성 깁스 에너지가 가장 큰 영향을 주는 파라메터이며, 각 정반응에서 K_2Sol과 물이 동시에 지배적인 염기로 작용한다는 것을 보였다. 또한 추정된 파라메터가 도입된 모델은 대부분의 실험의 출력을 95% 신뢰영역에서 만족함을 보였다.

주요어: 이산화탄소 포집, 저수계 아민 용매, 가우시안 프로세스 베이지안 최적화, 파일럿 스케일 테스트, 전역 민감도 분석, 베이지안 매개변수 추정
학번: 2011-21025

감사의 글

대학원에 입학한 지 9년 째, 연구실 선후배들에 비하면 턱없이 많은 시간이 소요 됐으나 어찌하였든 박사과정을 취득하여 졸업할 수 있게 되었다는 것에 큰 영광으로 생각합니다. 사실 이 글을 쓰는 지금도 나는 박사학위를 취득하기에는 너무나도 부족한 존재라는 것을 뼈저리게 느끼지만, 많은 분들의 도움이 있었기에 여기까지 올 수 있지 않았나 싶습니다.

먼저 지도교수님으로서 학위논문 지도와 함께, 졸업 후 갖춰야할 인격적 소양까지 큰 조언을 아끼지 않으신 이윤우 교수님께 감사의 말씀을 드립니다. 또한 화학공정설계라는 큰 분야에 뛰어들 수 있도록 박사과정 동안 기반을 제공해주신 한종훈 교수님께도 감사드립니다. 박사과정 중 군입대 및 제대를 하여 정신적으로 궁지에 몰리며 학문적으로 앞길을 찾지 못하였을 때 큰 지원을 해주신 임영섭 교수님과 제 졸업을 위해 자신의 일처럼 연구지원을 아끼지 않으시고 본 학위 논문의 큰 바탕이 된 파일럿 스케일 실험의 기회를 주신 이웅 박사님 감사합니다. 학위논문 심사에서 발전적인 코멘트로 도움을 주신 이종민 교수님, 남재욱 교수님께도 감사드립니다.

연구실 및 KIST 내의 학생연구원 생활 간, 저의 모난 성격과 모자른 지식, 게으른 성품 탓에 과연 무난히 졸업할 수 있을까 싶은 위기만이 연속이었다고 생각합니다. 지금과 같은 좋은 연구실에서 훌륭하신 선배님, 후배님, 동료님, 동기들이 함께 해 주시고 크나큰 배려와 도움이 있었기에 포기하지 않고 여기까지

올 수 있었습니다. 이 모든 한 사람 한 사람께 감사 인사를 드리고 싶습니다. 정말 도움이 되고 의지할 수 있는 일원이 되고자 하였으나, 오히려 도움만 받고 때로는 마음의 상처까지 주는 못난 인간 아닌 사람이었던 점에 대해 이 지면을 빌려 죄송하고 미안하다는 말씀을 드리고자 합니다.

마지막으로 사랑하는 어머니, 아버지, 동생, 모두에게 감사합니다. 부족했지만 연구에 대한 욕심으로 이 길에 발을 디뎠고, 그 이후 크나큰 고난들이 많았으나 가족들의 지지와 원호가 없었다면 끝까지 도달할 수 없었던 길이라 생각합니다. 받은 사랑만큼 더욱 성장하는 아들, 형으로서 모습을 보여드리고 싶고, 앞으로 모두에게 행복한 삶만이 있기를 기도합니다.

2019년 7월

김정남